UNIVERSITÀ DEGLI STUDI DI TRENTO
Dipartimento di Ingegneria Civile e Ambientale

QUEEN MARY
UNIVERSITY OF LONDON

Erasmus Mundus Joint Doctorate School in Science for MAnagement of Rivers and their Tidal System

---

Seyed Hossein Mohajeri

Hydrodynamics of Gravel Bed Flows (Implication on Colmation)

Erasmus Mundus

Autumn, 2014

Doctoral thesis in Science for MAnagement of Rivers and their Tidal System**,**

Cycle (I)

Primary Institution (Department of Civil, Mechanics and Environmental Engineering, University of Trento, Italy)
Secondary Institution (School of Geography, Queen Mary University of London, United Kingdom)
Associate Partner (School of Engineering, University of Aberdeen, United Kingdom)

Supervisors:
Dr. Maurizio Righetti, University of Trento
Dr. Geraldene Wharton, Queen Mary University of London

Associate Partner (External Advisor):
Prof. Vladimir Nikora, University of Aberdeen

Academic year 2011/2014

The SMART Joint Doctorate Programme

Research for this thesis was conducted with the support of the Erasmus Mundus Programme[1], within the framework of the Erasmus Mundus Joint Doctorate (EMJD) SMART (Science for MAnagement of Rivers and their Tidal systems),. EMJDs aim to foster cooperation between higher education institutions and academic staff in Europe and third countries with a view to creating centres of excellence and providing a highly skilled 21st century workforce enabled to lead social, cultural and economic developments. All EMJDs involve mandatory mobility between the universities in the consortia and lead to the award of recognised joint, double or multiple degrees.
The SMART programme represents a collaboration among the University of Trento, Queen Mary University of London, and Freie Universität Berlin. Each doctoral candidate within the SMART programme has conformed to the following during their 3 years of study:

(i) Supervision by a minimum of two supervisors in two institutions (their primary and secondary institutions).
(ii) Study for a minimum period of 6 months at their secondary institution
(iii) Successful completion of a minimum of 30 ECTS of taught courses
(iv) Collaboration with an associate partner to develop a particular component / application of their research that is of mutual interest.
(v) Submission of a thesis within 3 years of commencing the programme.

[1] This project has been funded with support from the European Commission. This publication reflects the views only of the author, and the Commission cannot be held responsible for any use which may be made of the information contained therein.

Acknowledgements

My thanks go to:

- ***Dr. Maurizio Righetti*** for the continuous support of my Ph.D study and research, for his motivation, enthusiasm, and immense knowledge. I could not have imagined having a better advisor for my Ph.D study.
- ***Dr. Geraldene Wharton*** whose expertise, understanding, and patience added considerably to my graduate experience, specifically in the field of physical geography.
- ***Prof. Vladimir Nikora*** for his invalueable advice not only for my thesis but also in my future career. I would like to thank him for encouraging my research and for allowing me to grow as a research scientist.
- my thesis committee: ***Dr. Markus Noack, Dr. Fluvio Boano , Dr. Stephen Krause*** *and* ***Prof. Marco Tubino***.
- ***Prof. Gian Paolo Romano*** and ***Dr Silvano Grizzi*** whose support on experimental data collection is appreciable.
- ***Dr. Jochen Aberle, Dr. Martin Detert*** *and* ***Prof. Kenneth Christensen*** who provided me with advice at times of critical need.
- ***Dr. Corrado Pellachini*** whose helps in the initial steps is laudable.
- The supportive crews of Hydraulic Laboratory of Trento University (***Fabio Sartori, Lorenzo Forti, Andrea Bampi*** and ***Paolo Scarfiello***).
- All my friends in Trento, London and Aberdeen, especially ***Iman Khaghanifard*** who is a unique friend and his helps are not forgettable.
- My friends, ***Mahdi Khademi, Tesfye Haimanot Tarekegn, Navid Maroofi*** who helped me during the measurements. I have truly fruitful discussion with them. I was lucky that I meet them throughout my study.
- My nice and lovely friends in SMART program, especially ***Cagri Gokdemir, Jean-Philipe Belliard, Marco Redolfi, Simone Zen, Prima Sekarsari, Sepideh Ramezani, Alex Albatros-Flugzeugwerke, Mathew Cashman, Francesca Pilotto*** and ***Ulfah Mardhiah.***

- ***My kind mother*** and ***good sister*** for their unconditional support throughout my degree.
- ***My wife*** for her understanding and love during the past two years. Her support and encouragement was in the end what made this dissertation possible.
- The last but not the least, ***my father*** who left us at the time we never think about it.

Seyed Hossein Mohajeri

September 2014

Abstract

Bottom of the mountainous rivers is generally composed of natural gravels. Flow depth in such rivers is generally shallow, with the ratio of water depth to size of bed materials (known as relative submergence) rarely higher than 20. In this type of flow, gravels intrusion induces significant spatial variation of the flow characteristics near bed region, which is known as roughness layer. The simultaneous effects of natural gravels and water surface cause formation of complicated flow structure which is to some extent different from the flow with high relative submergence (flow with relative submergence higher than 40). Despite abundance of studies in shallow flows, there are only a limited number of studies concerning spatial organization of near bed flow field for such type of flow, with also contradictory results.

The spatial organization of near bed turbulent flow characteristics is also important for transport of fine sediment. Transport of fine sediments is generally correlated to the asymmetry of vertical velocity. Asymmetry of vertical velocity also arises from a quasi-cyclic process of upward motion of low-velocity fluid parcels (ejection) and downward motion of high-velocity parcels (sweep), together known as bursting process. Spatial organization of bursting process and asymmetry of vertical velocity in near bed and respect to bed topography has not been inscribed properly.

In heterogeneous flows, the use of spatially averaged turbulent transport equations, known as Double Averaged Navier-Stikes equations (DANS), is common. In DANS equations viscous drag, form drag and correlation of spatial fluctuation of time averaged velocities (known as form induced stresses) are explicitly expressed. Despite prevailing usage of DANS equations in study of gravel bed flow, examination of vertical velocity has not been performed appropriately by applying double averaging method. Also, the role of form induced stresses in vertical momentum flux has not been highlighted.

In present thesis, Stereoscopic Particle Image Velocimetry at near bed horizontal layer and Digital Particle Image Velocimetry in vertical planes are employed together with laser scanning of bed elevations to study flow field and turbulence structure over a coarse immobile gravel bed in submergence conditions ranges from 5 to 10. Spatial organization of flow characteristics at the near bed region is analyzed respect to bed topography. This analysis is also composed of spatial distribution of bursting process and vertical momentum flux. Moreover, vertical profiles of double averaged turbulent flow characteristics and form induced stresses with different relative submergences are compared.

Results show that near bed flow field is characterized by a strip structure induced by secondary currents. Such structure tends to be disrupted by the effect of gravel protrusions. To better analyze the interaction between the flow field and gravel bed protrusions, cross-correlations of different velocity components and bed elevations in a horizontal layer just above gravel crests are computed. These results show that upward and downward flows occur not randomly on the bed, but in correspondence to upstream and downstream side of gravels. Also, turbulent momentum flux is directed downward in the downstream side of gravel crests and it is directed upward in upstream side of gravel crests. This is due to prevalence of

ejection and sweep events respectively in upstream and downstream sides of gravel crests. These results are in agreement with formation of separation and reattachment zones around gravel crests. Moreover, spatial distribution of sweep and ejection events are organized in streamwise elongated strips with high and low values which are consistent with presence of secondary currents cells.

Results obtained by double averaging method show that relative submergence affects the normalwise double averaged turbulence intensity profiles all along the flow depth, while only a weak effect, limited to the near bed region, is noticed on streamwise double averaged turbulence intensity profiles. Logarithmic law parameterization of double averaged velocity profiles shows that parameters change considerably with relative submergence and, in some cases, no clear log-law region was found. These results challenge application of log-law in such type of flow.

Analysis of the vertical velocity shows that far from the bed, vertical turbulence momentum flux is upward, while below gravel crests it is downward. This behavior is resulted by prevalence of ejection events far from the bed and sweep events below gravel crests. Results show that vertical momentum flux resulted by form induced component is not significant, except below gravel crests which are upward in to the water column.

A limited number of qualitative observations in the real case of fine sediments presence in the matrix of rough bed is in agreement with the results of turbulent flow characteristics. Sand ribbons are clearly formed due to secondary currents. Also, fine materials are mostly deposited and eroded respectively in downstream and upstream sides of gravel crests.

The results of present study show that in general some regions actively participate in transport, while the other regions do not participate in the transport. From this basis, Rouse criterion has been developed by considering spatial variation of vertical momentum flux.

Table of Contents

List of Figures

List of Tables

1 Colmation in Gravel Bed Rivers

***Abstract**:*

This chapter is an introduction to the rest of the present thesis. At first, colmation process is introduced and the importance of this process in the riverine area has been highlighted. Then, state of the art of gravel bed hydrodynamics is reported. The role of gravel bed hydrodynamics in fine sediment transport is also discussed. In the last part of this chapter, research questions and structure of present thesis is expressed.

"So study evermore is overshot:
While it doth study to have what it would
It doth forget to do the thing it should,
And when it hath the thing it hunteth most,
'Tis won as towns with fire, so won, so lost."

William Shakespeare (1564-1616)

1.1 INTRODUCTION

Gravel beds are common in nature, specifically most of mountainous rivers is composed of gravels in different sizes (Wohl, 2013). The transport and deposition of fine sediments in gravel bed rivers is also common in mountainous areas (Schälchli, 1992; Wohl, 2013). Improved knowledge of the distinct characteristics of fine sediments, which affects their erodibility (Grabowski et al., 2011) and the flow structures above gravel beds will further our understanding of fine sediment dynamics. This is important because fine sediments deliver benefits such as nutrient supply to biota but excessive fine sediment loads and the presence of sediment-bound contaminants can cause significant environmental impacts.

Fine sediment can be defined as all particles finer than gravel and comprising sand, silt and clay. Two scenarios are possible to change the state of a fine particle: in the transport state, it can be deposited and in the deposited state, it can be eroded. Colmation is the entry of finer material in the matrix of a gravel bed and its filtration to the deeper layer and then formation of a layer which reduces the permeability of a river bed compared to the initial conditions (Schälchli, 1992; Brunke and Gonser, 1997; Blaschke et al., 2003). These finer materials comprise particulate organic matters, such as seeds, and aggregates and/or flocs of organic and inorganic particles including invertebrate faecal pellets (Heppell et al., 2009).

There are several definitions of colmation. The term colmation is commonly used where there is more emphasis on the ecological and biological aspects of sediment deposition. In the context of the physical effects of sediment deposition, the

process is called clogging (Blaschke et al., 2003; Packman and Mackay, 2003; Rehg et al., 2005). Infilling is more used in the field of groundwater hydrology where the emphasis is on conductivity reduction (Mccloskey and Finnemore, 1996; Li, 1997) and finally ingress is a common term in geomorphology (Li, 1997). In the present study, the word colmation is used. In addition to fine deposition, colmation can also develop by production of polysaccharides by bacteria as biofilm which is called biological colmation (Ibisch, 2009).

Fine particle trapping in the matrix of a gravel bed can be affected by physical, chemical and biological variables (Schälchli, 1992). Physical variables consist of both ambient properties (e.g. porosity (Chen et al., 2008), hydraulic conductivity, gravel bed size distribution (Diplas and Parker, 1992) and hydraulic characteristics of both surface and subsurface flow (e.g. near bed turbulent properties and velocity (Sambrook Smith and Nicholas, 2005; Wren et al., 2011), surface-subsurface flow exchange (Packman and Mackay, 2003), suspended load (Diplas and Parker, 1992; Grams and Wilcock, 2007)). Chemical and biological variables like ambient acidity, available organic matter, nitrification and denitrification, oxidation state are important for biogeochemical processes (Doussan et al., 1997; Pretty et al., 2006; Dong et al., 2009). Although, physical, chemical and biological variables are interconnected, they have a reciprocal connection to colmation and so colmation results in other physico-chemical and biological processes (Brunke, 1998). This makes the comprehensive understanding of colmation processes complicated.

During a flood or as a consequence of up-welling ground water flow, colmated material can be resuspended in the water in the process of decolmation, also called declogging (Hiscock and Grischek, 2002; Blaschke et al., 2003). Colmation and decolmation form a natural cycle in river beds (Brunke, 1998; Blaschke et al., 2003). As explained in Figure 1-1a, in the low flow condition the process is initiated by internal or external colmation (Velickovic, 2005; Descloux et al., 2010).

External colmation refers to sediment deposition by lowering the flow velocities and water levels whereas internal colmation is the result of upward motion of the lower material toward an armour layer and the formation of a thin sealed layer (Brunke, 1998; Blaschke et al., 2003). Schälchli (1992) studied internal colmation and proposed a development mechanism composed of three phases and in each phase

large, medium and small particles play different roles (Brunke, 1998; Schälchli, 1992). The majority of studies of external colmation have been undertaken from a hydraulic engineering prospective since near bed flow properties and sediment transport are the most important factors (Diplas and Parker, 1992; Smits et al., 2011; Wren et al., 2011).

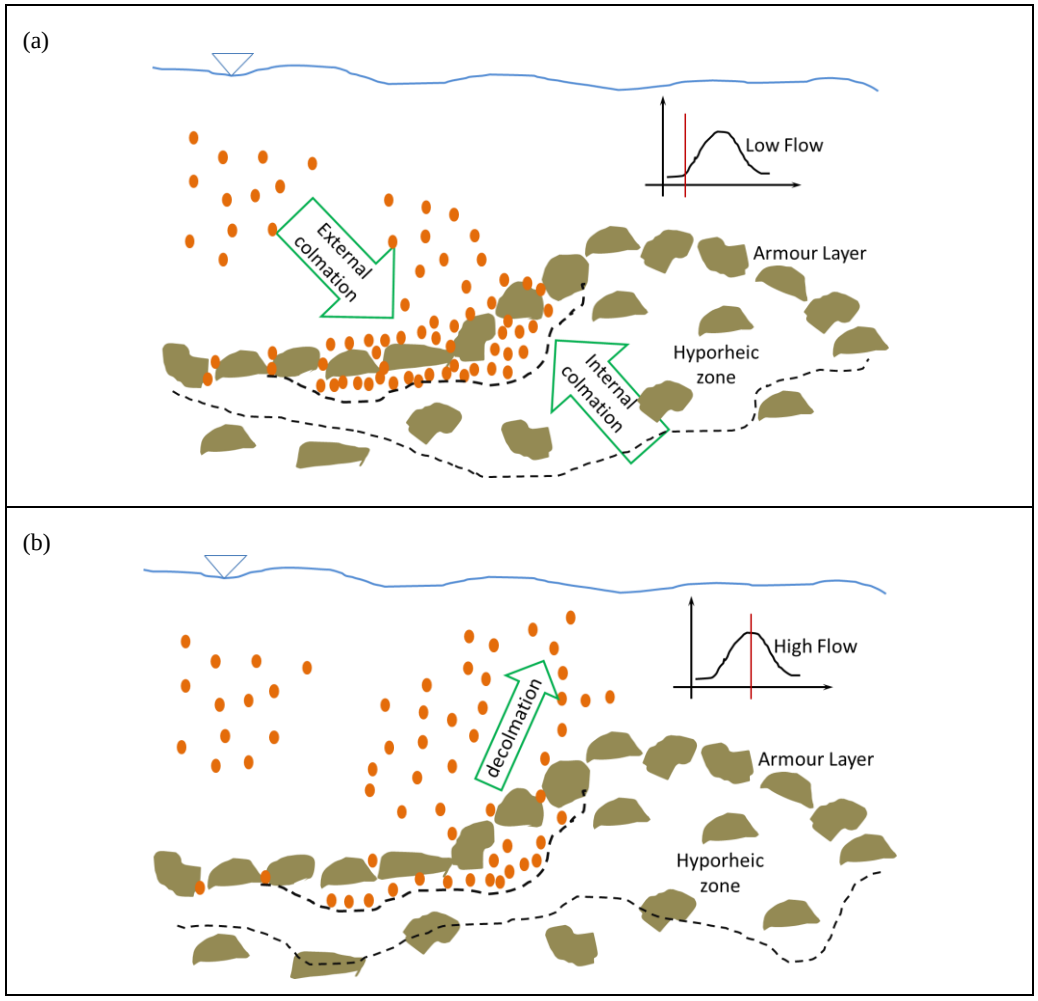

Figure 1-1: Colmation-decolmation cycle (a) Colmation (b) Decolmation.

It should be noted that there is another form of clogging where fine material is stored in an armour layer. This is called contact colmation or intermediate colmation or armour layer colmation which forms above internal and below external colmation

around an armour layer (Velickovic, 2005; Blaschke et al., 2003). External and intermediate clogging are visible, while internal clogging is hidden below an armour layer (Blaschke et al., 2003). In decolmation, the colmation layer is removed by exceedingly large shear stress or high ground water pressure and entrains and suspends fine sediment in the water as shown in Figure 1-1b (Brunke and Gonser, 1997; Blaschke et al., 2003; Velickovic, 2005).

The colmation takes place in bottom of river bed and in hyporheic zone. The hyporheic zone (HZ) is an active ecotone which connects surface water and ground water and riverine areas (Figure 1-2). The study of the HZ is an interdisciplinary research from hydrology to ecology in different spatial and temporal scales investigation (Boulton, 2007; Krause et al., 2011). Because of this variation, the exact definition of HZ is not clear. However, Krause et al. (2011) defined this layer as "a temporally and spatially dynamic saturated transition zone between surface water and groundwater bodies that derives its specific physical (e.g. water temperature) and biogeochemical (e.g. steep chemical gradients) characteristics from mixing of surface and groundwater to provide a dynamic habitat and potential refugia for obligate and facultative species".

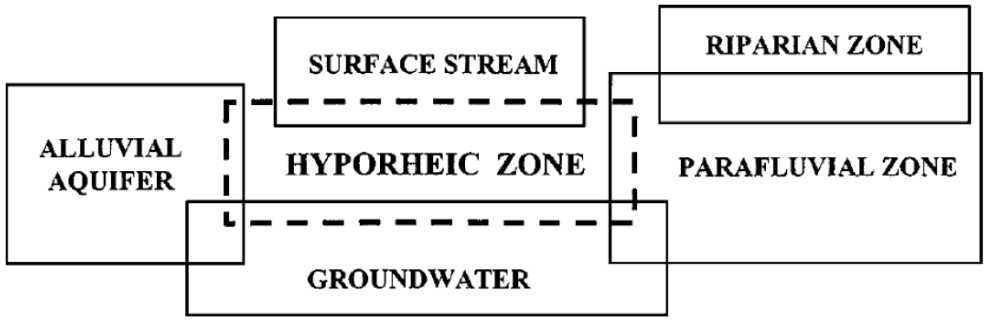

Figure 1-2: Simplified schematic diagram of the HZ and surrounding interconnected areas (Boulton et al., 1998).

A diverse array of aquatic invertebrates live in the interstitial space of HZ and which is called hyperheos (Boulton et al., 1998). Hyperheos activity (burrowing and fecal pellets formation) can alter the HZ porosity and forms an impermeable layer

(Boulton et al., 1998). Besides, filling the spaces by deposited river fine sediment affects hyperheos, too (Boulton et al., 1998). Granulometric features, hydraulic conductivity and porosity are important for physical, chemical and consequently biological processes in the HZ (Boulton et al., 1998). Flow patterns in the HZ can be turbulent, irregular with the presence of dead zone and rapid flow (Krause et al., 2011). Colmation changes flow patterns in the HZ and reduces hydraulic conductivity and consequently reduces the efficiency of hyporheic biogeochemical cycling and habitat conditions (Nogaro et al., 2006; Krause et al., 2011).

Although the study of colmation has a long history, only in recent years has a more inter-disciplinary approach been adopted. In the present study, we focus on the colmation from an inter-disciplinary approach. For this purpose, firstly, we firstly highlight the importance of colmation from ecological and environmental aspects and then we focus on physical process of colmation.

1.2 IMPORTANCE OF COLMATION

In natural streams, colmation and decolmation occurs intermittently as a result of changes in physical condition and this process is in equilibrium with the environment (Brunke and Gonser, 1997; Blaschke et al., 2003). Through increment in sediment load and changes in sediment quality, fine sediment deposition exacerbates and stream substratum compaction and cementation increases (Sternecker et al., 2013). Thus, colmation affects the fluvial system in various aspects from engineering to biology. Generally, these environmental effects can be classified in two groups: hydrological and hydraulic effects and ecological effects. The main focus of hydrological and hydraulic studies is the colmation process and the consequent problems such as changes in the HZ exchanges, sediment transport and near bed turbulent flow properties. While in ecological studies the main concern is the impact of colmation on fauna and flora. In the following sections, these effects will be explained in more detail.

1.2.1 Ecological Effects

Colmation can affect the taxa in the HZ by forming a impermeable thin layer which makes the surface-subsurface interaction difficult (Boulton et al., 1998; Pretty et al., 2006; Mueller et al., 2013). Moreover, it reduces spatial variation in river bed characteristics and produces more homogeneous condition which influences the biodiversity (Brunke and Gonser, 1997). The effects of colmation on biota in streams are directly and indirectly. Direct effects of colmation relates to infilling of porous spaces on the matrix of the gravel bed. It makes the growth of macro organism (such as mussels, fishes and algae) difficult and decreases the available area for their movement and refugial spaces during high flow and extreme drought events (Wood and Armitage, 1997; Brunke and Gonser, 1997; Bo et al., 2007). The increment in availability of fine sediments near bed increases possibility of abrasion which damage weak and unprotected invertebrates organs such as gills and filter-feeding (Jones et al., 2012). Also, burial can cause problem for some species like nymphs of the mayfly or in early stage of macro organisms' life (e.g. immotile eggs) (Wood et al., 2001; Jones et al., 2012). However, some species (e.g. tubificids worms or chironomid larvae) are able to move sediment and prepare enough space for their movement in the process of bioturbation (Statzner and Sagnes, 2008; Nogaro et al., 2010). The bioturbators can increase water-sediment interaction and initiate many biogeochemical and microbial processes in bottom of the rivers (Nogaro et al., 2006). So, the impact will be greater on species that do not perform bioturbation.

The indirect effects of colmation includes decreases in the concentration of dissolved oxygen in the HZ and disturbance of the normal breathing and feeding of communities living in the rivers (Bo et al., 2007; Jones et al., 2012); Restricting the amount of available oxygen increases the death rate among young fishes (Wood and Armitage, 1997; Jones et al., 2012) and there is some evidence that appropriate hydraulic exchange in the interstitial zone, is required to ensure the hatching success of brown trout eggs (Sternecker et al., 2013). In chalk stream rivers, colmation creates the conditions for methane production by some specific types of microbes at the lowest redox potential a process known as methanogenesis (Sanders et al., 2007; Krause et al., 2011). There is not so much information about methanogenesis in HZ (Trimmer et al., 2010). This process which is dominant in anaerobic sediment is the

final step in organic decay and during this process hydrogen, small organics and carbon dioxide become depleted (Sanders et al., 2007; Krause et al., 2011).

The bed composition is important in the colonisation mechanism and availability and composition of benthic communities (Bo et al., 2007). Crawling mayfly larvae prefers stable substrates comapring to fine material since they are not strong enough to grip (Jones et al., 2012). Unlike Crawling mayfly larvae, certain Chironomidae and Ephemeridae prefer finer sediment since they can bore them (Armitage and Cannan, 2000; Jones et al., 2012). Some species, such as Oligochaeta, improve under the effect of colmation and thus biodiversity is affected (Maridet and Philippe, 1995; Bo et al., 2007). Also, some species such as Bivalve molluscs and Cladocera are able to reject unwanted particles from their gills and filter combs (Macisaac and Rocha, 1995; Jones et al., 2012), while the other like Blackfly and Caddis fly larvae are more sensitive to receiving particles (Armitage and Blackburn, 2001; Jones et al., 2012). These examples show that colmation alters the competition between species as some species can adopt (e.g. through bioturbation) or thrive in the altered condition. Thus, it dangers the community structure in the river bed and HZ (Statzner and Sagnes, 2008; Jones et al., 2012).

In the rivers, where instream vegetation (e.g. macrophytes) is present, reciprocal relationship of colmation and vegetation is important. In the presence of a patch of macrophyte stands the current velocity reduces (Wharton et al., 2006; Warren et al., 2009). The current velocity reduction promotes fine sediment deposition, accumulation and colmation layer progress (Wood and Armitage, 1999; Clarke and Wharton, 2001). However, there are some evidence that fine sediment deposition is higher in the absence of instream vegetation (Warren et al., 2009). On the other hand colmation affects instream vegetation spatial distribution by covering river bed roughness and disrupting subsurface nutrient concentration and subsurface water movement (Eglin et al., 1997; Boulton et al., 1998).

A suitable connection between surface and subsurface water is not only important for hyporheos and benthos, but also is vital because of its effects on riparian area (Stromberg and Tiller, 1996; Brunke and Gonser, 1997; Webb and Leake, 2006) . In the area where infiltration is important for feeding of ground water, the colmation induces lower ground water level (Kondolf and Mathews, 1991 ;

Brunke and Gonser, 1997). The low ground water disturbs riparian vegetation which is an important area for biodiversity and productivity at the plant patch scale and at the reach scale (Webb and Leake, 2006). Colmation can change a perennial river to an ephemeral river (Webb and Leake, 2006) and can lead to lowering of ground water level in the riparian zone and floodplain. This can have detrimental effects on the riparian vegetation (Stromberg and Tiller, 1996; Webb and Leake, 2006) and such losses can have further impacts on other biota in the riparian zone (Lambs, 2004; Webb and Leake, 2006).

1.2.2 Hydrological and Hydraulic Effects

Ground water flow is a stable flow which holds a variety of useful inorganic compounds for hyporheic and surface organisms. Flow in the HZ moves in three different directions: exfiltration (up-welling movement of subsurface flow), infiltration (down-welling movement of surface flow) and vertical advection (streamwise water movement) (Brunke, 1998). Exfiltration brings nutrients for micro and macro organism, while infiltration brings dissolved oxygen and organic substances for these communities (Boulton et al., 1998). Hyperhoic exchanges are responsible of the mixing, transport, redox conditions, moderating habitat life condition in the riverbed and spatio-temporal patterns of dissolved oxygen, nutrients and contaminants (Krause et al., 2009). The associated physico-chemical gradient is important for invertebrate communities, salmonid habitat and plant distribution (Pretty et al., 2006; Wharton et al., 2006; Warren et al., 2009; Sternecker et al., 2013). The rate of this exchange depends on the hydraulic conductivity which is a function of bed morphology and bed materials size (Pretty et al., 2006). Coarser gravel has a greater hydraulic conductivity and so the exchange rate is high, but the addition of finer material decreases conductivity (Brunke, 1998; Boulton et al., 1998). The progressive deposition of finer materials disturbs surface-subsurface fluxes, excludes river bed organisms from up-welling nutrients and down-welling oxygen and alters the community of organisms (Pretty et al., 2006; Statzner and Sagnes, 2008; Mueller et al., 2013).

Oxic processes such as respiration and nitrification reduces when dissolved oxygen reduces and bacterial activities intensify in clogged area and anoxic processes such as denitrification, fermentation become prevalent (Boulton et al., 1998; Pretty et al., 2006; Dong et al., 2009; Nogaro et al., 2006). Lefebvre et al. (2004) observed nitrate concentration reduction and ammonium concentrations increment in fine sediments deposited rural streams. Fine sediment deposition, enlarge the surface area colonisable by bacteria and stimulates growth of biofilm and heterotrophic microbial processes (Boulton et al., 1998; Nogaro et al., 2010). Also, nitrate dominant conditions increase the reproduction of nitrate reducing bacteria (Mueller et al., 2013) which accelerates the process of biological colmation.

Ground water is also important for regulating river temperature (Brunke and Gonser, 1997; Krause et al., 2011). Up-welling ground water flux injects the cooler water to the river in summer and warmer water in winter and moderates the surface water temperature. Also, hyporheic flow in daytime cool down 25% of the heat associated with net radiation (Webb et al., 2008). Appropriate temperature is key feature for benthic and hyporhic habitat condition (Lambs, 2004; Webb et al., 2008). Water temperature is important for fish spawning and incubation, invertebrate development and microbial activity in HZ (Brunke and Gonser, 1997; Burkholder et al., 2008). Acornley (1999) reported hatching and alevin emergence of brown trout eggs in chalk stream spanning bed is earlier than predicted time by stream temperature as a result of warmer intragravel temperature comparing to stream temperature. colmation weakens the intragravel temperature gradient and produces more uniform spatial thermal distribution comparing to natural condition. In addition, the water temperature is important for water viscosity and density and so the hydraulic conductivity and water stratification affects surface and subsurfece exchanges (Brunke and Gonser, 1997).

Moreover, entry of pollutant such as fertilizers, pesticides and agricultural wastes to the rivers increases the organic materials in the river which reduces the diversity of river bed species (Grabowski et al., 2011; Von Bertrab et al., 2013). Colmation faced with pollution can be harmful or useful. It behaves as barrier for pollutant to enter ground water, while it forces pollutant to store in the river bed (Velickovic, 2005). Also, the ingredients of sediment load are important in colmation

process by their effects on organism and increasing the fine particulate organic matter (Warren et al., 2009; Scheurer et al., 2009).

Although colmation layer mostly causes negative effects, in some situations it can be helpful in protecting the ground water environments against containments and enhancing process of bank filtration. The surface flow bears significant amount of pollutants since agricultural activities perform near banks of rivers and they produce lots of nitrate (Doussan et al., 1997). The colmated layer behaves as a barrier which prevents passing of the containment (Brunke and Gonser, 1997). Colmation can also improve purification by bank filtration processes by reducing the hydraulic conductivity and increasing resistance time (Doussan et al., 1997; Brunke and Gonser, 1997; Hiscock and Grischek, 2002). There is mutual interaction of colmation and near gravel bed turbulent flow characteristics. Colmation reduces effective roughness and increases velocity near bed (Sambrook Smith and Nicholas, 2005). Besides, it reduces shear stress and increases turbulent fluxes which increase the mobility of fine sediment comparing to coarser materials (Sambrook Smith and Nicholas, 2005). The presence of fine particle disarranges balance between near bed sediment concentration and entrainment rate which is common in gravel bed and in equilibrium condition (Grams and Wilcock, 2007). Wren et al. (2011) studied the process of clomation and observed changes in shear stress, turbulent fluxes similar to Smith and Nicholas (2005). Pellachini (2011) developed a theoretical framework for sand transport in gravel bed by considering level of the sand presence. Pellachini (2011) showed that in mixed sand-gravel systems, shear velocity can be scaled with the bed elevations distribution function. Recently, Kuhnle et al. (2013) showed that sand transport rate is related to bed shear stress which is scaled with the cumulative probability distribution function of the gravel bed elevations.

Despite the fact that fine sediment deposition and infiltration to lower levels has been widely studied (Schalchi, 1992; Geldner, 1982), many engineering aspects of colmation have not been addressed so far. Indeed, while the effect of colmation on near bed turbulent flow has been defined, the role of turbulent flow on external colmation has not highlighted. In present thesis, we focus on turbulent structure of near gravel bed flow in order to enhance our knowledge on external colmation. In the

following paragraphs, state of the art of gravel bed flow and transport of fine sediment respect to turbulence are reviewed.

1.3 FLOW AND TRANSPORT PROCESS IN GRAVEL BED

1.3.1 Gravel Bed Flow

Study of flow over rough beds has been advanced over the past years due to interest for possible applications in broad range of various disciplines (Jimenez, 2004; Nezu and Nakagawa, 1993). For example, gravel beds are widely studied in environmental and hydraulic engineering where protrusions induce significant spatial heterogeneities at near bed region of flow field, which is known as roughness layer (Nikora et al., 2001; Buffin-Bélanger et al., 2006).

Nowadays, spatially averaged Navier-Stokes equations, called double averaging (DA) equations in hydraulic sciences, are widely used to study rough bed heterogeneous flows (Finnigan, 2000; Nikora et al., 2001; Nikora et al., 2007a). Double averaging induces loss of information on the local variation of flow variables, but some hydraulic concepts such as flow uniformity, two dimensionality and bed shear stress are more properly defined. Moreover, spatially averaged viscous drag, form drag and additional terms due to spatial heterogeneity, known as form induced (or dispersive) stresses, appear explicitly in the double averaged equations (Nikora & Rowinsky, 2008). In this way, double averaged flow variables and bed shear stress are coupled consistently with spatially averaged roughness parameters.

Concerning open channel gravel bed flows, Nikora et al. (2007b) introduced four regimes of flow as a function of relative submergence (H/Δ where H is water depth and Δ is the roughness scale). As shown in Figure 1, Flow Type (I) is the high relative submergence ($H/\Delta > 40$), Flow Type (II) is intermediate relative submergence ($5 < H/\Delta < 40$) where water depth is shallow with respect to rough element scale, Flow Type (III) is low relative submergence ($1 < H/\Delta < 5$) and, lastly, partially inundated flow ($H/\Delta < 1$) is Flow Type (IV) (Nikora, 2007; Nikora et al., 2007b). Other expressions like *depth-limited flows* (Buffin-Bélanger and Roy, 1998; Hardy et al., 2007; Hardy et al., 2009; Hardy et al., 2010), *small relative submergence* (Manes et al., 2007) and *shallows streams* (Katul et al., 2002) are

referred to conditions where both low submergence and intermediate submergence are considered.

Generally shallow streams are quite common in the nature, with Relative Submergence (RS) values less than 5 (Hardy et al., 2007; Hardy et al., 2010). Therefore, in many studies there have been efforts to describe behavior of shallow flows. Buffin-Bélanger and Roy (1998) found that flow field around pebble clusters shows spatial heterogeneities. Manes et al. (2007) by applying double averaged method, observed that flow statistics do not change with relative submergence except for the form-induced stress. Aberle et al. (2008) found that form induced stresses are small at greater distance from the bed and increase slightly toward gravel crests. Also Recently, Cooper et al. (2013) studied the role of submergence ratio on spatial flow variations. They showed that the effect of relative submergence is more notable in streamwise than in the normalwise direction.

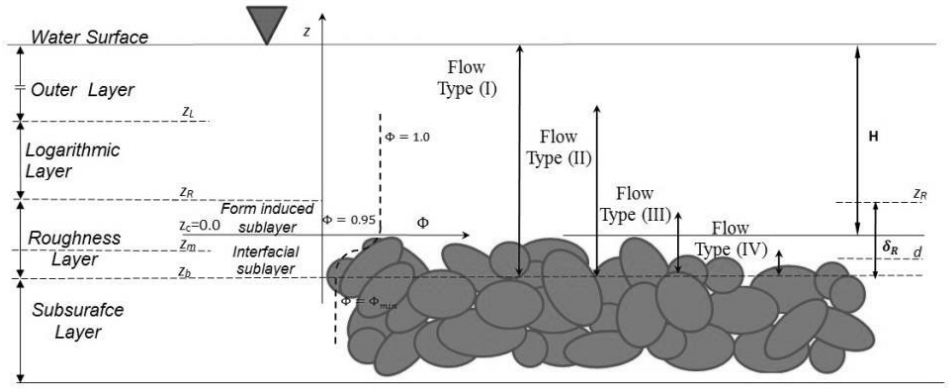

Figure 1-3: Subdivision of free surface boundary layer to sub layers (Nikora et al., 2001).

In the inner region of flow type (I), logarithmic law is valid (Nikora et al., 2001; Jimenez, 2004), however, new findings in wall-bounded turbulent flows do not support the idea of universal log-law even in smooth wall conditions (George, 2007; Smits et al., 2011; Marusic et al., 2010). As far as smooth bed flows are considered, the viscous influence in velocity profile extends considerably further from the bed rather than previously expected and log-law parameters change by flow conditions (Marusic et al., 2010; Smits et al., 2011). On the other side, in rough bed Flow Type (II), it has been observed that the shape of double averaged velocity profile is still

logarithmic (Bayazit, 1976; Koll, 2006; Nikora, 2007), but von Kàrmàn constant, zero-plane displacement position and log-law bounds can vary based on flow condition and bed geometry (Koll, 2006; Nikora, 2007; Gaudio et al., 2010). What makes velocity profile in Flow Type (II) more complicated is that zero-plane displacement should be determined together with bounds of logarithmic region and values of log-law parameters. The process of estimating zero-plane displacement position, log-law bounds and parameters in Flow Type (II) is a substantial challenge which has not yet addressed appropriately.

Despite abundance of studies in Flow Type (II), there are only a limited number of studies concerning spatial organization of near bed velocity field for such type of flow, with also contradictory results. Dancey et al. (2000) studied variation of vertical component of velocity above closely packed spheres of the same diameter. They found strong vertical downward motion with upward fluctuating fluid motions. Buffin-Bélanger et al. (2006) reported spatial organization of both time averaged velocity and turbulence kinetic energy in near bed region related to local bed micro-topography. These findings are confirmed also by analogous experiments of Lamarre and Roy (2005). However, sampling spacing in both the studies were too coarse for accurate analysis of possible consistent dependency of flow spatial organization on bed properties at finer scales. Moreover, Mclean and Nikora (2006) found significant correlation between both streamwise and normalwise form induced velocity components ($\tilde{u}$, $\tilde{w}$) and bed topography in gravel bed. In contrast, Cooper and Tait (2008) did not observe any significant correlation between near bed flow and bed topography. Instead, they highlighted presence of alternating high and low time averaged velocity strips at the bed, with width changing with relative submergence. They argued that the observed strips cannot be ascribed to secondary current cells, given the high aspect ratio B/H (where B is channel width) in the experiments. Generally, secondary currents are important in narrow channels where $B/H < 5$ (Nezu and Nakagawa, 1993). However, they have been observed also in rough bed channels with higher aspect ratios (Nikora et al., 1998b; Rodríguez and García, 2008; Albayrak and Lemmin, 2011). Presence of secondary current in wide gravel bed open channel deserve to be deeper studied, considering not only streamwise time-averaged

velocity, but also normal and spanwise time-averaged velocities and higher order velocity moments.

In summary, there is still a lack of systematic information on gravel bed flow at intermediate relative submergence conditions. The relation between bed topography, mean flow and turbulence characteristics in near bed regions has not clarified properly. Also, it is not clear how the effects of bed topography and presence of secondary current cells combine together at different relative submergence.

1.3.2 Fine Sediment Transport in Gravel Bed

Transport of fine sediment in a free surface flow is triggered by near-bed turbulence (Bagnold, 1966; Sutherland, 1967; Nino and Garcia, 1996; Papanicolaou et al., 2001). The interaction between particles and bed turbulence influences the diffusion and transport processes of suspended sediment in the outer part of the flow field. Different studies of the turbulent flow structure have recognized the importance of the near bed bursting-sweep cycle for particles entrainment and transport. Bursting is a phenomenon common in turbulent boundary layer and open channels. It gives evidence of the turbulent coherent structures that develop in the near bed region of the flow field. It is composed of quasi-cyclic process of upward motion of low-velocity fluid parcels (ejection) and downward motion of high-velocity parcels (sweep) (Nezu and Nakagawa, 1993), which is associated with short-duration large-amplitude wall pressure fluctuations (Thomas and Bull, 1983; Snarski and Lueptow, 1995).

Recent developments in research suggest the conception of a turbulent burst being a succession of ejections due to the passage of a packet of hairpin vortices, the smallest hairpin creating the strongest ejection velocity (Adrian et al., 2000b). The bursting process in the near-wall region, interacts with outer layer-large scale coherent structure (Adrian et al., 2000b; Shvidchenko and Pender, 2001; Tamburrino and Gulliver, 2007) and is considered to play an important role in the overall dynamics of the boundary layer and to sediment transport processes. Ejections are considered mainly responsible for particles entrainment and

resuspension (Bagnold, 1966; Grass, 1971; Wei and Willmarth, 1991; Nelson et al., 1995; Bennett et al., 1998; Righetti and Romano, 2004; Singh et al., 2007). A significant bed load transport is also attributed to sweeps impinging on the bed (Drake et al., 1988; Sterk et al., 1998; Detert et al., 2010).

There is experimental evidence that the main features of bursting phenomena are common on both smooth and rough beds (Grass, 1971; Shvidchenko and Pender, 2001; Singh et al., 2007). On the other hand, there are fundamental differences between the two classes of bed. In smooth wall conditions, bursting is related to flow instabilities taking place in the alternating high and low velocity streaks belonging to the viscous sublayer, while for rough bed, roughness elements protrusion disrupt viscous sublayer and buffer layer and bursting seems to be triggered by the wake-like vortex shedding at roughness crests (Bandyopadhyay and Watson, 1988; Bomminayuni and Stoesser, 2011; Guala et al., 2012). Moreover, these features of the bursting phenomena on a gravel bed flow are accompanied by the experimental evidence that for this kind of flow the time averaged velocity field and higher order turbulence moments at the near bed region (the roughness layer, sensu Nikora et al. (2001)) vary spatially in accordance with bed topography (Buffin-Bélanger et al., 2006; Mclean and Nikora, 2006).

As mentioned above, to consider spatial variation of turbulent flow characteristics double averaged equations are developed. Despite prevailing usage of double averaging method in study of gravel bed flow, vertical momentum transport in gravel bed flow has not been examined in detail by applying the double averaging method. In this condition, form induced stresses in DANS equations cause momentum flux in addition to Reynolds stresses (Pokrajac et al., 2007). The role of form induced stresses in vertical momentum flux (i.e. sediment transport) has not been the focus of previous works. Therefore, vertical momentum in gravel bed flow needs to be examined through development of a theoretical frame work.

1.4 RESEARCH OBJECTIVES AND THESIS OVERVIEW

Following information reported in the previous sections (Gravel Bed Flow, page 28 and Fine Sediment Transport in Gravel Bed, page 31), in the present study,

hydrodynamics of gravel bed flow in the intermediate relative submergence conditions is studied in the context of sediment transport. Two series of Particle Image Velocimetry (PIV) data in both horizontal layer and vertical planes are coupled with bed topography measurements to assemble a detailed description of near bed flow in comparison to gravel bed statistical properties. Also, the spatial variability of the turbulence structure at the near bed region and along water depth is analyzed in the context of fine sediment transport. Specifically, the main objectives of the this research are:

1) To study the flow field features with particular attention to the near bed region in Flow Type (II).

2) To address the relationship between near bed flow structure and bed topography.

3) To describe process of fine sediment transport in gravel with respect to turbulent flow characteristics.

The present thesis is organized in eight chapters. Information reported in these chapters are as follow:

- The present chapter (*Colmation in Gravel Bed Rivers*) is an introduction for the rest of the thesis. Also, state of the art of colmation is explained in this chapter.
- The governing equations and mathematical description of the methods used for analysis of the data are explained in *Theoretical Background* (Chapter 2).
- The laboratory set-up and measurements arrangement are described in *Methodology* (Chapter 3).
- *Gravel Bed Characteristics* (Chapter 4) is about all information related to description of bed properties. These properties are classified as statistical characteristics of bed materials and also their spatial organization.
- General results related to the turbulent flow characteristics are reported in *Characteristics of Turbulent Flow* (Chapter 5).
- *Sediment Transport* (Chapter 6) is complementary to Chapter 5. In this chapter, vertical component of velocity is analyzed. Also, spatial variation of near bed flow is studies in accordance with bursting process.

- In Chapter 7 (*Discussion*), results which are reported in Chapter 4 to 6 are discussed and implemented in predicting initiation of external colmation (entry of fine sediment in matrix of gravels).
- In Chapter 8 (*Conclusions*) a summary of the present thesis findings is reported. Also, recommendations and open questions for future works are proposed in the last part of this Chapter.

2 Theoretical Background

Abstract:

In this chapter theoretical aspect of gravel bed flow is described. At first, governing equations of turbulent gravel bed flows in the double averaging frame work are introduced. Then, turbulent flow in the context of sediment transport is considered. To this end, statistical characteristics of vertical velocity (especially asymmetry of vertical velocity) should be examined. The available method for analysis of vertical velocity is presented. Moreover, it is useful to compare statistical characteristics of vertical velocity with bursting process. Quadrant analysis which is a detecting method for bursting process is also explained in this chapter.

2.1 GOVERNING EQUATIONS OF GRAVEL BED FLOWS

In order to consider turbulence in motion of Newtonian fluid (i.e. fluids that their viscous stress and strain rate are related by a constant viscosity) like water, Navier-Stokes equations are averaged in time. These equations are famous as Reynolds Averaged Navier-Stokes (RANS) equations (Pope, 2000). As width of open channels or rivers is generally wide, it is common to simplify RANS equations with two dimensional flow assumption (Nezu and Nakagawa, 1993). Also, in straight open channels and rivers, it is assumed that flow does not change in streamwise direction (uniformity assumption). However, in the conditions like gravel bed or vegetated flows, where protrusion of obstacles is significant, near bed flow is heterogeneous. Therefore, both 2D flow assumption and uniformity can be questionable.

In order to apply 2D flow and uniformity assumptions to rough bed flows, time averaged equations of motion should be supplemented by averaging in space. The spatial-averaging methodology initiated from multiphase and porous media hydrodynamics (Whitaker, 1999) and it has been developed since the 1960s (Nikora et al., 2007a). In the 1970s, a spatial averaging approach was introduced in the aerodynamics of canopy flows where it was used to smooth time-averaged hydrodynamic fields (Nikora et al., 2007a). The development of this technique was primarily conducted by atmospheric flow scientists for describing and predicting turbulent flows within and above terrestrial canopies such as forests or bushes (Raupach and Shaw, 1982; Finnigan, 2000). Spatial averaging (known as Double Averaging Method (DAM) in hydraulic sciences) in the river engineering and environmental fluid mechanics has been used extensively due to heterogeneous nature of flow in near boundaries (Nikora et al., 2007b; Nikora and Rowiński, 2008). The general form of double averaged Navier-Stokes (DANS) equations are as follow (Nikora et al., 2007a):

$$\frac{\partial\langle\bar{u}_i\rangle}{\partial t}+\langle\bar{u}_j\rangle\frac{\partial\langle\bar{u}_i\rangle}{\partial x_j}=g_i-\frac{1}{\rho}\frac{\partial\langle\bar{p}\rangle}{\partial x_j}-\frac{1}{\Phi}\frac{\partial\Phi\langle\tilde{u}_i\tilde{u}_j\rangle}{\partial x_j}-\frac{1}{\Phi}\frac{\partial\Phi\langle\overline{u'_j u'_i}\rangle}{\partial x_j}+\frac{1}{\Phi}\nu\nabla^2\Phi\langle\bar{u}_i\rangle+\frac{1}{\rho}\frac{1}{V_f\Phi}\iint_{S_{int}}pn_i dS-\frac{1}{V_f\Phi}\iint_{S_{int}}\left(\nu\frac{\partial\bar{u}_i}{\partial x_j}\right)n_j dS \quad (2\text{-}1)$$

In this equation, the overbar denotes time/ensemble average, the angle brackets denotes space average, fluctuations from time and space averaged values are respectively shown by prime and tilde. Also, u_i is velocity in three different directions, p is pressure ,g_i is gravitational acceleration, ρ is fluid density, Φ is roughness geometry function and ν is viscosity. The last two terms in this equation are representative of pressure and viscous drags. Note that the Eq. (2-1) is written in Einstein summation form.

In steady, uniform rough bed open channel flow, for 2D equations, the following simplifying assumptions are applied: 1) $\partial\langle\,\bar{}\,\rangle/\partial x = 0$; 2) $\partial/\partial t = 0$; and 3) $\langle\overline{w}\rangle = 0$. In such a condition, the double averaged equation in the vertical direction reduces to (Nikora et al., 2001):

$$-g\cos\theta - {}^{1}\!/_{\rho}\frac{1}{\Phi}\frac{\partial\Phi\langle\bar{p}\rangle}{\partial z} + \frac{1}{\Phi}\frac{\partial\Phi\,\langle-\overline{w'^2}\rangle}{\partial z} + \frac{1}{\Phi}\frac{\partial\Phi\langle-\tilde{w}^2\rangle}{\partial z} + \frac{1}{\Phi}\nu\nabla\Phi\nabla\langle\overline{w}\rangle = 0 \tag{2-2}$$

where θ is the angle between the bed and the horizontal line. Bear in mind that in vertical direction, drag forces (two last terms in Eq. (2-1)) are also negligible.

By neglecting the effect of viscosity ($\nu\nabla\Phi\nabla\langle\overline{w}\rangle \approx 0.0$), this equation after integration along water depth leads to:

$$\langle\bar{p}\rangle = \rho(H-z)\cos\theta - \rho\,\langle\overline{w'^2}\rangle - \rho\langle\tilde{w}^2\rangle - \int_{z}^{z_c}\left[\frac{1}{\Phi}\frac{\partial\Phi}{\partial z}\left(\rho\,\langle\overline{w'^2}\rangle + \rho\langle\tilde{w}^2\rangle + \langle\bar{p}\rangle\right)\right]dz \tag{2-3}$$

In Eq.(2-3), $\rho(H-z)\cos\theta$ is static pressure, $-\rho\,\langle\overline{w'^2}\rangle$ and $-\rho\langle\tilde{w}^2\rangle$ are double averaged vertical Reynolds stress and vertical form-induced stress, respectively. The last term in Eq.(2-3) is the results of vertical variation of the roughness geometry function. This term is equal to zero above the gravel crests. Double averaged vertical Reynolds stress is turbulent momentum flux and the vertical form-induced stress is the transfer of local momentum caused by spatial disturbances in time-averaged flow (Pokrajac et al., 2007; Nikora et al., 2001).

This equation shows that, above the gravel crests, double averaged pressure ($\langle\bar{p}\rangle$) is composed of static pressure ($\rho(H-z)cos\theta$) and a form of dynamic pressure ($-\rho\,\langle\overline{w'^2}\rangle + -\rho\langle\tilde{w}^2\rangle$) caused by turbulence and bed geometry. Below the gravel crests, variation of bed geometry due to the presence of gravels ($\partial\Phi/\partial z$) contributes an additional term which makes understanding of the relationship between double averaged pressure and turbulent flow characteristics more complicated. Nevertheless, the terms in the Eq.(2-3) show that among all turbulent fluctuation components only vertical components ($-\rho\,\langle\overline{w'^2}\rangle$ and $-\rho\langle\tilde{w}^2\rangle$) are important for vertical momentum transport. Also, Bagnold (1966) highlighted the importance of the vertical velocity component in sediment transport in the vertical direction. He stated that the asymmetric probability density of vertical velocity causes net vertical momentum flux which keeps particles in suspension despite the influence of gravity.

2.2 ANALYSIS OF VERTICAL VELOCITY

Following Bagnold (1966) hypothesis, it has been attempted to study sediment transport in association with vertical velocity (Leeder, 1983; Wei and Willmarth, 1989). They generally correlate transport of fine sediments to asymmetry of vertical velocity component. Wei and Willmarth (1991) proposed a method to study statistical characteristics of the vertical velocity.

In this method, as shown in Figure 2-1, the intervals of positive vertical velocity (Δt_+) are separated from the interval of negative vertical velocity (Δt_-). Accordingly, the total duration of measurement (T) is divided to total duration of positive vertical velocity (T_+) and negative vertical velocity (T_-) i.e. $T = T_+ + T_-$. In this case, the time averaged vertical velocity can be expressed as (Wei and Willmarth, 1991):

$$\bar{w} = \frac{1}{T}\left(\bar{w}_+ T_+ + T_-\,\bar{w}_-\right) \qquad (2\text{-}4)$$

where positive and negative vertical velocities are defined as ($\bar{w}_+, \bar{w}_-$):

$$\bar{w}_+ = \frac{1}{T_+}\sum w_+^i \Delta t_+^i \qquad (2\text{-}5)$$

$$\overline{\mathrm{w}}_{-} = \frac{1}{\mathrm{T}_{-}} \sum w_{-}^{i} \Delta t_{-}^{i} \qquad (2\text{-}6)$$

and w_{-}^{i} and w_{+}^{i} are instantaneous values of velocity that are negative and positive, respectively.

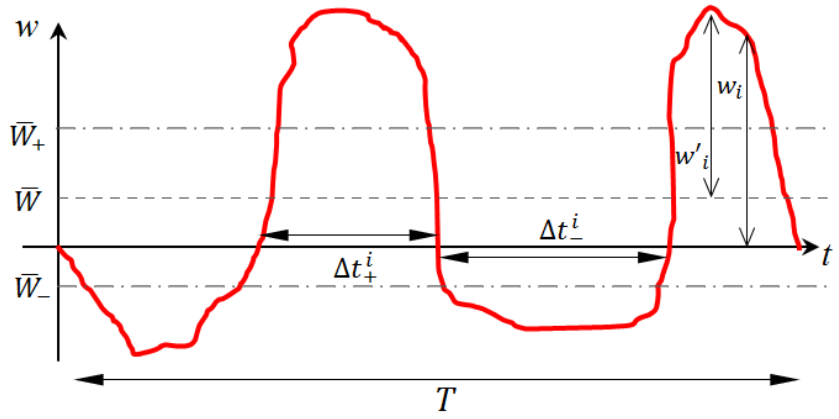

Figure 2-1: Schematic view of vertical velocity signal with Wei and Willmarth (1991)'s parameters.

The difference between the absolute values of $\overline{\mathrm{w}}_{+}$ and $\overline{\mathrm{w}}_{-}$ shows asymmetry of vertical velocity in time. Like vertical velocity, upward and downward turbulent vertical momentum fluxes can also be defined as (Wei and Willmarth, 1991) :

$$\overline{\mathrm{w'^2}}_{+} = \frac{1}{\mathrm{T}_{+}} \sum {w'^2_{+}}^{i} \Delta t_{+}^{i} \qquad (2\text{-}7)$$

$$\overline{\mathrm{w'^2}}_{-} = \frac{1}{\mathrm{T}_{-}} \sum {w'^2_{-}}^{i} \Delta t_{-}^{i} \qquad (2\text{-}8)$$

where $\overline{\mathrm{w'^2}}_{+}$ and $\overline{\mathrm{w'^2}}_{-}$ are respectively upward and downward turbulent momentum fluxes. Thus, net momentum flux (upward turbulent momentum flux minus downward turbulent momentum flux) is expressed as (Wei and Willmarth, 1991):

$$\overline{\mathrm{w'^2}}^{\mathrm{NF}} = (\mathrm{T}_{+}\overline{\mathrm{w'^2}}_{+} - \mathrm{T}_{-}\overline{\mathrm{w'^2}}_{-})/\mathrm{T} \qquad (2\text{-}9)$$

Note that in the present study $\overline{w'^2}^{NF}$ is the net momentum flux due to the turbulence. In other words, as shown in Figure 2-1, the effect of mean vertical velocity ($\overline{w}$) was subtracted before estimation of momentum flux.

Previous studies show that vertical velocity and momentum similar to other turbulent flow properties are heterogeneous near rough bed (Dancey et al., 2000; Buffin-Bélanger et al., 2006; Manes et al., 2007). In such condition, positive and negative vertical velocity and momentum fluxes must also be averaged spatially. Besides, in this condition spatial variation of time-averaged vertical velocity induces additional momentum flux which is considerable in the near bed region (Nikora et al., 2007a).

To study this additional momentum flux, the method of Wei and Willmarth (1991) should be applied to the spatial vertical velocity fluctuations. For this purpose, as shown in Figure 2-2, spaces with positive contributions to $\overline{w}$ (a_+^i) should be distinguished from spaces with negative contributions (a_-^i).

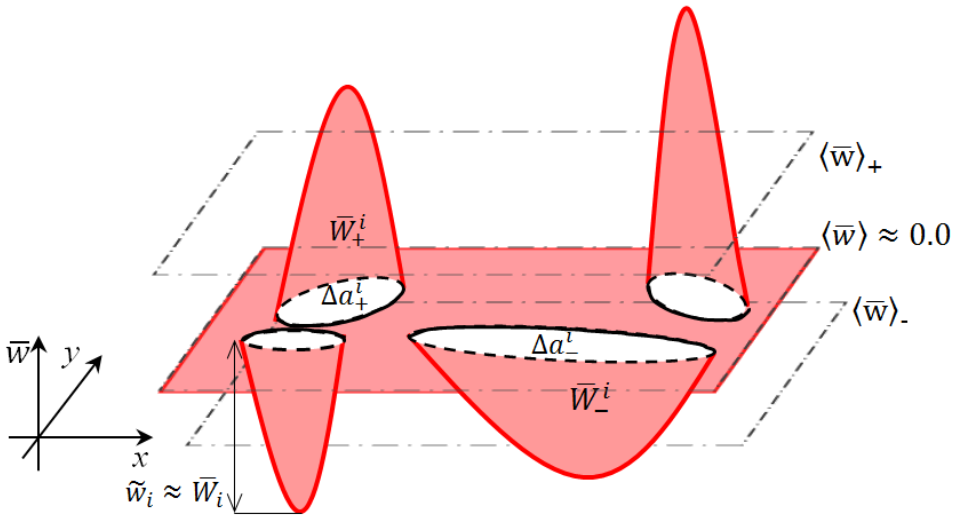

Figure 2-2: Schematic view of spatial mean vertical velocity distribution with parameters used in extended Wei and Willmarth (1991)'s method in present study.

So, total measurement area (A) is divided into the area with positive vertical velocity (A_+) and the area with negative vertical velocity (A_-) i.e. $A = A_+ + A_-$. In

this case, double averaged positive and negative vertical velocities are defined as $(\langle\overline{\mathrm{w}}\rangle_+, \langle\overline{\mathrm{w}}\rangle_-)$:

$$\langle\overline{\mathrm{w}}\rangle_+ = \frac{1}{\mathrm{A}_+}\sum \overline{w}_+^i \mathrm{a}_+^i \tag{2-10}$$

$$\langle\overline{\mathrm{w}}\rangle_- = \frac{1}{\mathrm{A}_-}\sum \overline{w}_-^i \mathrm{a}_-^i \tag{2-11}$$

where $\overline{\mathrm{w}}_-^{\mathrm{i}}$ and $\overline{\mathrm{w}}_+^{\mathrm{i}}$ are time-averaged values of velocity that are negative and positive, respectively. In this case, the difference between $|\langle\overline{\mathrm{w}}\rangle^+|$ and $|\langle\overline{\mathrm{w}}\rangle^-|$ shows asymmetry of vertical velocity fluctuations in space.

Also, turbulent upward and downward momentum fluxes can be supported by double averaging. The double averaged turbulent upward and downward momentum fluxes $(\langle\overline{\mathrm{w}}^2\rangle_+, \langle\overline{\mathrm{w}}^2\rangle_-)$ are defined as:

$$\langle\overline{\mathrm{w}}^2\rangle_+ = \frac{1}{\mathrm{A}}\sum \overline{\mathrm{w'^2}}_+^{\,i} \tag{2-12}$$

$$\langle\overline{\mathrm{w}}^2\rangle_- = \frac{1}{\mathrm{A}}\sum \overline{\mathrm{w'^2}}_-^{\,i} \tag{2-13}$$

As shown in Eq. (2-3), double averaged turbulent vertical momentum flux $(\langle\overline{w'^2}\rangle)$ and double averaged vertical form induced momentum flux $(\langle\tilde{\mathrm{w}}^2\rangle)$ are important for the transport in vertical direction. The results obtained from Eq. (2-12) and Eq. (2-13) show what percentage of the double averaged turbulent momentum flux is in upward and downward directions. Similar analysis can be also applied to double averaged vertical form induced momentum flux. Positive and negative vertical form-induced momentum fluxes are also defined as:

$$\langle\widetilde{w}_i^2\rangle_+ = \frac{1}{\mathrm{A}_+}\sum \widetilde{w}_+^{2\,i} \mathrm{a}_+^i \tag{2-14}$$

$$\langle\widetilde{w}_i^2\rangle_- = \frac{1}{\mathrm{A}_-}\sum \widetilde{w}_-^{2\,i} \mathrm{a}_-^i \tag{2-15}$$

where $\widetilde{w}$ is velocity fluctuation respect to double averaged vertical velocity ($\langle\overline{w}\rangle$). We should note that in theory, in order to satisfy continuity, double averaged vertical velocity should be zero ($\langle\overline{w}\rangle \approx 0.0$) and there is not significant difference between form induced vertical velocity and time averaged vertical velocity ($\overline{W} \approx \widetilde{w}$).

In analogy to what is explained for net momentum flux due to vertical velocity fluctuations in time, net momentum flux (upward flux minus downward flux) due to spatial variation is expressed as:

$$\langle\widetilde{w}^2\rangle^{NF} = (\mathrm{A}_+\langle\widetilde{w}^2\rangle_+ - \mathrm{A}_-\langle\widetilde{w}^2\rangle_-)/A \tag{2-16}$$

Finally, to estimate total net vertical momentum flux, net vertical momentum flux due to spatial fluctuations ($\langle\widetilde{w}^2\rangle^{NF}$) should be accumulated with double averaged of net vertical momentum flux due to time fluctuations $\langle\overline{\mathrm{w}'^2}^{\mathrm{NF}}\rangle$ which can be expressed as:

$$\langle\widetilde{w}^2\rangle^{NF} = \frac{1}{A}\sum \overline{w'^2}^{NF^i} \tag{2-17}$$

So, total net vertical momentum flux (TNWF) will be:

$$\mathrm{TNWF} = \langle\overline{\mathrm{w}'^2}^{\mathrm{NF}}\rangle + \langle\widetilde{w}^2\rangle^{NF} \tag{2-18}$$

2.3 BURSTING PROCESS DETECTING METHOD

Previous studies have shown that upward momentum flux is related to bursting process (Kline et al., 1967; Grass, 1971; Wei and Willmarth, 1991). To study the cause of asymmetrical behavior of vertical velocity component, it is useful to compare statistical properties of vertical velocity components with bursting process detecting methods (Wei and Willmarth, 1991). The bursting process is generally studied through quadrant analysis (after Lu and Willmarth (1973)). Quadrant analysis is a method based on the premise that correlation of u' and w' is related to bursting events (Nezu and Nakagawa, 1993). Based on quadrant analysis, upward motion of low velocity ($\mathrm{u}' < 0,\ \mathrm{w}' > 0$), known as ejection, is the second

quadrant (Q_2) and downward motion of high velocity ($u' > 0$, $w' < 0$), known as sweep, is the fourth quadrant (Q_4) (Lu and Willmarth, 1973; Nezu and Nakagawa, 1993). First and third quadrants (Q_1, Q_3) are outward and inward interactions, respectively (Nezu and Nakagawa, 1993).

Generally, in quadrant analysis only intense fluctuations should be considered. Indeed, small fluctuations cancel each other out and are not important in the flux process (Narasimha et al., 2007). To eliminate small instantaneous fluctuations, it is assumed that intense instantaneous fluctuations should be greater than one of the specific characteristics of the flow. As first approximation, this statistical threshold was a portion of Reynolds shear stress ($\chi\overline{u'w'}$, Where χ is a constant known as "*hole size*") (Willmarth and Lu, 1972). Later, Lu and Willmarth (1973) and Bogard and Tiederman (1986) compare instantaneous fluctuation ($u'(t)w'(t)$) with turbulence intensities in streamwise and vertical directions ($\chi\sigma_u\sigma_w$). Recently, Narasimha et al. (2007) suggested root mean square of instantaneous $u'(t)w'(t)$ fluctuations ($\chi\sigma_{u'w'}$) as the threshold. The fraction of fluctuations which is discarded in quadrant analysis is also depended on hole size (χ). In the present study, we used the Bogard and Tiederman (1986) threshold with hole size equal to 1.0 ($\chi = 1$). This threshold and hole size have been widely used in clear water open channel flows (Righetti and Romano, 2004; Hardy et al., 2009).

According to the quadrant analysis, the fractional contributions to the total Reynolds shear stress from each quadrant based on a constant hole size can be estimated by:

$$\overline{u'w'}_i = \lim_{T\to\infty} \frac{1}{T} \int_0^T u'(t)w'(t)\xi_i dt \tag{2-19}$$

where $\overline{u'w'}_i$ is the fractional contribution of quadrant i to total shear stress, T is total duration of the measurement and ξ_i is the detecting function defined as follow:

$$\xi_i = \begin{cases} 1.0 & u'(t)w'(t) > \sigma_u\sigma_w \; and \\ & located \; in \; i^{th} \; quadrant \\ 0.0 & elsewhere \end{cases} \tag{2-20}$$

Also, in the same manner, the fractional contribution of different events to the total vertical momentum flux can be estimated through quadrant analysis with the following equation:

$$\overline{w'^2}_i = \lim_{T\to\infty} \frac{1}{T} \int_0^T w'(t)^2 \xi_i dt \tag{2-21}$$

where $\overline{w'^2}_i$ is the fractional contribution of the quadrant i to the total vertical momentum flux.

3 Methodology

Abstract:

This chapter discuss laboratory experiments arrangement for the measurements of turbulent flow field and gravel bed characteristics. At first, general laboratory apparatus are introduced. After, fundamentals of particle image velocimetry are presented accompanying with characteristics of particle image velocimetry in the present study. Then, the instruments used in characterizing gravel bed are described. Finally, in the last part of this chapter measurement errors analysis is reported.

3.1 LABORATORY FACILITIES

The measurements were performed at the Hydraulic Engineering Laboratory at University of Trento. Experiments were conducted in a 0.4 m wide, up to 0.4 m deep, and 6 m long polymethylmethacrylate rectangular tilting open channel, shown in Figure 3-1. To achieve uniform flow conditions, an adjustable tailgate weir located at the end of the flume was used. Small surface waves at the entrance of the flume were eliminated with a polystyrene plate held parallel to the upper water surface just downstream of the intake. Also, a steel mesh at the entrance was used to help formation of uniform flow in shorter distance from entrance.

Free surface profiles were measured by an ultrasonic distance transducer. Also, each 50cm a plastic ruler was installed for controlling water depth. The discharge at the flume inlet was controlled by an inverter for pump speed regulation and the discharge was measured by an electromagnetic flowmeter.

The standard right-handed x, y, z coordinate system is defined as follows. The x-coordinate is oriented along the main flow positive downstream and parallel to the mean bed elevations. The z-coordinate refers to the vertical direction, pointing upward, crest of the bed materials, which will be introduced clearly in the next section, being the reference of the z-axis ($z_c = 0.0$). The y-axis is directed spanwise and is positive from right to left wall.

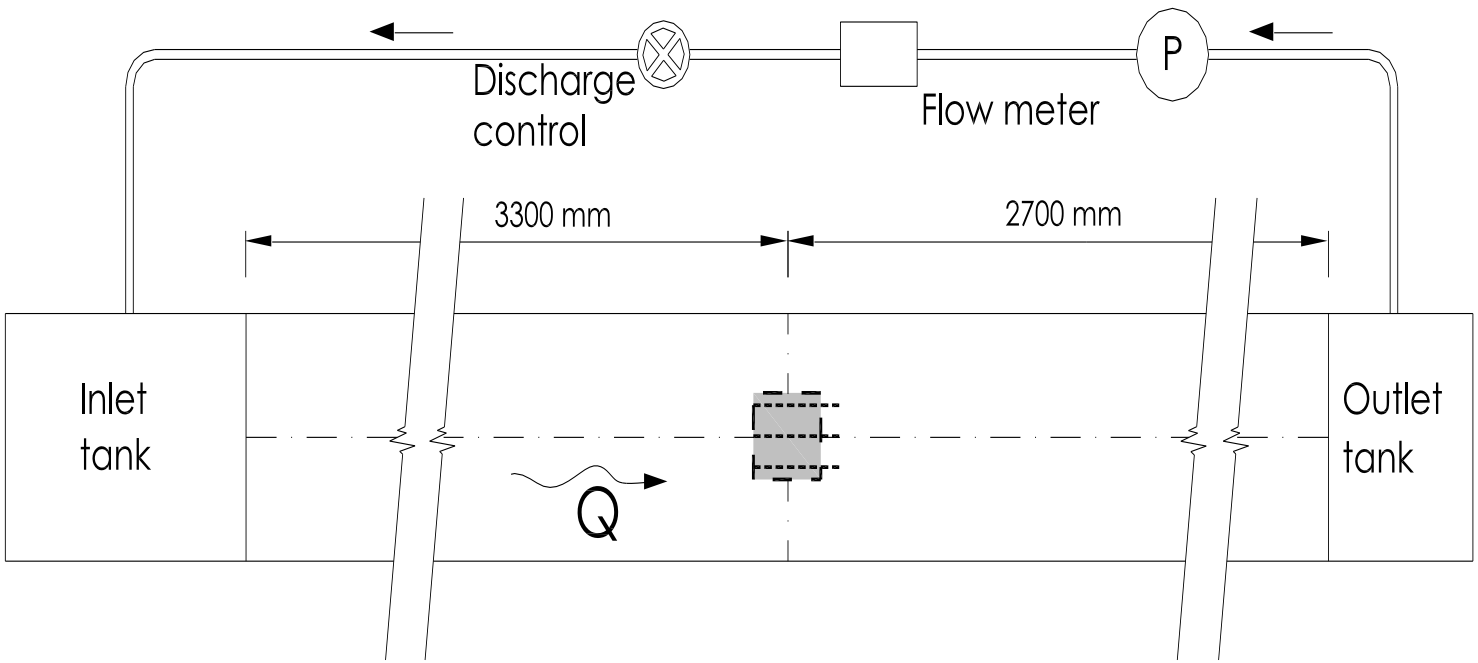

Figure 3-1: Sketch of the laboratory open channel.

3.2 PARTICLE IMAGE VELOCIMETRY

All flow field measurements were done by Particle Image velocimetry (PIV). Particle Image Velocimetery (PIV) is one of the most common measurement techniques in environmental hydrodynamics as well as fluid mechanics (Nezu and Sanjou, 2011). Up to know this technique has been applied to study of various turbulent phenomena in the laboratory experiments related to natural rivers, e.g. bursting phenomena near the bed, mixing layers observed at confluences, wake turbulence around dikes and piers, and so on (Nezu and Sanjou, 2011). This technique is considered as the main category of flow visualization techniques albeit the particle tracking technique is common as well as PIV technique[2].

Unlike probe measurements, PIV is a non-intrusive technique and does not affect natural conditions of the flow field (Nezu and Sanjou, 2011). This allows usage of PIV even in high-speed flows with shocks or in boundary layers close to the wall, where the flow may be disturbed by the presence of the probes (Raffel et al., 2007). Besides, with PIV it is possible to measure whole the field of study simultaneously which can be useful in study of large scale turbulence and coherent structures (Nezu and Sanjou, 2011).

Generally PIV system consists of four elements which are shown in Figure 3-2. The first element is tracer. Tracer is a liquid or a powder which is seeded to the flow and has to be illuminated in the measurement plane at least twice within short time interval (Raffel et al., 2007). The choice of correct tracer particles is one of the important part of the PIV measurement. The tracer must show the velocity of the fluid and on the other hand must be visible in the captured photos. Besides, it must be neutrally buoyant in the fluid. The second element is an illumination device which is generally a laser beam. The illuminated tracer in laser sheet is captured by the high speed camera and the finally the captured photos should be stored in a hard disk.

---

[2] The differences between Particle imaging and particle tracking is related to the density of tracing particles. When the density is low, the flow visualization is named particle tracking when we have medium density of traces is called particle imaging. It should be mentioned that flow visualization with higher density is called laser speckle velocimetry.

The general rules in velocity calculation by PIV technique is not complicated. It works based on the definition of velocity i.e. the displacement of a particle divided by time interval between two sequential photos is equal to the velocity. The calculation process is started by dividing the area of the interest to the sub areas which are called interrogation areas (Raffel et al., 2007). The displacement vector for each interrogation area between two sequential photos is calculated by means of cross-correlation based on the following equation:

$$C(\Delta x, \Delta y) = \sum_{x=0,y=0}^{x<n,y<n} I_1(x,y) I_2(x+\Delta x, y+\Delta y) \qquad (3\text{-}1)$$

where I_1 and I_2 are image intensities of sequential photos. The C is a factor which shows correlation of I_1 and I_2 for all integer displacement $(\Delta x, \Delta y)$ between the the two interrogation areas and n is the size of interrogation areas.

Figure 3-3 shows the correlation coefficient obtained from Eq. (3-1). In this photo the peak considered as the most probable displacement.

Lastly, the velocity can be calculated by:

$$[u, v] = \frac{[\Delta x, \Delta y] C_{max}}{\Delta t} \qquad (3\text{-}2)$$

where u, v are velocity compoents in the measurement photo, C_{max} is maximum value of cross-correlation in each interrogation area and Δt is the time difference between two consecutive photos.

In Stereoscopic Particle Image Velocimetry (SPIV) all three components of velocity are reconstructed by implementing additional PIV recording from different direction of view (Raffel et al., 2007). The fundamental principles of stereoscopic PIV are similar to human eye-sight. Indeed, additional view from different direction allows human to distinguish far objects from near objects (Prasad, 2000).

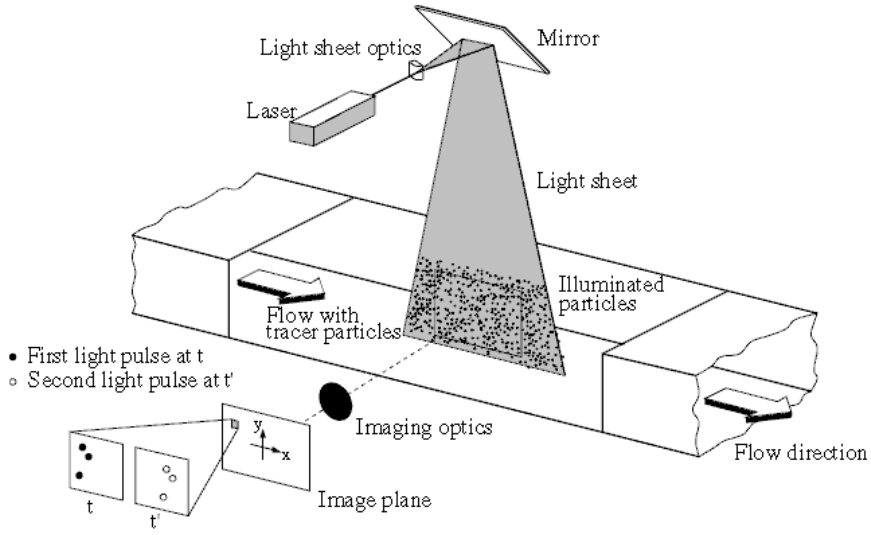

Figure 3-2: Experimental arrangement for particle image velocimetry (Raffel et al., 2007).

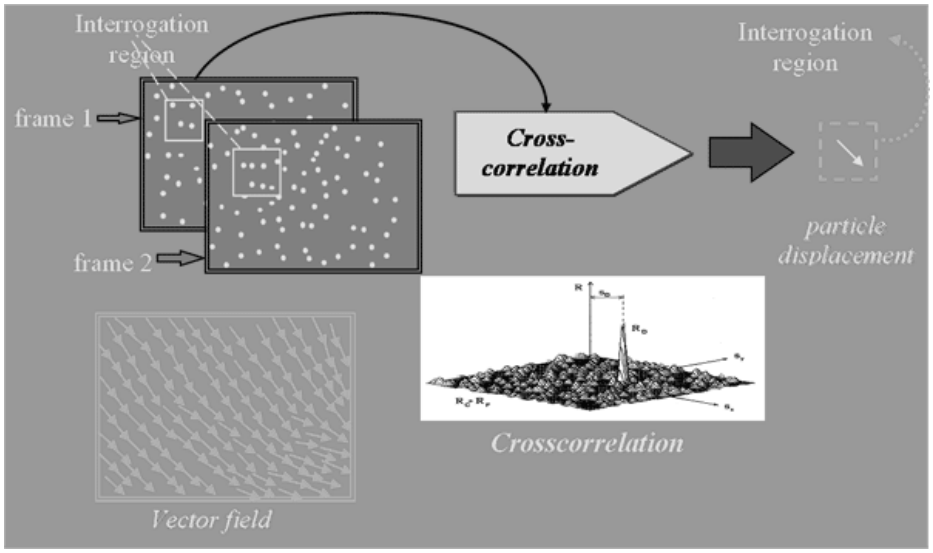

Figure 3-3: Priciple of PIV technique (sourse: http://www.erc.wisc.edu/piv.php).

There are different configuration for stereoscopic PIV apparatus. Among all configurations two forms of translation and rotation systems are more common. In translation system (Figure 3-4a), the axis of two camera's are placed parallel to each

other (Soloff et al., 1997). As in this method, object plane, lens plane and image plane are all parallel, preparation of apparatus is simple and easy. In rotation system, axes of cameras are not parallel to each other, however cameras' axes intersect object axis at the system axis (Figure 3-4b). As shown in Figure 3-4b in this system different from translation system, object plane, lens plane and image plane are collinear. This condition is known as "*Schiempflug condition"* which assures good focus of all particles in image plane (Raffel et al., 2007).

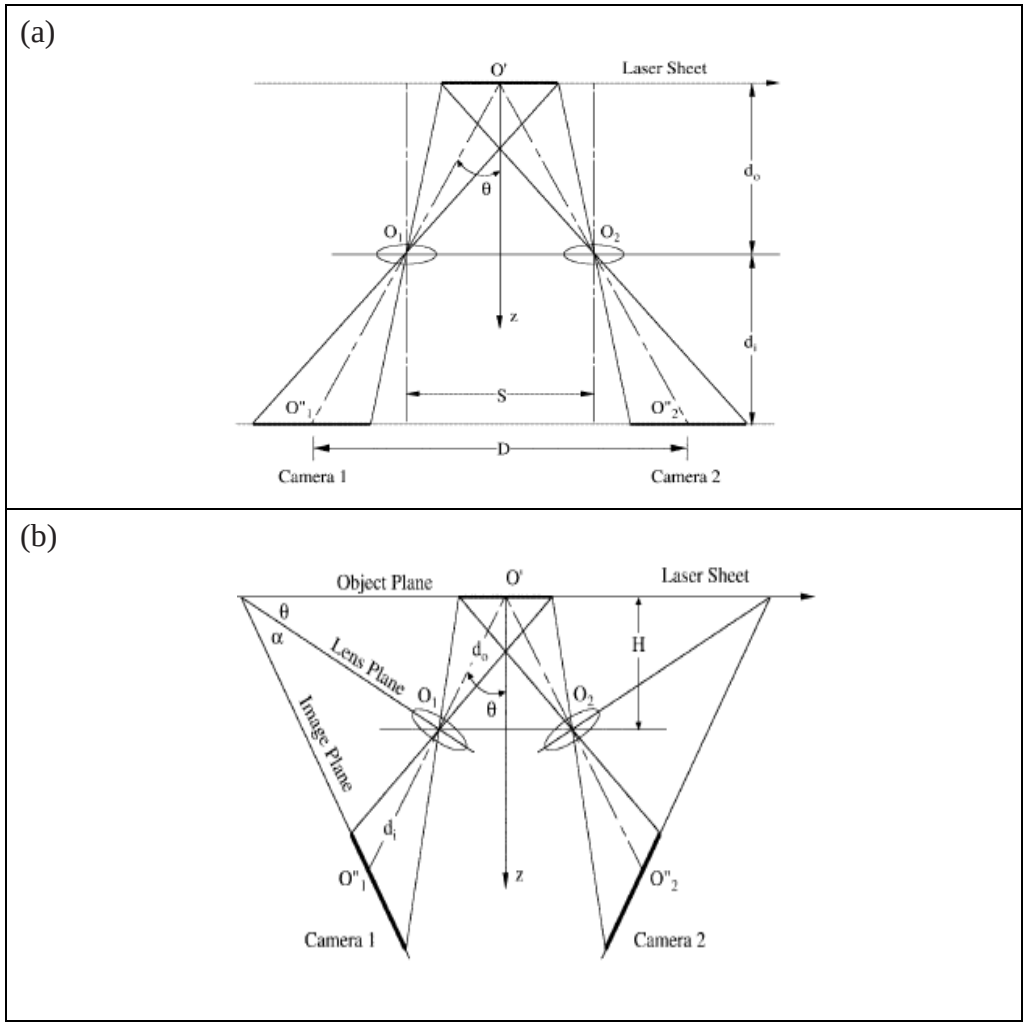

Figure 3-4: Configuration of stereoscopic PIV system (a) translation system (b) rotation system (Prasad, 2000).

In stereoscopic PIV, measurements from two different views are combined

using a specific algorithm to reconstruct three dimensional flow field. In other words, apparent displacement recorded by two cameras ($\Delta X_1, \Delta X_2$) are combined to obtain in-plane real displacements ($\Delta x, \Delta y$), plus out of plane displacement (Δz). The process of reaching to real in-plane displacements and out-plane displacement from measurement of two different cameras is called reconstruction method (Raffel et al., 2007). The process of reconstruction can be preceded along two different way of geometric reconstruction and calibration-based reconstruction. Calibration based reconstruction can also be classified as 2d and 3d calibration based reconstruction. In geometric reconstruction, complete information of recording configuration geometry is necessary. In calibration based method, placement of the target in object plane in necessary (Prasad, 2000). The calibration target is an object containing a mesh grid with specific size. In 3d calibration based reconstruction method, different from geometric method and 2d calibration based method, information related to recording geometry is not required. In 3d and 2d calibration based method the real function for projection of the image plane to the object plane is approximated by Soloff et al. (1997)'s polynomial function.

When the reconstruction process is completed, the instantaneous velocity field can be extracted from combination of two photos data. If the process repeated for the photos recorded in different instant at the same location, the velocity time series of instantaneous velocities can be achieved. Please note that the spatial and temporal quality of the collected data is a function of the optical quality of the camera system, the tracer particles and the illumination and the computer power.

3.2.1 PIV in Present Study

Two series of time-resolved Particle Image Velocimetry data on vertical planes and horizontal layer, as shown in Figure 3-5, were carried out during measurement. In the first series of measurements, SPIV was applied to measure three components of velocity (streamwise *u*, spanwise *v* and vertical component *w*) at *x*-*y* horizontal plane located 1mm above the crests. In this condition, video-cameras were installed above the channel in a symmetric 45^{o} configuration, using a surface prism to avoid optical deformations, and laser sheet was aligned

horizontally. The acquisition area was approximately $140mm$ long and $140mm$ wide, its centre was placed approximately at the middle of the channel (see Figure 3-1). In the second series of measurements, two dimensional Particle Image Velocimetry was employed in three vertical planes ($x-z$ plane) located at the centreline, 50mm left and 50mm right of the channel center line as shown in Figure 3-7. The camera was placed at the left side of the channel and the laser beam came from the top of the channel. In all measurements, high-speed Fastcam X 1024 PCI Photron cameras with a super light sensitive 10-bit CMOS sensor were used. The laser was a Nd:Yag in continuous mode. Sieved pollen particles (particle size of 0.075-0.125mm and particle density of 1.07g/cm^3) were used as tracers. For each run, tracers were inserted at the entrance of the channel and the density of tracer particles and the contrast between the white spots and background was controlled to obtain homogeneous distribution of particles, especially near the bed region. To eliminate the region in images covered by bed, a mask based on the measured bed elevations data was prepared and applied to data. The acquired region was equal to $1024 \times 512 px^2 \approx 128 \times 64\, mm^2$ in vertical planes and $1024 \times 1024 px^2 \approx 140 \times 140\, mm^2$ in horizontal layer. For each run, vertical planes in total cover at least 12 gravel bed particles (D_{50}) along *x*- direction. In Figure 3-6, two snapshots of a single PIV recording in vertical plane (Figure 3-6a) and horizontal layer (Figure 3-6b) are shown.

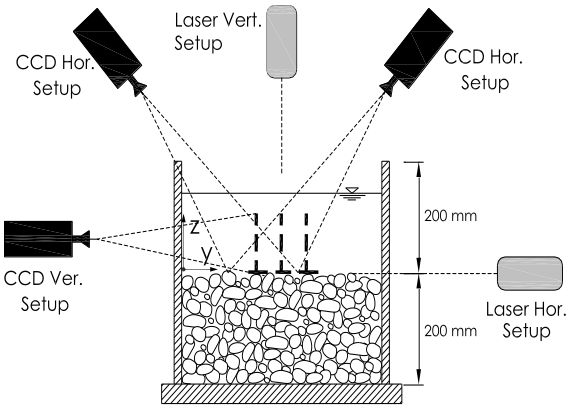

Figure 3-5: cross-section view of laboratory open channel with both 2D-PIV and Stereoscopic PIV set-ups.

Image analysis and processing were also performed by PIVDEF software (CNR-INSEAN) (Florio et al., 2002). In the first step, in order to reduce the effects of laser flare, the minimum value of image intensity for each pixel was subtracted from PIV recording. The flow field was reconstructed by iterative cross-correlation method with smallest interrogation size equal to 32×16 (75% overlapped) in vertical plane and 64 × 64 to 28 × 28 zero padded algorithm (50% overlapped) in horizontal layer by applying windows deformation and subpixel refinement (Scarano, 2002). Also, in order to reduce the number of spurious vectors, a 4 points (2 × 2) local median filter (Westerweel and Scarano, 2005) was applied to measured data. In horizontal plane, the 2d-3C reconstruction was performed using Soloff polynomial algorithm 332 degree (Soloff et al., 1997).

The resulted vector spacing (l_{IA}) is approximately 1mm in both horizontal and vertical planes. For each measurement, the sampling frequency was $500Hz$. Flow was sampled for 38.4 and 13 seconds in each vertical plane and horizontal layer, respectively. Cooper and Tait (2010) studied effect of measurement properties on velocity over gravel beds. Comparison of present study with Cooper and Tait (2010) shows that measurement duration in vertical plane is long enough to ensure statistical convergence of measured flow field. Ratio of vector spacing to bed material size (l_{IA}/D_{50}) in present study is approximately 0.05. This allows depicting flow behavior among gravels which has not measured in previous studies.

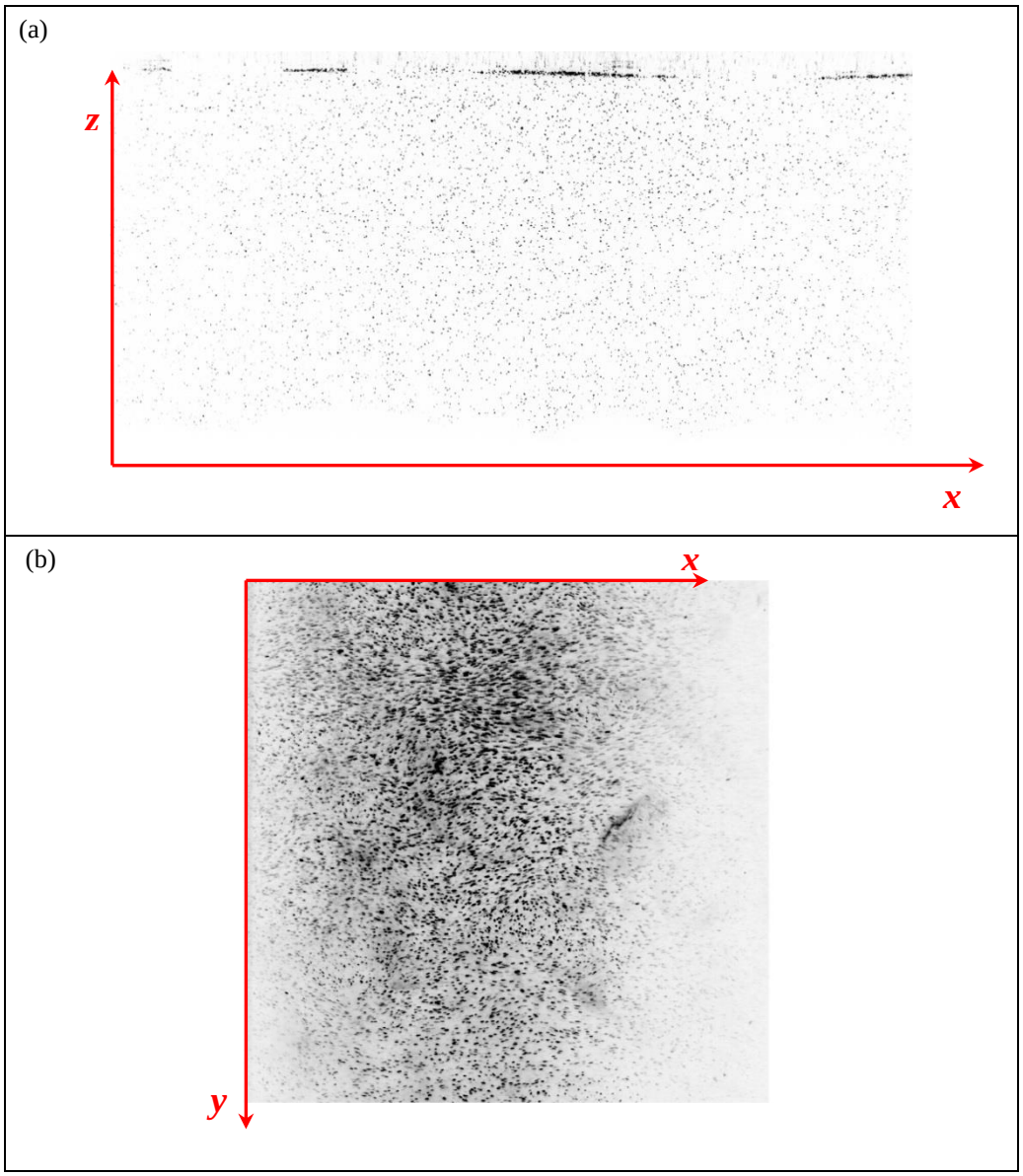

Figure 3-6: Single PIV frame (negative print) (a) Vertical plane measurement (b) Horizontal layer measurement.

3.3 BED PROPERTIES MEASUREMENTS

Bed materials were spread randomly at the bottom of the channel and about half of the channel depth was filled by bed materials, for a thickness of about 20cm

(Figure 3-8). Before measurements, gravel bed surface distributed and regularized mechanically by moving a wooden scraper along a longitudinal guide from upstream to downstream, in order to avoid gravel clustering and produce condition similar to water-worked gravel beds, as reported by Aberle and Nikora (2006). The topography of bed elevation was measured by Mitsubishi ML200 roughness meter, having linearity error of $600\mu m$, distance resolution of $60\mu m$ and a spatial resolution of $1.5mm^2$. The bed topography details were measured from $x = -200mm$ to $x = +300mm$ along all cross-sections where flow field measurements were performed. Before any analysis, noise was removed from bed elevation measurements by applying both range validation and median filters. Finally, least square fitting method was applied to remove the planar trend of the bed topography. Result of bed topography after applying filters and detrending is shown in Figure 3-7.

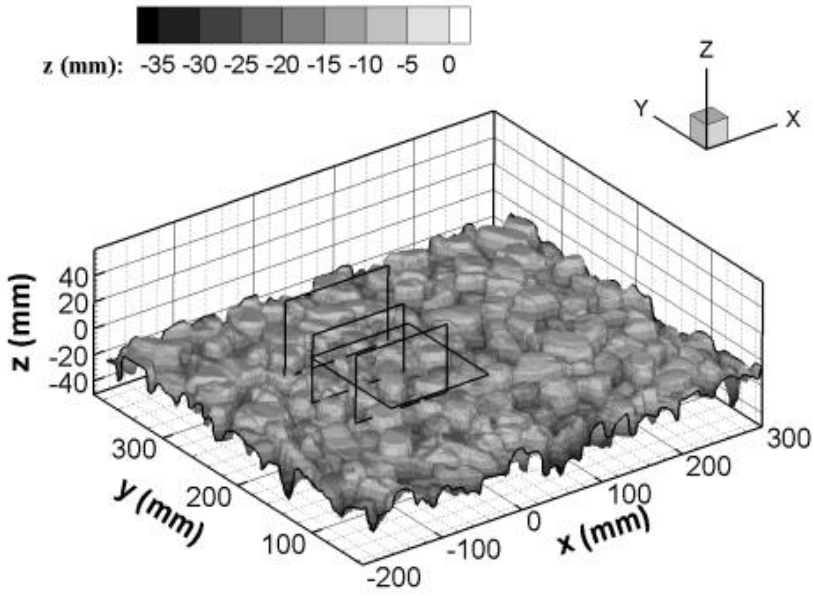

Figure 3-7: Relative location of PIV vertical planes and horizontal layer above measured gravel bed.

Figure 3-8: Photo of the gravel bed.

3.4 EXPERIMENTAL PROGRAM

Three series of experiments were performed, at different discharges (named Run (I), Run (II) and Run (III)), changing the slope so that three different flow depths were obtained, maintaining almost constant the Froude number. In Table 3-1, the experimental conditions of measurement are summarized. In this table, dimensionless Nikuradse sand equivalent roughness $k_s{}^+ = k_s u_* / \nu$ (where k_s is the equivalent roughness evaluated by stage-discharge measurements using Colebrook and White formula, ν is the water kinematic viscosity) shows that the present flows are in hydraulically rough condition (Nezu and Nakagawa, 1993). For gravel beds, Nikora et al. (1998a) proposed standard deviation of bed surface fluctuation (σ_l) as representative of roughness scale (Δ) and this value is 6.1mm in the present study. Relative submergence (H/σ_l where H is water depth) is in conditions of intermediate submergence flows (Flow Type (II)). The aspect ratio (B/H where B is channel width) shows measurements can be classified in wide open channels (Nezu and Nakagawa, 1993). Measurements were performed in a region far from side walls at the distance of 3.3 m far from the entrance of the channel (shown in Figure 3-1), where the velocity profile is fully developed and the effects of downstream weir are negligible. Length for fully developed conditions (X_L) was achieved and verified by

comparison with the Nikora et al.'s formula (Nikora et al., 1998b) (reported in Table 3-1). Moreover, in order to precisely control if the flow was in fully developed conditions, velocity profiles were measured along seven different transversal y positions with UVP (Ultrasonic Velocity Profiler, METFLOW-SA) at different longitudinal *x* positions. The comparison of the double averaged velocity profiles at different longitudinal distances (see Figure 3-9) show that at the measurement region the velocity profiles are almost overlapping ($x = 3m$ and $x = 3.5m$), thus indicating that the flow at the measurement section is in fully-developed condition.

In Table 3-2 shear velocity (u_*) obtained from extrapolation of Reynolds shear stress profile to gravel crest and that obtained by momentum balance (u_m) based on hydraulic radius are shown for three runs (Pokrajac et al., 2006). Estimated shear velocities agreed within 9%. It should be noted that as von Kàrmàn parameter of vertical velocity profile in intermediate submerged flows is affected by relative submergence (Gaudio et al., 2010), a shear velocity based on logarithmic law cannot be estimated.

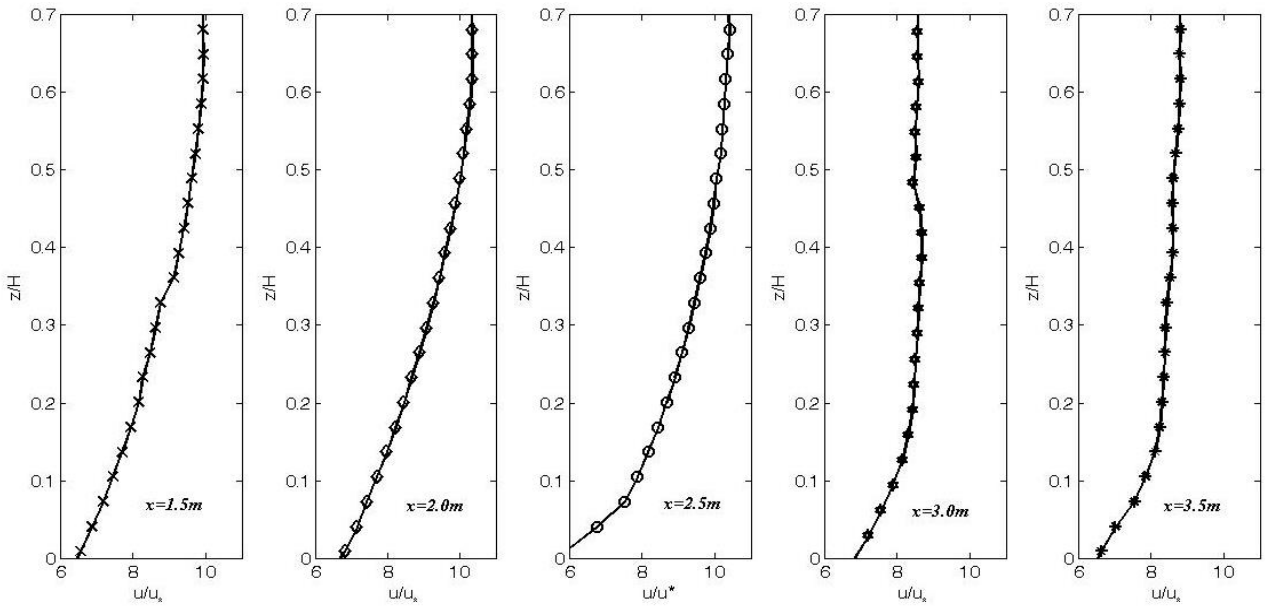

Figure 3-9: Spanwise averaged velocity profiles along x-direction.

Table 3-1: Hydraulic condition of laboratory measurements.

-	Run (I)	Run (II)	Run (III)
H (m)	0.040	0.052	0.060
S (-)	0.0028	0.0026	0.0029
Fr (-)	0.51	0.47	0.51
$Re_H \times 10^3$ (-)	12.75	17.63	23.32
B/H (-)	10.0	7.7	6.7
Q (10^{-3} m^3/s)	5.1	7.05	9.33
U_{ave} (m/s)	0.32	0.34	0.39
k_s [mm]	6.75	8.55	8.7
k_s^+ (-)	190	284	354
X_L (m)	1.37	1.61	1.74
H/σ_l	6.5	8.5	9.8

S: channel slope, $Fr = U/\sqrt{gH}$: Froude number where g is acceleration of gravity and U in mean velocity, $Re_H = UH/v$: Reynolds number, Q: water discharge

Table 3-2: Estimated bed shear velocity based on different techniques, u_m (m/s): momentum balance, u_* (m/s): Reynolds stresses accompanying with confidence interval.

Experiment	u_m (m/s)	u_* (m/s)
Run (I)	0.030±0.001	0.028±0.006
Run (II)	0.036±0.001	0.033±0.003
Run (III)	0.041±0.001	0.041±0.009

3.5 MEASUREMENTS UNCERTAINTIES

It has been sown that if the ratio of particle-image diameter to the size of a CCD pixel on the photograph is larger than 3-4, the uncertainty of the measurement is equal to one-tenth to one-twentieth of the particle diameter (Prasad et al., 1992).

For better understanding of our PIV measurement error, following method of Detert (2008), a spectral analysis was performed. Based on this method, the quality

of PIV measured data can be estimated by the ratio of resolved turbulent intensities to total turbulent intensities of velocity signal (Detert et al., 2010; Weitbrecht et al., 2011), i.e. :

$$\frac{\sigma_{PIV}}{\sigma_{total}} \tag{3-3}$$

where σ_{PIV} is resolved turbulent intensity by the PIV measurements and σ_{total} is the total turbulent intensity of the velocity signal. Also, the following relationship is valid between variance of the resolved velocity signal with PIV and total variance of velocity signal:

$$\sigma_{tot}{}^2 = \sigma_{PIV}{}^2 + \sigma_r{}^2 \tag{3-4}$$

where $\sigma_r{}^2$ is the residual of the velocity which does not resolved with PIV. Based on the Eq. (3-4), the Eq. (3-3) can be rewritten as:

$$\frac{\sigma_{PIV}}{\sigma_{total}} = \sqrt{\frac{\sigma_{PIV}{}^2}{\sigma_{PIV}{}^2 + \sigma_r{}^2}} \tag{3-5}$$

Resolved turbulent intensity is estimated from area below experimental spectra (Lavoie et al., 2007). Velocity signal which is resolved by PIV does not cover small scales which cuase difference between $\sigma_{PIV}{}^2$ and $\sigma_{tot}{}^2$. To estimate this difference ($\sigma_r{}^2$), an extrapolation of the $\kappa^{-5/3}$ cascade to small scales can be used as:

$$\sigma_r{}^2 = -3/2\,\frac{S_{uu}(k_N)}{K_N{}^{-5/3}}\,\frac{1}{(2\pi)^{\frac{2}{3}}}\,(\eta_k{}^{2/3} - L_N{}^{2/3}) \tag{3-6}$$

where L_N is the smallest resolved scale applied in vector processing, $K_N = 2\pi/L_N$ is the corresponding wave number and S_{uu} is the one sided spectra of streamwise velocity. Finally, η_k is the smallest relevant scales which was considered to be three times of Kolmogorov micro scale ($\eta_k = 3\eta$) (Weitbrecht et al., 2011). Kolmogorov

micro scale is also estimated from the following equation (Nezu and Nakagawa, 1993):

$$\eta = 1.1 L_x / R_L{}^{3/4} \qquad (3\text{-}7)$$

where L_x is macro length scale of the turbulence and $Re_L$is a form of Reynolds stress based on root mean square of streamwive velocity signal and macro length scale of the turbulence. In Figure 3-10, spatial spectra of streamwise velocity of plane in channel center line for $z/H = 0.4$ are shown. The spectra are estimated based on Welch's method with $n = 2^5$ and no overlapping. Also, in order to make vector spacing equal to PIV spatial resolution, no overlapping is applied in PIV data processing. The results show that at least 96% of turbulence intensities are retrieved during measurements.

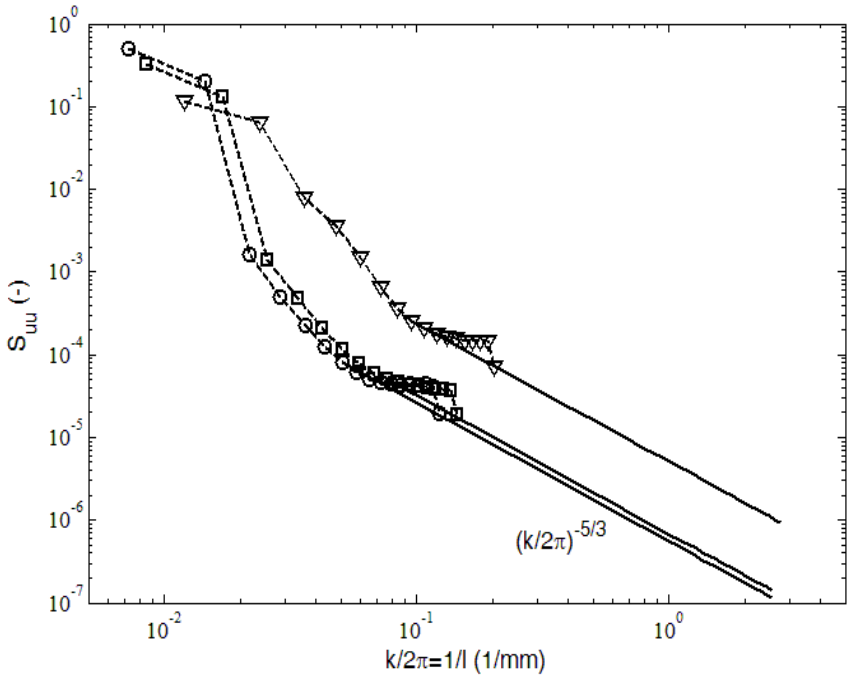

Figure 3-10: One sided spectra (S_{uu}) from PIV data, bold line indicates extrapolation of spectra to 3η where η is Kolmogrov length scale, estimaed from (Nezu and Nakagawa (1993)), page 30; Δ Run (I) □ Run (II) ○ Run (III).

Finally, statistical uncertainty due to the sampling of random process should also be reported. The relative error can be estimated based on the following equation:

$$Er_x = \frac{{s_x}^2/N}{\bar{x}} \tag{3-8}$$

where Er_x is relative error of x, ${s_x}^2/N$ is the variance of estimated mean ($\bar{x}$). We assume that the samples collected during measurements are uncorrelated and they have standard normal distribution. In this case, value of ${s_x}^2/N$ can be estimated from available formula (Benedict and Gould, 1996). These formulas are presented in Table 3-3.

Based on Eq.(3-8) and the formulas reported in Table 3-3 relative error of different quantities are estimated. The mean values of estimated relative errors for different runs are reported in Table 3-4. As reported, relative error of vertical and transversal components of velocity are higher in comparison to other quantities. This fact resulted by smaller values of mean vertical and transversal velocity (dominator of Eq.(3-8)) in comparison to other statistical characteristics of flow.

Table 3-3: Variance estimator of different statistics.

Statistics	Variance Estimator
$\bar{x}$	$\overline{x^2}$
$\sqrt{\overline{x^2}}$	$\overline{x^2}/2$
$\overline{x_1 x_2}$	$(1-\frac{\overline{x_1 x_2}}{(\overline{{x_1}^2})^{0.5}(\overline{{x_2}^2})^{0.5}})(\overline{{x_1}^2})(\overline{{x_2}^2})$
$\overline{x^2}$	$2(\overline{x^2})^2$

Table 3-4: Mean of relative sampling error in present study.

	Vertical Planes (%)			**Horizontal Layer (%)**		
	Run (I)	**Run (II)**	**Run (III)**	**Run (I)**	**Run (II)**	**Run (III)**
$\bar{u}$	*0.90*	*0.83*	*0.91*	*1.13*	*1.84*	*1.81*
$\bar{v}$	-	-	-	*8.60*	*13.11*	*25.25*
$\bar{w}$	*28.14*	*24.41*	*30.36*	*15.91*	*15.28*	*29.87*
σ_u	*2.34*	*2.68*	*2.57*	*2.42*	*3.03*	*2.94*
σ_v	-	-	-	*1.62*	*2.12*	*2.03*
σ_w	*1.40*	*1.53*	*1.49*	*2.21*	*2.29*	*2.21*
$-\overline{u'w'}$	*0.43*	*0.53*	*0.51*	*0.75*	*1.05*	*0.89*

4 Gravel Bed Characteristics

Abstract:

This chapter concerned with gravel bed characteristics. In present study, random gravel bed is regularized by a scraper along streamwise direction. We regulated the bed with scraper in order to prepare a condition similar to natural water-worked beds. In this chapter, the characteristics are reported under the title of "statistical characteristics of gravel bed" and "spatial organization of gravel bed". Comparison of gravel bed characteristics in present study with gravel bed characteristics in other studies, show that while some of the bed properties are similar to the natural water-worked beds (e.g. near Gaussian distribution of bed elevations and range of obtained characteristic length scales), some differences are still present (e.g. negative skewness of bed elevation and different scaling exponent value in comparison to water worked beds).

4.1 STATISTICAL CHARACTERISTICS OF GRAVEL BED

Before discussing details of the flow field, it is useful to describe general bed properties. This provides the possibility to compare the present laboratory gravel bed to previously studied natural water-worked and artificial unworked beds. Also, it can be helpful for understanding the relation of gravel bed characteristics with flow field. The size distribution curve of bed material is shown in Figure 4-1. To produce this curve, three diameters of each particle (large (a), intermediate (b) and small (c)) from a bed materials sample around 10 kg was measured. The volume of each particle is equal to the product of these diameters. So, cumulative density function of particles volume is considered as bed material size distribution curve.

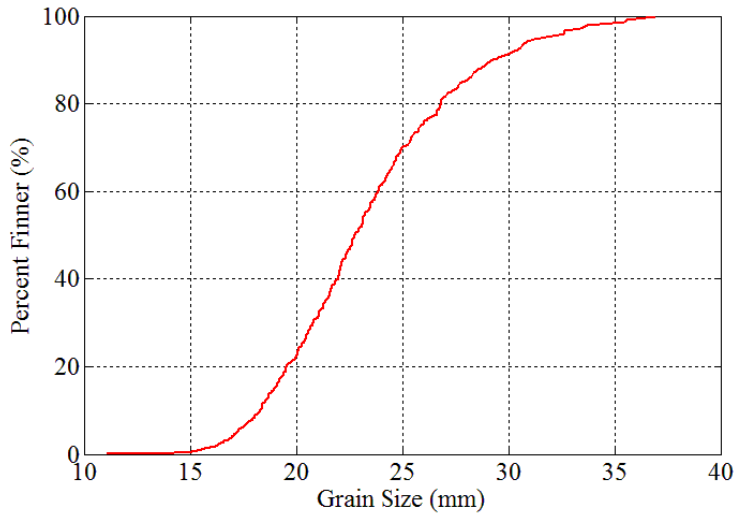

Figure 4-1: Grains size distribution curve.

Complementary statistical representative of bed materials are reported in Table 4-1. As reported, the grading parameter ($\sigma_g = (D_{84}/D_{16})^{0.5}$) is smaller than 1.4 and coefficient of uniformity ($C_u = D_{60}/D_{16}$) is smaller than 3, so bed materials have well-graded uniform distribution (Tigrek and Aras, 2011). Also, comparison of three different particles diameters shows that bed materials shape are generally spherical (46%), while there are also stones in the blade (25%), disc (18%) and roller (11%) shapes (Selley, 2000).

Table 4-1: Statistical properties of gravel bed.

D_{50}^{*}	D_{90}^{**}	C_u	σ_g	Sk	K
21.5mm	28mm	1.3	1.2	-0.41	-0.02

*** D_{50} is the grain diameter at 50% passing, ** D_{90} is the grain diameter at 90% passing**

Histogram of gravel surface elevations as measured by roughness meter is shown in Figure 4-2. Bed elevations distribution has mild negative skewness (*Sk* in Table 4-1) and its kurtosis value (*K* in Table 4-1) is close to zero. Applying Kolmogorov-Smirnov test shows that hypothesis of normality is rejected at significance level of 0.01 due to the presence of negative skewness.

Figure 4-3 reports the porosity function (Φ) evaluated by two different methods: water displacement method and roughness meter measurements (digital elevation method) (Aberle, 2007). The mean bed level (z_m) was 12.7mm lower than gravel crest level (z_c), the latter defined as the elevation corresponding to 95% of cumulative frequency of measured bed surface elevation values. Bottom of roughness layer (z_b) was determined as the level of constant porosity function based on water displacement method.

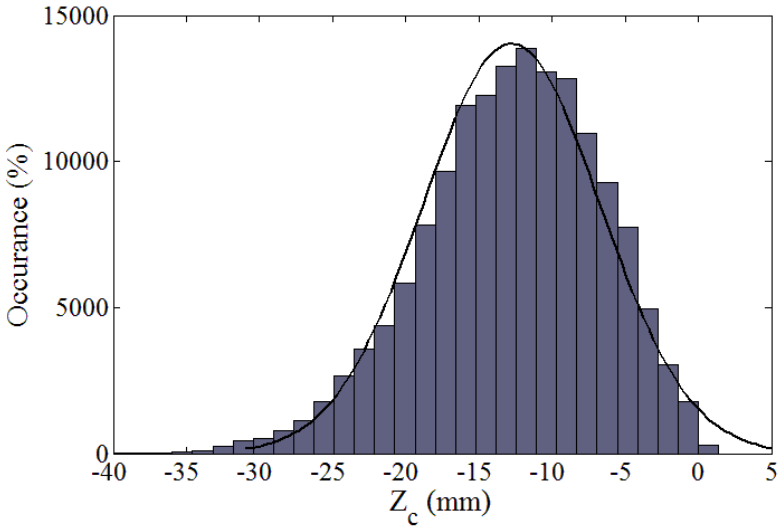

Figure 4-2: Histogram of bed surface elevation.

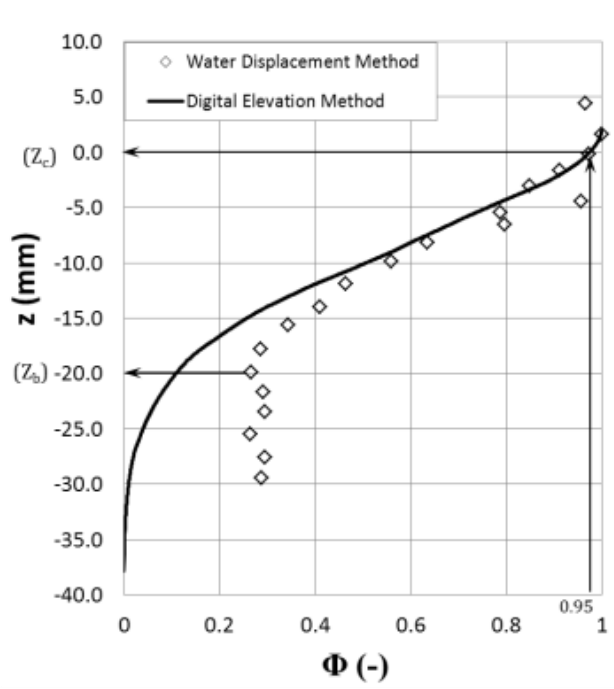

Figure 4-3: Porosity function Φ as measured with water displacement method and with digital elevation method.

4.2 SPATIAL ORGANIZATION OF GRAVEL BED

Description of gravel bed will be completed by consideration of bed materials spatial organization. Generally, this type of information can be extracted by variogram and higher order structure functions of gravel bed surface elevations (Robert, 1991; Nikora et al., 1998a; Nikora and Walsh, 2004). In present study, generalized longitudinal and transversal structure functions are examined and shown in Figure 4-4a, b. In this figure, D_p is *p*-order structure function and l_x, l_y are spatial lags in streamwise and spanwise directions, respectively. In both directions, scaling, transition and saturation regions are evident. The *p*-order generalized structure function, at small spatial lags, follows power function ($D_p(\Delta x) = \left[\left|\Delta x^{\xi_p}\right|\right]$ and $D_p(\Delta y) = \left[\left|\,\Delta y^{\xi_p}\right|\right]$), where ξ_p is an exponent related to the structure function order, $|\ \ |$ defines absolute value and $[\ \ ]$ defines averaging over many points (Nikora and Walsh, 2004). For simple scaling condition, $\xi_p$is linear ($\xi_p = pS$, where *S* is scaling

exponent).

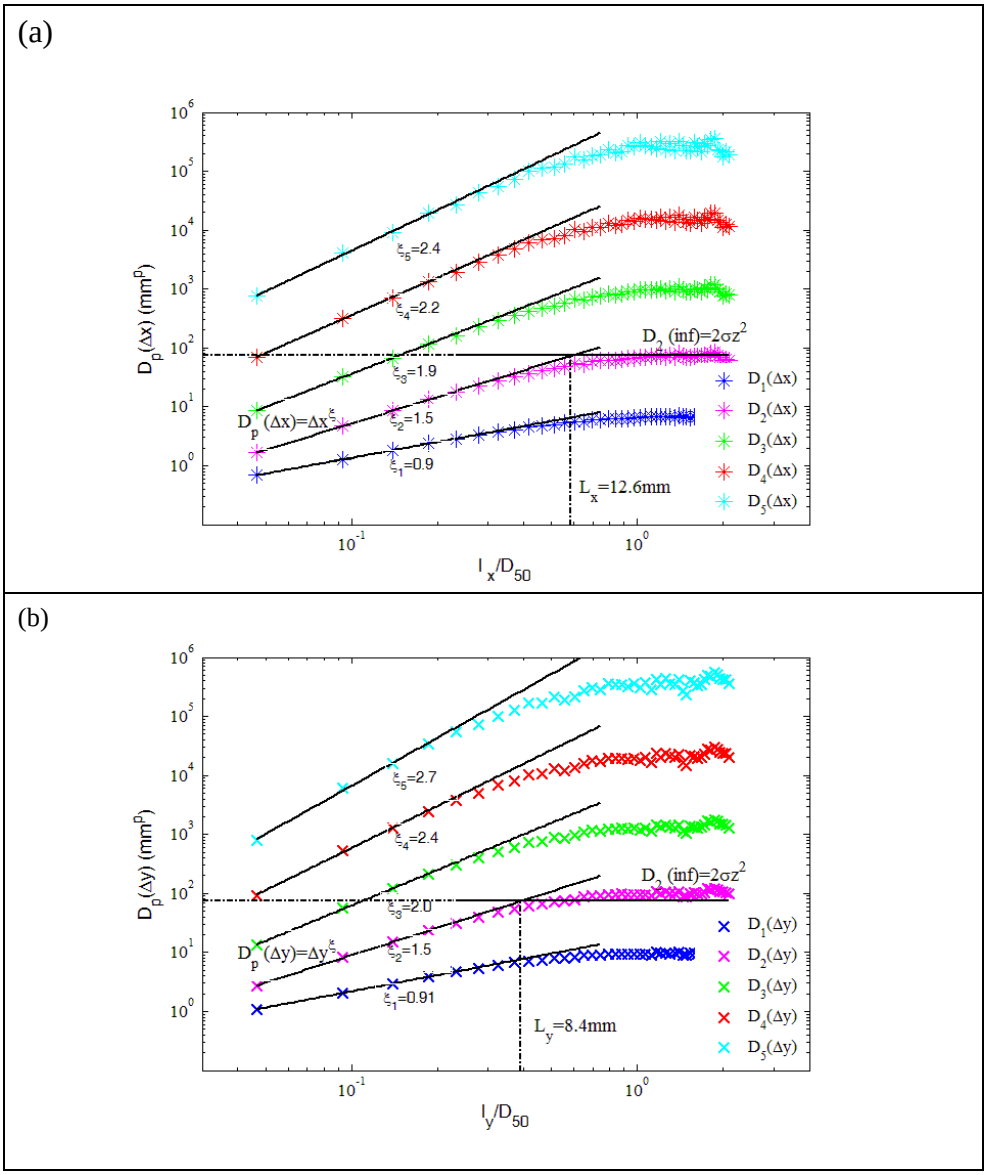

Figure 4-4: 1D higher-order structure functions (a) in streamwise direction (b) in spanwise direction.

In Figure 4-5, ξ_p accompanying with error bar resulted by linear regression versus order of structure function is shown. For better comparison, line of $\xi_p = pS$ with $S = 0.9$ which should have been observed in the case of simple scaling (similar

scaling exponent for strucuture function with different orders) is also shown. Both longitudinal and transversal components deviated from linear function as a consequence of multi-scaling behavior (Davis et al., 1994). Similar results were found by Nikora and Walsh (2004) for both water-worked and artificial unworked gravel bed surfaces. Moreover, scaling exponents in longitudinal and transversal directions for first and second order moments are equal, while by increasing order of structure functions their differences increase. However, as shown in Figure 4-5, by increasing order of structure function linear regression error increases and so the confidence intervals of longitudinal and transversal structure functions overlap.

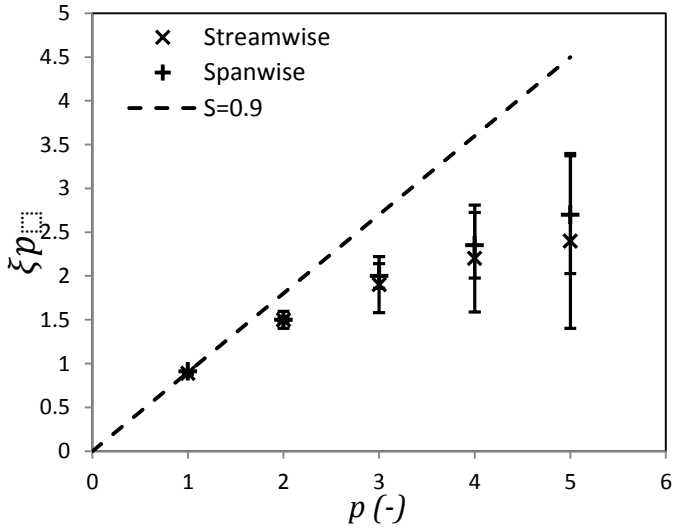

Figure 4-5: Scaling exponents of generalized structure function in comparison to linear function with S=0.9.

Rough bed characteristics scales (L_x, L_y) in longitudinal and transversal directions are defined as spatial scales where scaling region and saturation region are separated in the corresponding variogram (Nikora et al., 1998a). For present study these values are calculated by defining intersection of constant structure function values in saturation region with extrapolation of linear relation in scaling region, as proposed by Nikora et al. (1998a). Results are reported in Table 4-2 and Figure 4-4. These values are in agreement with observation of Aberle and Nikora (2006) who

relate rough bed characteristics scale in *x*-direction to $0.5D_{50}$. Obtained scaling value in longitudinal direction is larger than the transversal one. Comparison between ratio of longitudinal to transversal characteristic scales and ratio of large to intermediate mean diameters of bed material ($\bar{a}, \bar{b}$) show that these values are close to each other. This issue resulted by aforementioned fact that, before any measurement, bed surface has been regularized mechanically, thus large and intermediate diameters of particles mostly lie in longitudinal and transversal directions respectively.

Moreover, 2D-2nd order structure function is calculated and shown in Figure 4-6. For natural water-worked beds, it has been observed that contours of 2D-2nd order structure function at small scales is circular, while at larger scales it become significantly elliptical with maximum axis inclined with respect to x-axis (Goring et al., 1999). Also, Aberle and Nikora (2006) reported largest diameter of 2D-2nd order structure function aligned in *x*-direction for small spatial lags, but inclined for large lags during armouring process. This comes from different behavior of small particles to large particles during armouring. In present study, as shown in Figure 4-6, shape of small scale contour lines has a mild inclination with respect to *x*-axis, which increases for larger scales.

To compare longitudinal and transversal scales, ratio of largest to smallest diameters of the ellipse in an arbitrary contour line at the border of scaling and saturation regions (l_ξ, l_η in Figure 4-6) is calculated and reported in Table 4-2. Value of this ratio is also close to that of longitudinal and transversal characteristic scales (L_x/L_y) and to that of large to intermediate mean diameters of particles ($\bar{a}/\bar{b}$). Also, standard deviation, skewness and kurtosis of bed elevations in longitudinal and transversal directions are separately calculated and reported in Table 4-2. As seen, there is not a significant difference between standard deviation, skewness and kurtosis values in longitudinal direction to the corresponding values in transversal direction.

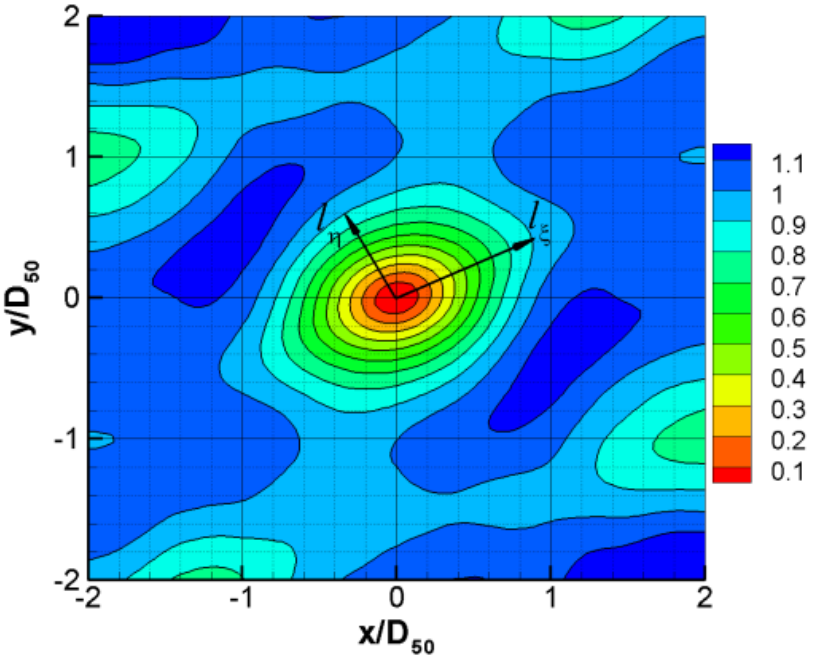

Figure 4-6: Contour map of 2D variogram.

Table 4-2: Comparison of longitudinal and transversal statistical properties of gravel bed in present study.

	Longitudinal	**Transversal**	**Ratio**
$\boldsymbol{L_x, L_y(mm)}$	12.6	8.4	1.5
$\boldsymbol{l_\xi, l_\eta(mm)}$	20.9	14.8	1.4
$\boldsymbol{sk_x sk_y}$	-0.4	-0.4	1.0
$\boldsymbol{k_x k_y}$	-0.1	-0.1	1.0
$\boldsymbol{\sigma_{lx}, \sigma_{ly}(mm)}$	5.8	5.8	1.0
	Averaged Particles Diameters		
	Large, $\bar{a}$ (*mm*)	Intermediate, $\bar{b}$ (*mm*)	Ratio
	30.1	22.00	1.4

In present study, we attempted to produce conditions similar to natural water-worked gravel beds by spreading gravels randomly in bottom of channel and then regularizing them mechanically in main flow direction. However, it was found that while some of the bed properties are similar to natural water-worked beds (e.g. near Gaussian distribution of bed elevation and range of obtained characteristic scales), some differences are still present (e.g. negative skewness of bed elevation and different scaling exponent value in comparison to water worked beds).

5 Characteristics of Turbulent Flow

Abstract:

This chapter is concerned with flow field and turbulence structure over a coarse immobile gravel bed in intermediate submergence condition, with particular attention to the near bed region. Results show that near bed flow field is characterized by striped structure induced by secondary currents. However, these striped structures tend to be disrupted by the effects of gravel protrusions. These results show that upward and downward flows occur not randomly on the bed, but in correspondence to upstream and downstream sides of gravels, respectively. Analysis of instantaneous flow field shows formation of vortices in accordance with presence of secondary currents and gravel protrusions. Logarithmic law parameterization of double averaged velocity profiles in this type of flow was reviewed and applied to experimental data. It was found that log-law parameters change considerably with relative submergence and, in some cases, no clear log-law region was found.

5.1 TIME AVERAGED TURBULENCE STATISTICS

In Figure 5-1 colour maps of time averaged velocity components in horizontal layer at 1mm above crest are shown. All velocity components are normalized with u_* as computed in Table 3-2. For comparison, bed topography is shown in the background and those parts of bed topography which are lower than z_m are not shown in the background. The results of streamwise velocity ($\bar{u}/u_*$) in In Figure 5-1a, b, c show that for all the three runs low and high velocity strips alternating in spanwise direction are evident. Contour maps of spanwise velocity ($\bar{v}/u_*$ in In Figure 5-1d, e, f) and normalwise velocity ($\overline{w}/u_*$ in Figure 5-1g, h, i) also show analogous longitudinal strips of positive and negative velocities, even if less evident in comparison to that of $\bar{u}/u_*$. These strips can be a consequence of turbulence secondary currents (Nezu and Nakagawa, 1993). For better analysis, spanwise profile of longitudinally averaged velocities accompanying with idealized sketch of correspondent secondary current cells in water depth are shown in Figure 5-1. From these profiles, it is clear that strips of negative *w*-component (downflow) correspond to high streamwise velocity strips, while positive *w*-component strips (upflow) correspond to low- streamwise velocity strips. Moreover, in spanwise velocity, a tendency of changes in sign where streamwise and normalwise velocities are minimum or maximum was also noted. This behavior recalls convergence and divergence of transversal flow in secondary current cells. The lateral spacing of lower longitudinal streamwise velocity strips is near 1.2 times the water depth (see Figure 5-2), which is smaller than those measurement by Kinoshita (1967) ($2H$) in wide river and Albayrak and Lemmin (2011) ($1.85H$) in open channel at free surface. Concerning normalwise and spanwise velocity components, approximately the same strips spacing ($1.2H$) were found in present study.

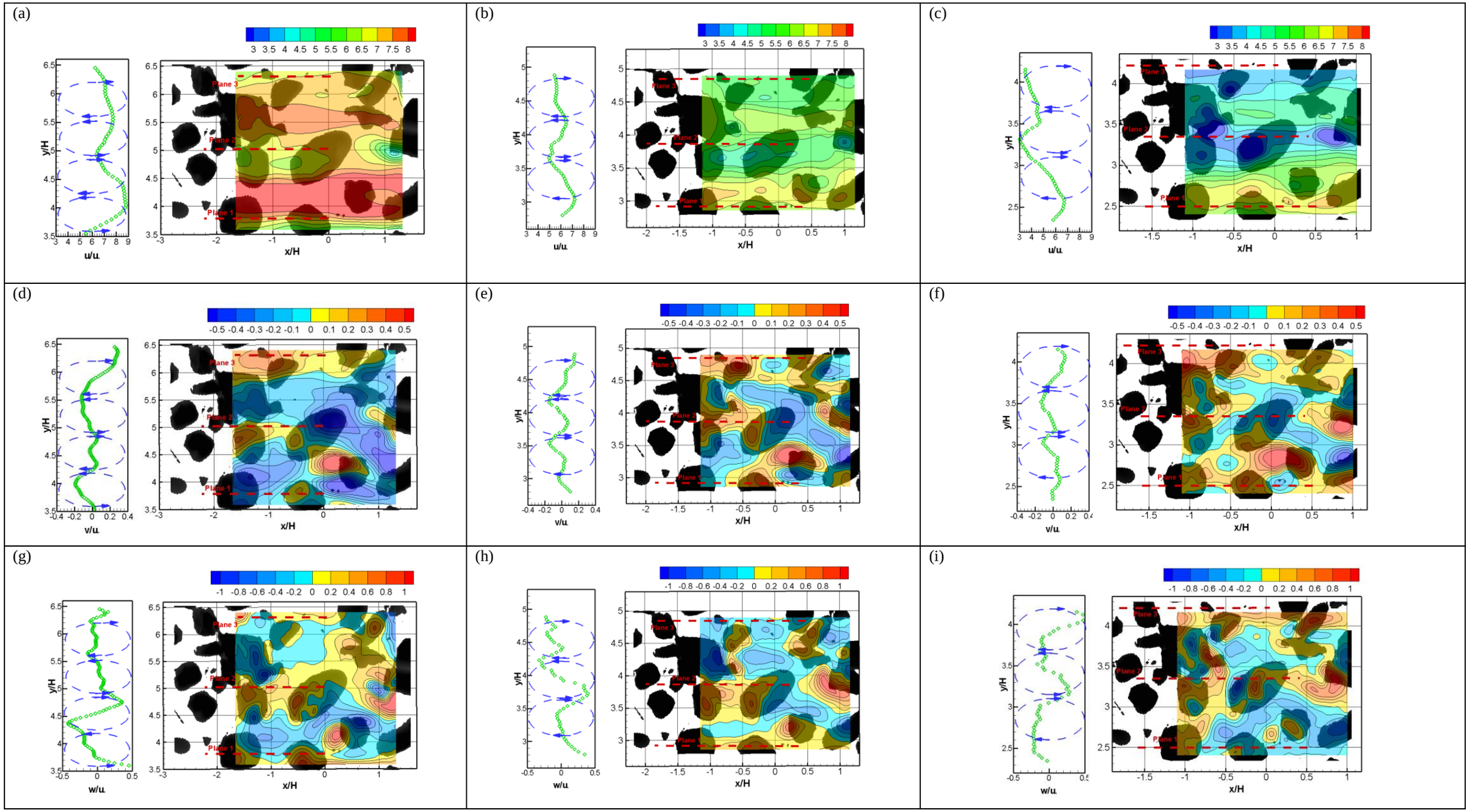

Figure 5-1: Contour map of velocity components in horizontal plane just above the crest (a) $\bar{u}/u_*$ in Run (I) (b) $\bar{u}/u_*$ in Run (II) (c) $\bar{u}/u_*$ in Run (III) (d) $\bar{v}/u_*$ in Run (I) (e) $\bar{v}/u_*$ in Run (II) (f) $\bar{v}/u_*$ in Run (III) (g) $\bar{w}/u_*$ in Run (I) (h) $\bar{w}/u_*$ in Run (II), crest (i) $\bar{w}/u_*$ in Run (III), flow from left to right.

Smaller lateral spacing of velocity strips in present study in comparison to previous studies can be explained by new observation of Mejia-Alvarez and Christensen (2013) and Barros and Christensen (2014). Mejia-Alvarez and Christensen (2013) and Barros and Christensen (2014) observed similar low and high (positive and negative) velocity strips in rough bed boundary layer. They found that there is consistency between bed topography and locations of low and high (positive and negative) velocity strips. Specifically, high streamwise velocity strips ("*high momentum path way"* based on the terminology used by Barros and Christensen (2014)) are placed where averaged value of bed elevations in the x-direction is higher than mean bed elevations and vice versa (Barros and Christensen, 2014). Consequently, they found scaling values of lateral spacing of high and low streamwise velocity strips different to what obtained by Kinoshita (1967), Nezu and Nakagawa (1993) and Albayrak and Lemmin (2011). In Horizontal PIV measurements of present study, only 35% of the channel width is covered and just two pairs of velocity strips are depicted. Therefore, it is not possible to evaluate the average spacing of velocity strips all along the cross-section.

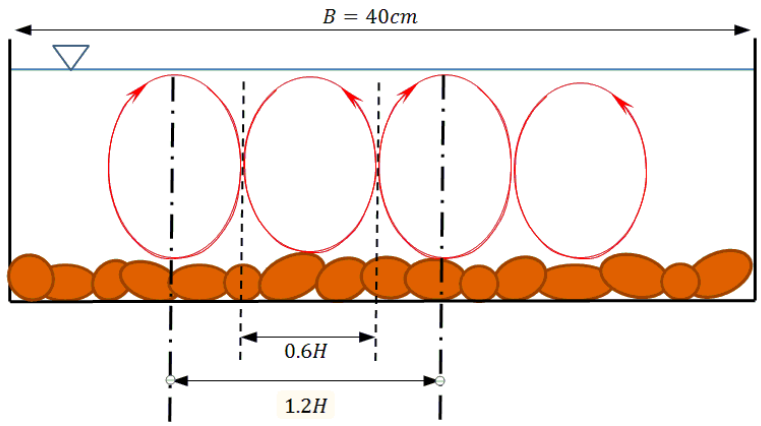

Figure 5-2: Flow pattern of cellular secondary currents.

In Figure 5-1, it can be also recognized that described strips in previous paragraph are disrupted, at least in part, by the protrusions of gravel crests. The effect of gravels protrusion varies on the different velocity components. As far as

streamwise velocity is concerned, gravel protrusions lead to deceleration and form a region of lower velocity at the downstream side of gravel crests (Figure 5-1a, b, c). Normalwise velocity component has mostly positive local values at upstream side of the gravel crests, depending on their shape, orientation and neighbor features, while the values are mostly negative at the downstream side of the gravel crests (Figure 5-1g, h, i). Finally, in spanwise component, strong variations are observed around each gravel crest, again depending on gravel shape and orientation.

The presence of secondary currents and bed topography effects are also visible in turbulence statistics. As an example, in Figure 5-3 turbulent intensities (σ_u/u_* streamwise, σ_w/u_* normalwise) for Run (I) and Reynolds shear stress ($-\overline{u'w'}/{u_*}^2$) for Run (I) and Run (III) are shown. As one can see, turbulent intensities and Reynolds stress contour maps alternates transversally. Lateral spacing of these quantities is almost in agreement with stripes spacing noticed in the maps of the time averaged velocity components. However, striped structures in second order moments are less clear in comparison to time averaged velocity field, especially in normalwise turbulent intensity. Surprisingly, despite the fact that aspect ratio reduces from Run (I) to Run (III) (Table 3-1), transversal variation of $-\overline{u'w'}/{u_*}^2$ caused by secondary currents is less clear in Run (III) than in Run (I). Indeed, the tendency to less clear striped structure for increasing relative submergence is noticed in all turbulent intensities and Reynolds stresses measurements (not reported). What comes out from the analysis of the velocity measurements in horizontal layer is that the striped structure is more evident for higher aspect ratio and lower relative submergence. Similar trends were found by Cooper and Tait (2008). They observed that strips of time averaged streamwise velocity are less clear for higher relative submergence. However, they did not believe that secondary currents are present in their measurement. Nevertheless, if the strips can be considered as result of secondary currents, actual observation are contradictory to the common idea that secondary currents are more important for smaller aspect ratio conditions (Nezu and Nakagawa, 1993).

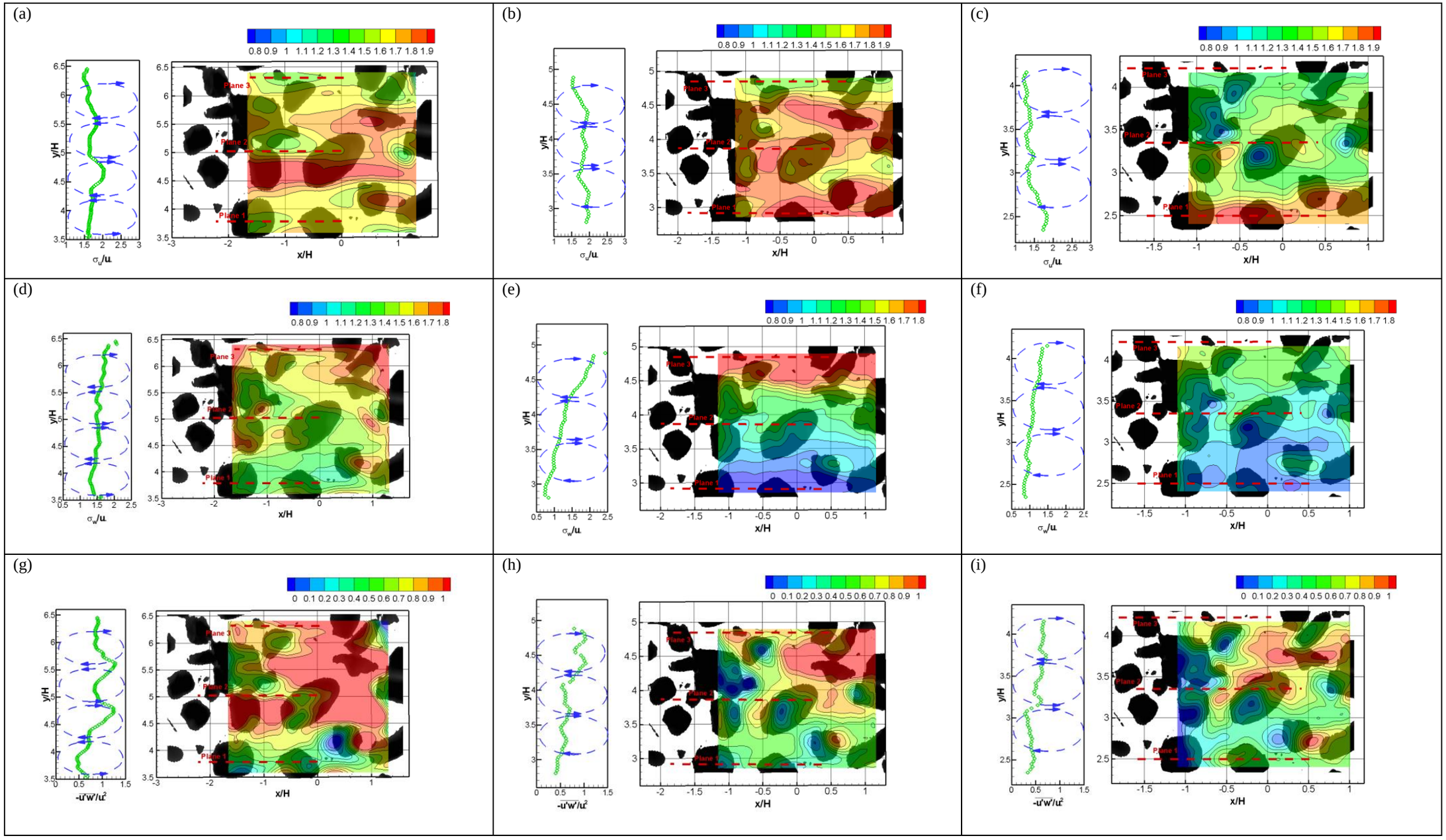

Figure 5-3: Contour map of velocity components in horizontal plane just above the crest (a) σ_u/u_* in Run (I) (b) σ_u/u_* in Run (II) (c) σ_u/u_*in Run (III) (d) σ_w/u_* in Run (I) , (e) σ_w/u_* in Run (II) (f) σ_w/u_* in Run (III) (g) $-\overline{u'w'}/u_*^2$ in Run (I) (h) $-\overline{u'w'}/u_*^2$ in Run (II) (i)$-\overline{u'w'}/u_*^2$ in Run (III) , flow from left to right.

On the other side, bed topography affects also second order moments. Bed topography induces local variations which tend to hide striped structure in the near bed flow field. This can be observed in Figure 5-3, in which regions of strong turbulent intensities formed at the downstream side of gravels, whereas gravel spacing is sufficiently large for development of a wake. The behavior of Reynolds stress is similar to that of turbulent intensities and local high values are measured at the downstream side of gravels.

Contour maps of streamwise velocity for the three different runs in three different planes are given in Figure 5-4. These contour maps are also in agreement with horizontal layer findings. Previous studies showed that near gravel bed velocity field is affected by bed topography (Hoover and Ackerman, 2004; Hardy et al., 2010; Mignot et al., 2009a). In present study, flow can be divided into two regions (Figure 5-4): in near bed region, which starts from bottom of plane and continues approximately until σ_l above gravel crests, velocity variations are high. In region above σ_l velocity field is almost homogenous. Looking at Figure 5-4, shows that variation of velocity in near bed region is driven by gravel bed protrusions. Similar to horizontal layer, in vertical plane streamwise velocity reduces due to the protrusion of gravel crests. This behavior in free space between adjacent gravels is analogous to wake-like motion.

Figure 5-5 reports the contour map of measured turbulence intensities and Reynolds stress in plane 1 for three different measurement conditions. Like velocity contour maps, in this figure near bed region is heterogeneous and region away from the bed is homogenous. In comparison to streamwise velocity contour maps, difference between near bed region and outer region is more distinct. Moreover, based on the Figure 5-5, thickness of near bed region is about $2.5\sigma_l$, which is larger than observed value in streamwise velocity contour maps. This shows that extension of roughness layer is different when the time averaged streamwise velocity or the time averaged turbulent intensity are considered. Therefore, it can be concluded that the definition of roughness layer may not be universal and depends on the particular turbulence parameter which is considered. In all contour maps of Figure 5-5, patchiness in spatial distribution of near bed flow is not random and it is mostly associated with protrusion of gravel crests and depression due to interstices between

gravels.

Looking deeper in Figure 5-5, one can also see turbulent intensities dimensionless with bed properties are higher for lower submergence ratio. In addition, it can be noticed that for Run (I) a peak of turbulent intensity is present at the downstream side of gravel crest protrusion, in analogy to what could be expected in the wake of a bluff body (see e.g. Braza et al., 2006; Dong et al., 2006), however this peak tends to reduce in Run (II) and disappears in Run (III). These results are in part analogous to what reported by Hardy et al. (2009), which found that for flow at low Reynolds number the wakes dynamics at gravel crests is more evident with respect to flow at high Reynolds number, so inducing a higher spatial heterogeneity of the near bed turbulence field, while for the latter the skimming flow phenomenon tends to prevail. Nevertheless there is a distinction between actual findings and that of Hardy et al. (2009). On the contrary of Hardy et al. (2009), which claims that the turbulence intensity increases with Reynolds number, when turbulent intensity is made dimensionless with the shear velocity, the local peaks seem to be higher for lower submergences (and so, in present case for lower Reynolds number). This apparent contradiction will be better analyzed with double averaging of second order moments.

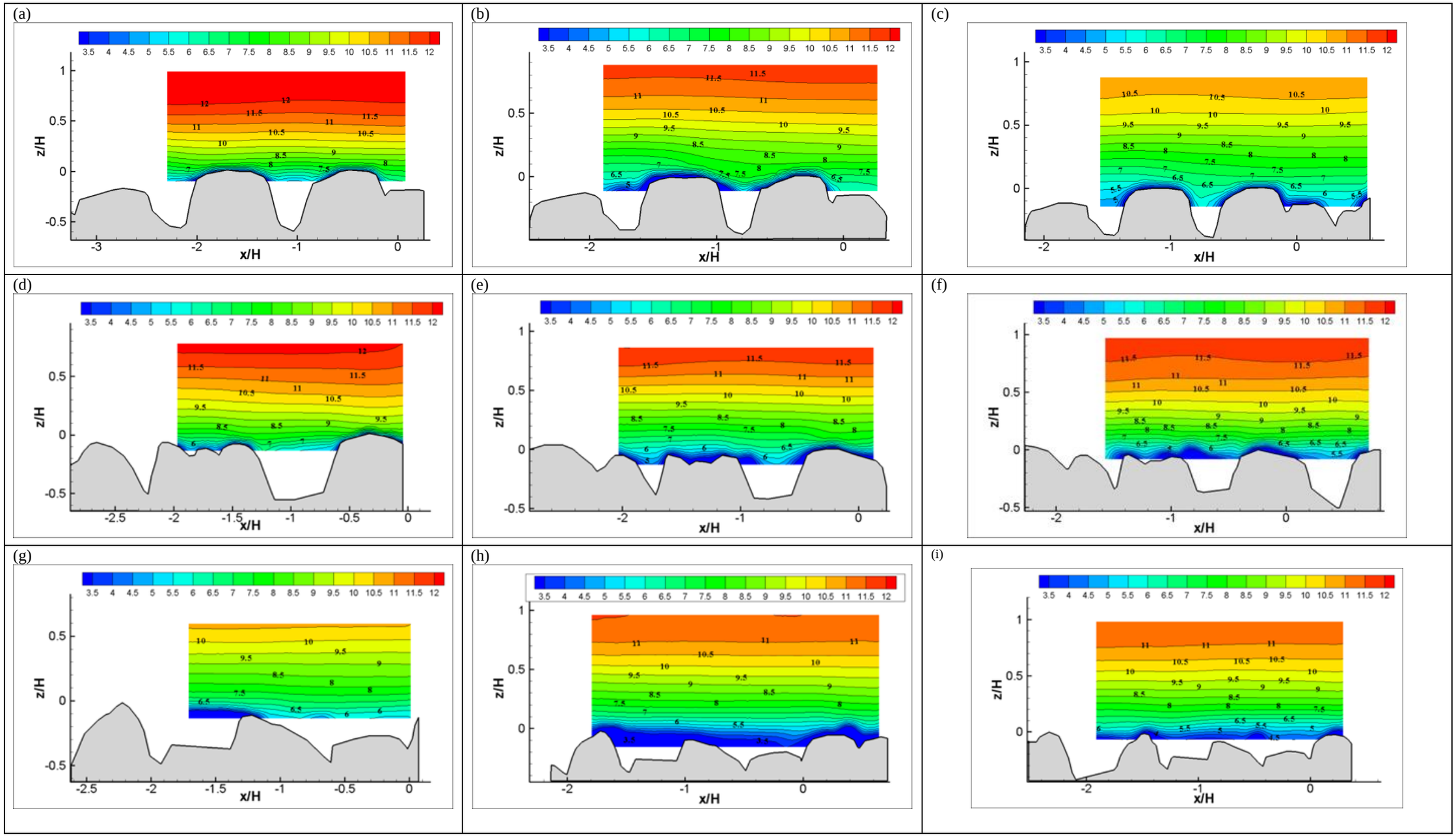

Figure 5-4: Contour map of $\bar{u}/u_*$ in vertical planes (a) plane 1, Run (I) (b) plane 1, Run (II) (c) plane 1, Run (III) (d) plane 2, Run (I) (e) plane 2, Run (II) (f) plane 2, Run (III), (g) plane 3, Run (I) (h) plane 3, Run (II) (i) plane 3, Run (III),flow left to right.

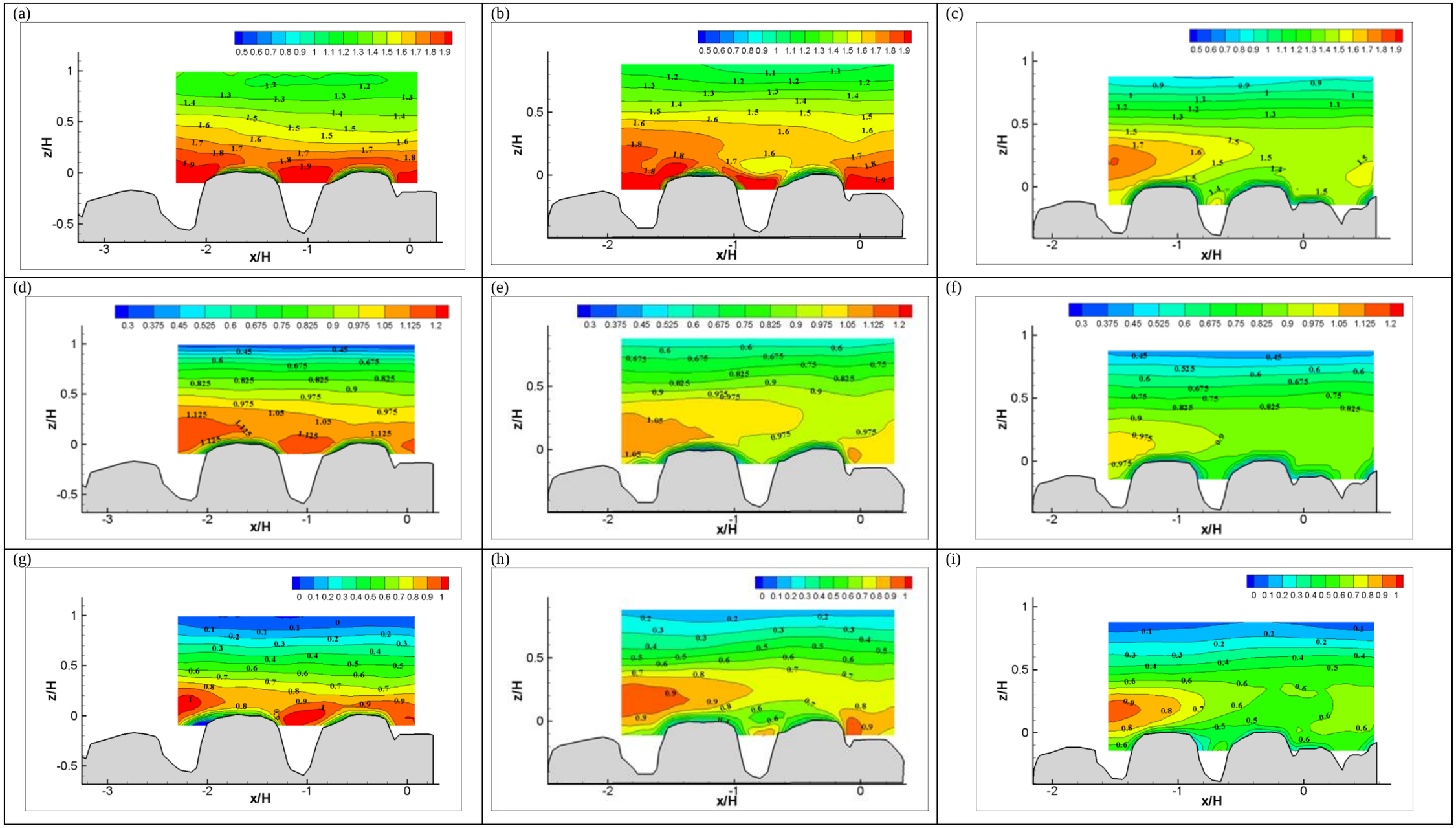

Figure 5-5: Contour map of turbulent intensities and Reynolds stress in vertical plane (plane 1) (a) σ_u/u_* for Run (I) (b) σ_u/u_* for Run (II) (c) σ_u/u_* for Run (III) (d) σ_w/u_* for Run (I), (e) σ_w/u_* for Run (II) (f) σ_w/u_* for Run (III) (g) $-\overline{u'w'}/{u_*}^2$ for Run (I) (h) $-\overline{u'w'}/{u_*}^2$ for Run (II) (i) $-\overline{u'w'}/{u_*}^2$ for Run (III),flow left to right.

5.2 DOUBLE AVERAGED TURBULENCE STATISTICS

Double Averaged Reynolds Shear Stress (DARSS) profiles along three different planes in Run (II) are shown in Figure 5-6. In this figure, $-\langle\overline{u'w'}\rangle$ is DARSS where $\langle\overline{....}\rangle$ denotes a DA quantity (first in time, $\overline{...}$ and after in space, $\langle...\rangle$). One can see that DARSS profiles in plane 1 and plane 2 have negative curvature and experimental points tend to be located above the expected theoretical triangular profile, while DARSS profile in plane 3 has positive curvature and is located below triangular profile. This is consistent with presence of secondary currents which causes deviation of $-\langle\overline{u'w'}\rangle$ distribution from linear distribution in 2D open channel flows (Nezu and Nakagawa, 1993; Albayrak and Lemmin, 2011). Plane 1 and plane 2 are located in regions where upward flow is predominant, while plane 3 is in downward flow region (see Figure 5-1). Similar trend has been observed in previous studies (Nezu and Nakagawa, 1993; Nikora et al., 1998b; Albayrak and Lemmin, 2011). Difference of DARSS profiles in the three planes shows that its transversal variations are significant. This leads to the conclusion that when DA is performed, different longitudinal planes at different transversal positions have to be considered in order to properly take into account also spatial heterogeneities induced by secondary currents. In present study, double averaging is done among all measured planes in order to consider transversal variation as much as possible. As an example, red line in Figure 5-6 is DARSS profile averaged along three planes for Run (II). This line is close to triangular distribution expected for 2D open channel flows.

Measured Double Averaged Turbulent Intensities (DATI) for the three runs reported in Figure 5-7, together with semi-empirical best fitted curves proposed by Manes et al. (2007). Figure 5-7a shows that profiles of streamwise DATI are similar and almost overlap. Only at the near bed region ($z/H < 2.5\sigma_l$) small differences are notable. In particular, streamwise DATI tend to reduce for relative submergence increase, i.e. for increasing. roughness (k_s^+). This finding is in agreement with the results of Grass (1971), Bayazit (1976), Nezu & Nakagawa (1993) and Wang et al. (1993). On the other side, Manes et al. (2007) did not find any significant changes of

DATI with RS variation.

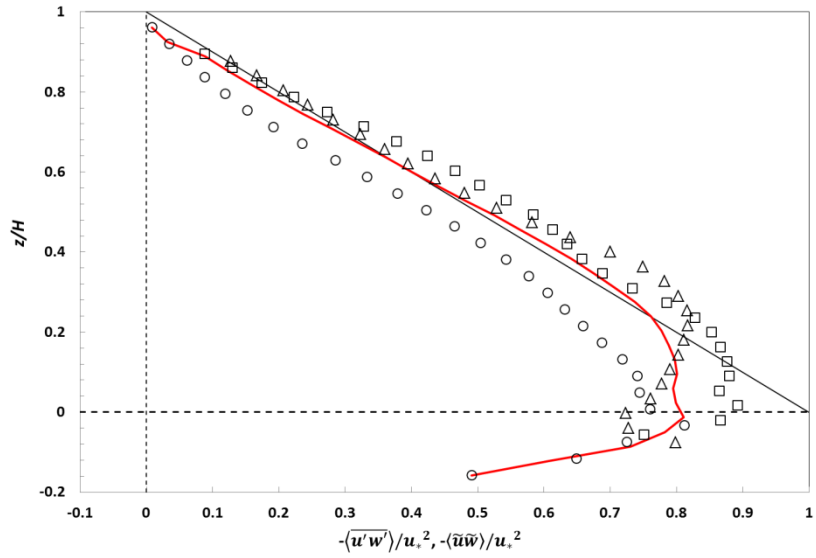

Figure 5-6: Comparison of double averaged Reynolds shear stress (DARSS) among cross-section: Δ Plane 1; □ Plane 2 ○ Plane 3, red line is averaged values among three planes.

As far as the normalwise DATI profiles are concerned, different to Manes et al. (2007) findings which did not notice any dependence on RS, it can be clearly observed that in present data DATI values tend to increase all along the flow depths for decreasing RS (see Figure 5-7b). Bearing in mind that in present experiments decreasing relative submergence corresponds to decreasing bed roughness, actual findings are in contrast to what reported by Grass (1971) and Nezu and Nakagawa (1993), for which as the roughness increases, a tendency to an increase in the normalwise component of turbulent intensity is expected in the near bed region ($z/H < 0.3$). This behaviour calls in present data for a dependence of the turbulent structure of the flow field on the relative submergence more than on the bed roughness.

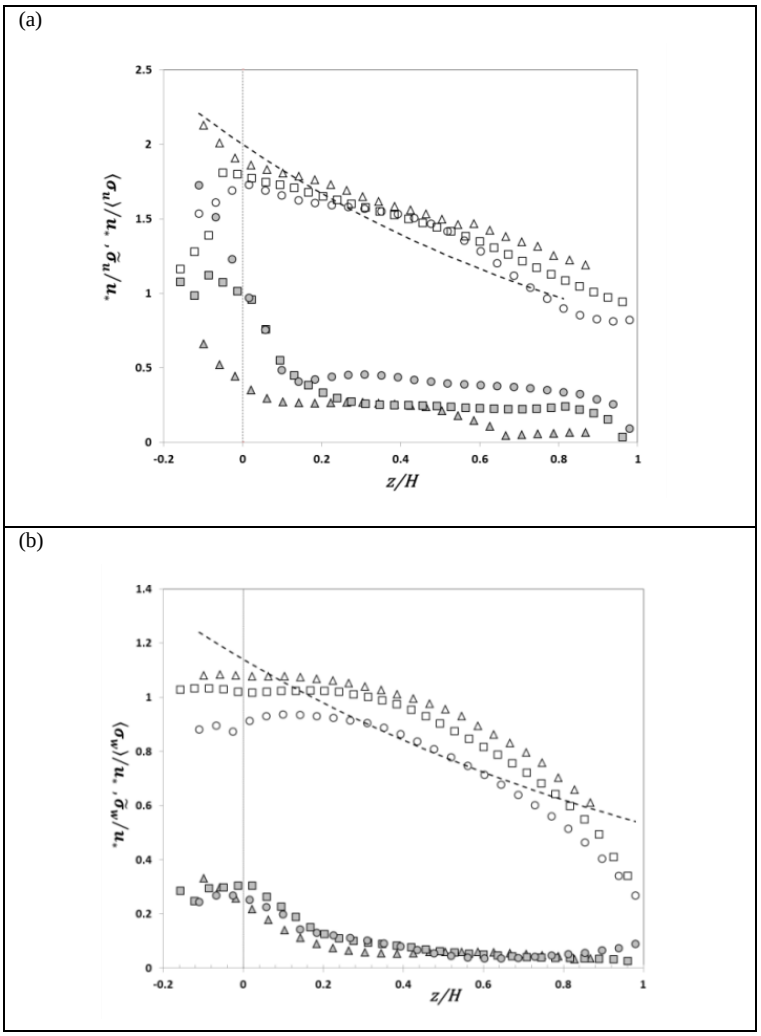

Figure 5-7: Double averaged turbulent intensity (DATI) profiles (open symbols) and Form induced (FITI) profiles (filled symbols): (a) Streamwise component, $\langle\sigma_u\rangle/u_*$, $\langle\tilde{\sigma}_u\rangle/u_*$ (b) Normalwise component, $\langle\sigma_w\rangle/u_*$, $\langle\tilde{\sigma}_w\rangle/u_*$; Δ Run (I); □ Run (II) ○ Run (III).

The analysis of Form Induced Turbulent Intensities (FITI) profiles (Figure 5-7a, b) indicates that on the contrary of Manes et al. (2007) and of Dey and Das (2012) findings, no clear peak for FITI is detected at the gravel crests region. The normalwise component of FITI assume values at the crest ranging between 0.2 and 0.3, similar to that obtained by Manes et al. (2007) and by Dey and Das (2012). The maximum measured values of the streamwise component of FITI in the roughness layer ranges between 0.7 and 1.7, that are less than one half of the

maximum values measured in the same region by Manes et al. (2007), but very similar to that obtained by Dey and Das (2012). However, looking deeper at the streamwise FITI shows that they increase with relative submergence, especially in the interfacial-sublayer.

5.3 DOUBLE AVERAGED VELOCITY PROFILE

As mentioned in introduction (see page 28, Gravel Bed Flow), shape of double averaged velocity profile in flow type (II) follows logarithmic formula:

$$\frac{\langle \bar{u} \rangle}{u_*} = \frac{1}{\kappa_{(H/\Delta)}} ln\left(\frac{z-d}{\Delta}\right) + C = \frac{1}{\kappa_{(H/\Delta)}} ln\left(\frac{z-d}{z_o}\right) \quad (5\text{-}1)$$

where κ is von Kàrmàn constant, d is zero-plane displacement level, z_o is hydrodynamic roughness length and C is additive constant. In this study, roughness scale (Δ) is assumed to be the standard deviation of bed elevation (σ_l). Estimation of log-law parameters together with zero-plane displacement level and log-law bounds is complicated in flow type (II). Following Nikora et al. (2002), these values can be extracted from equation:

$$(d\langle \bar{u} \rangle / dz)^{-1} = \frac{\kappa}{u_*}(z-d) \quad (5\text{-}2)$$

This linear relation is valid only in the logarithmic region. Thus, bounds of log-law can be assumed as region where Eq. (5-2) is valid. Moreover, in this equation, d can be determined from ratio of intercept to slope of linear regression equation in logarithmic region, without any needs to estimate shear velocity (Nikora et al., 2002). Also, von Kàrmàn constant can be obtained from equation:

$$\kappa = \frac{u_*}{(z-d)} (d\langle \bar{u} \rangle / dz)^{-1} \quad (5\text{-}3)$$

Once d is estimated from Eq. (5-2) and u_* is estimated by DARSS profile, Eq.(5-3), which is equivalent to Eq. (5-2), may be useful also as an additional diagnostic tool to check the bounds of log-law. In present study, this method applied to each measurement plane, separately. Summary of estimated values are reported in Table 5-1. Estimation of d, κ from Eq.(5-2) and Eq.(5-3) in different planes and runs are shown in Figure 5-8 to Figure 5-10. Table 5-1 shows that variation of d, κ and estimated log-law bounds in different planes are notable. In Table 5-1, estimated shear velocity for different planes based on extrapolation of double averaged Reynold shear stress to gravel crests is also reported. The results show that, while in some planes detection of log-law region is clear (see e.g. Figure 5-8: a, b), it is difficult to accept that this region be present in some other planes (see e.g. Figure 5-9a, b).

Table 5-1: Summary of estimated zero-plane displacement level, log-law bounds and von Kàrmàn constant in present study.

	Run (I)						
	d (mm)	κ	Z_R (mm)	Z_R/H	Z_L (mm)	Z_L/H	u_* (m/s)
Plane 1	-12.8	0.2	4.1	0.1	17.0	0.4	0.029
Plane 2	-11.4	0.3	2.7	0.1	19.0	0.5	0.028
Plane 3	-9.8	0.3	13.3	0.3	20.3	0.5	0.025
	Run (II)						
	d (mm)	κ	Z_R (mm)	Z_R/H	Z_L (mm)	Z_L/H	u_* (m/s)
Plane 1	-18.0	0.2	9.4	0.2	30.4	0.6	0.035
Plane 2	-17.3	0.2	12.3	0.2	35.2	0.7	0.034
Plane 3	-17.4	0.2	9.0	0.2	34.9	0.7	0.031
	Run (II)						
	d (mm)	κ	Z_R (mm)	Z_R/H	Z_L (mm)	Z_L/H	u_* (m/s)
Plane 1	-18.7	0.2	14.1	0.2	37.0	0.6	0.040
Plane 2	-14.0	0.3	11.4	0.2	34.8	0.6	0.040
Plane 3	-12.1	0.3	5.5	0.1	32.2	0.5	0.041

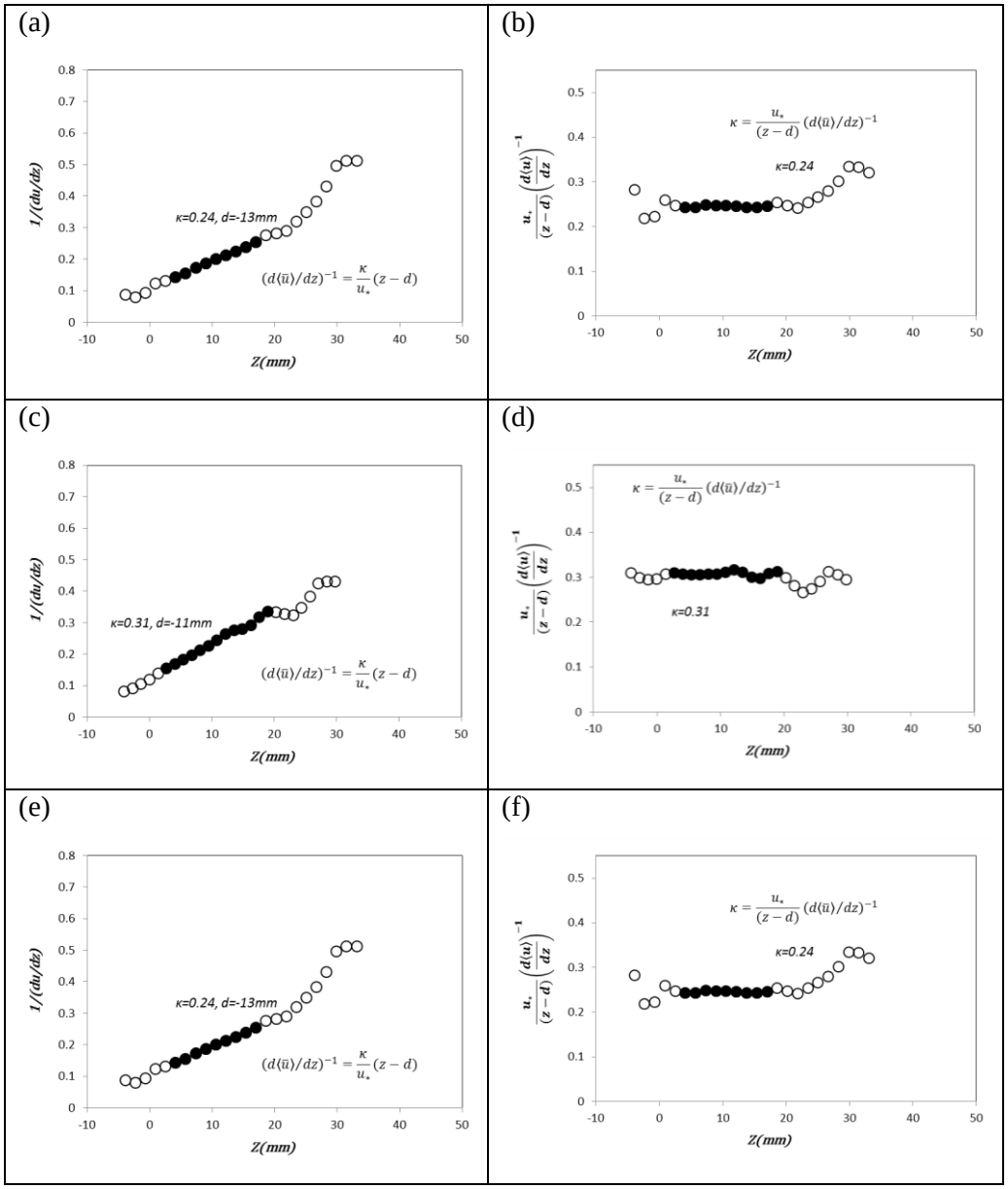

Figure 5-8: Determination of κ, d for three planes in Run (I) (a) Estimation of κ, d (b) Estimation of κ in plane 1 (c) Estimation of κ, d (d) Estimation of κ in plane 2 (e) Estimation of κ, d (f) Estimation of κ in plane 3; ○Experimental data in total depth ●Experimental data in estimated log-law region.

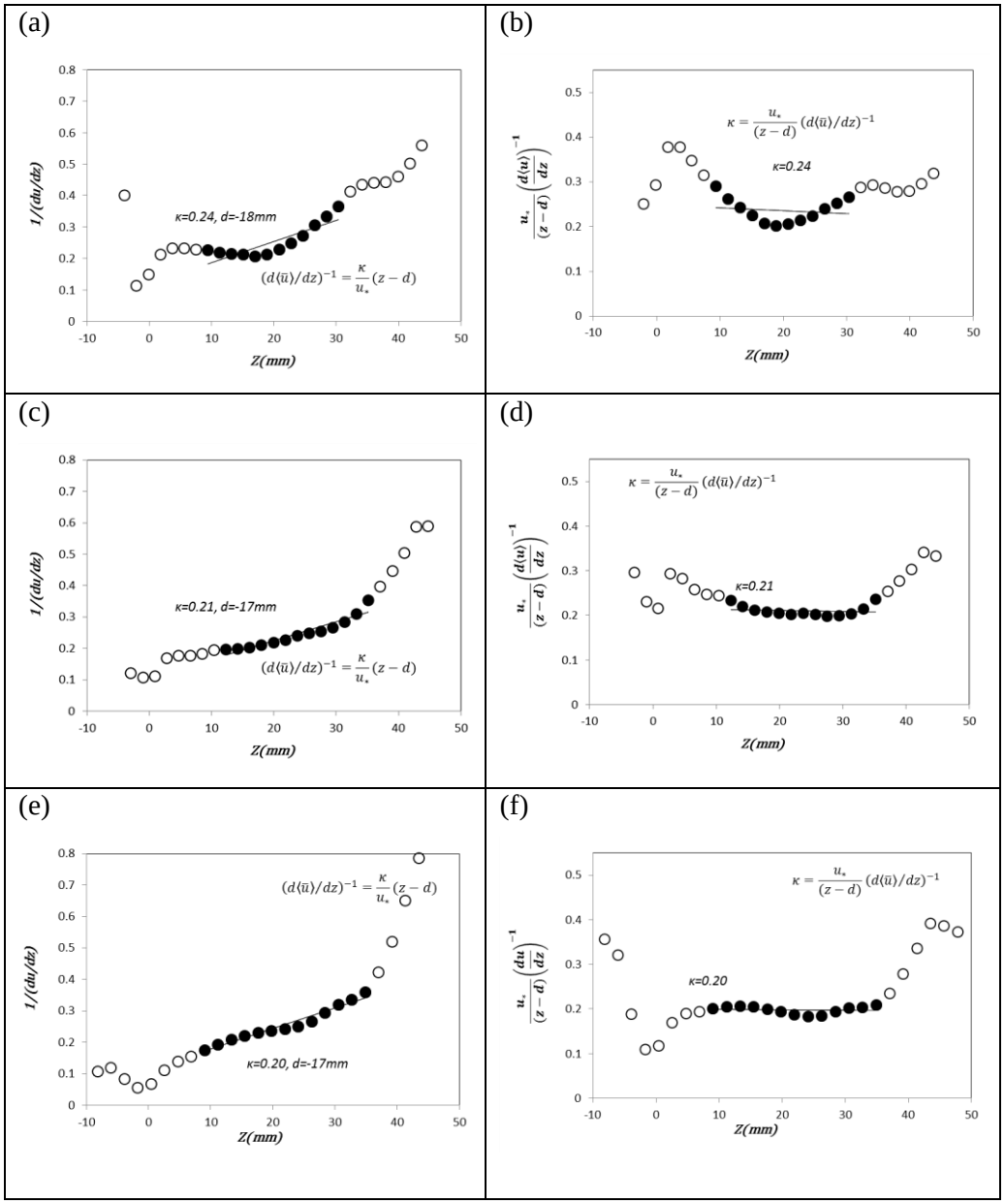

Figure 5-9: Determination of κ, d for three planes in Run (II) (a) Estimation of κ, d (b) Estimation of κ in plane 1 (c) Estimation of κ, d (d) Estimation of κ in plane 2 (e) Estimation of κ, d (f) Estimation of κ in plane 3; ○Experimental data in total depth ●Experimental data in estimated log-law region.

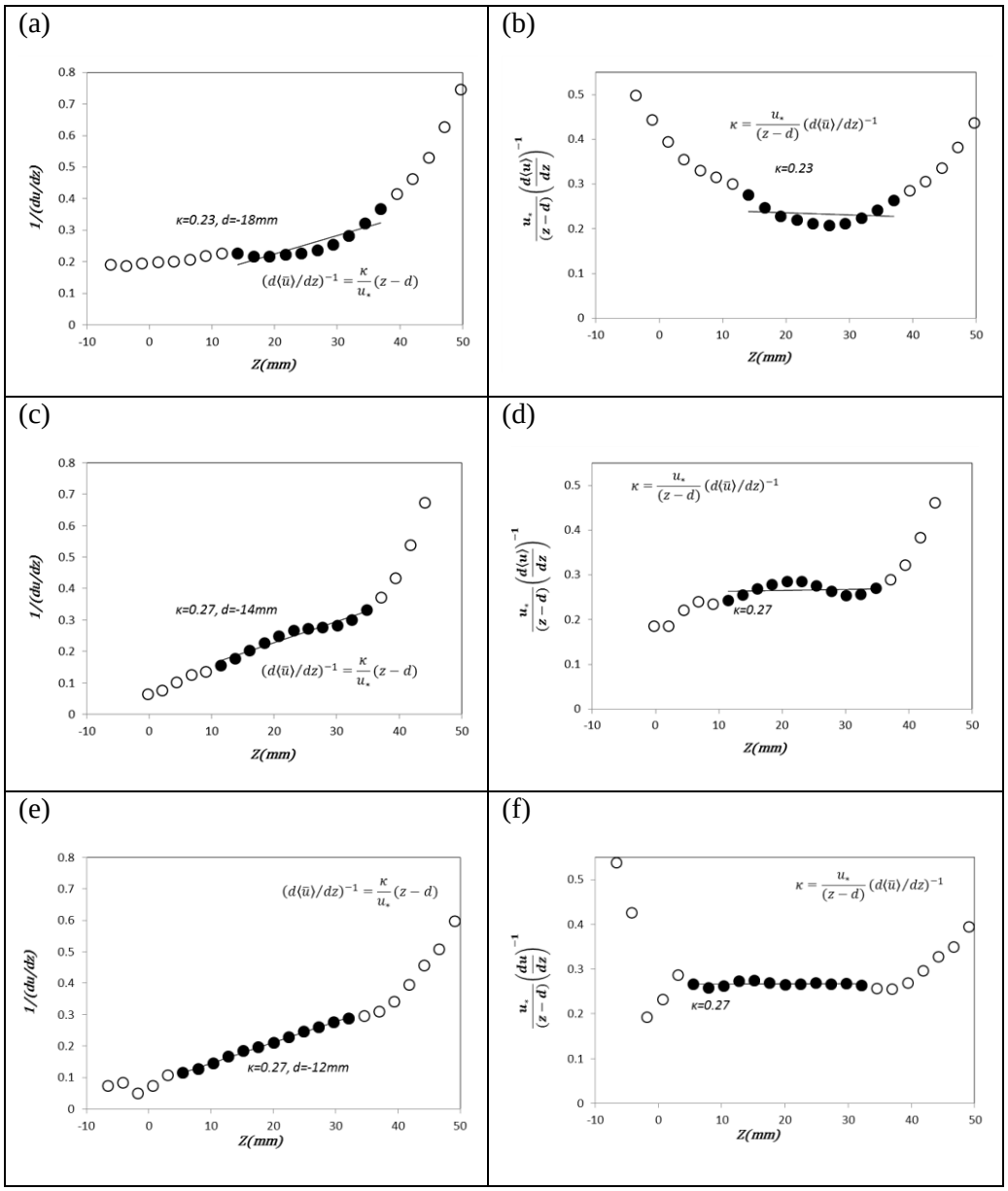

Figure 5-10: Determination of κ, d for three planes in Run (III) (a) Estimation of κ, d (b) Estimation of κ in plane 1 (c) Estimation of κ, d (d) Estimation of κ in plane 2 (e) Estimation of κ, d (f) Estimation of κ in plane 3; ○Experimental data in total depth ●Experimental data in estimated log-law region.

It has been observed that in shallow flows, von Kàrmàn constant assumes

values smaller than 0.41 which vary with relative submergence (Koll, 2006; Gaudio et al., 2010). However, effect of relative submergence on zero-plane displacement level has not been specified yet. In fact, it is not clear whether zero-plane displacement level is only a function of bed geometry or if and how does it change with flow conditions. In present study, while zero-plane displacement level varies, its variations are not systematic. This problem needs to be better clarified in future studies.

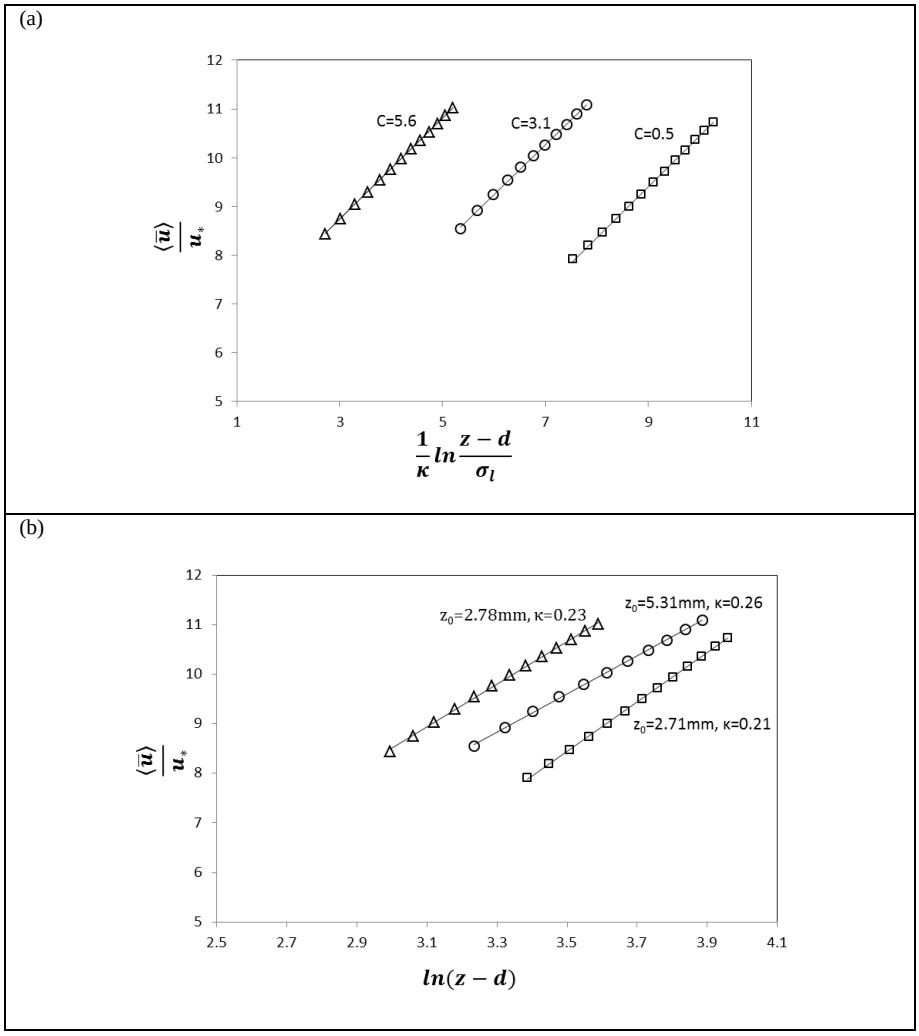

Figure 5-11: Results of applying logarithmic velocity profile in plane 2 (middle of channel) (a) with constant C form (b) with hydrodynamic roughness length (z_0) and κ estimated from Eq. (1) instead of Eq. (2); Δ Run (I); □ Run (II) ○ Run (III).

5.4 INSTANTANEOUS FLOW FIELD

In Figure 5-12a, b, two snapshots sequence of instantaneous vorticity field accompanying with vector field measured in streamwise vertical plane (3) for Run (I) is shown. In these figures, velocities are decomposed based on Galilean approach with convective velocity u_c=[0.85U, 0] instead of Reynolds decomposition (Pope, 2000). The main reason for this choice is that shear between structures with Galilean decomposition are preserved. Also, as Navier-Stokes equations are not sensitive to Galilean transformation, the convection velocity can be consider directly in the Navier-Stokes equations with no necessity to Reynolds stress modification (Adrian et al., 2000b).

In the boundary layer flows, the background shear is significant and vorticity cannot identify vortexes properly (Hunt et al., 1988; Jeong and Hussain, 1995). Complex eigen values of velocity gradient tensor have been proposed to solve this problem (Jeong and Hussain, 1995; Adrian et al., 2000a).

The two-dimensional swirling strength (λ) defined as in Eq. (5-4) is used to identify vortex cores:

$$\lambda = \max[0, -\frac{\partial u}{\partial y}\frac{\partial v}{\partial x} + \frac{1}{2}\frac{\partial u}{\partial x}\frac{\partial v}{\partial y} - \frac{1}{4}\left(\frac{\partial u}{\partial x}\right)^2 - \frac{1}{4}\left(\frac{\partial v}{\partial y}\right)^2] \qquad (5\text{-}4)$$

Lines of constant value of λ are shown in Figure 5-12c and Figure 5-12d with red color. In both of snapshots, there is good agreement between information obtained from vorticity, velocity and swirling strength fields. In Figure 5-12a wedge-like structure of the flow field is recognizable, with two well noticeable regions of high velocity and low velocity. Similar features of the flow field were present also in all the vertical planes of other runs. The shear layer between these regions is inclined in streamwise direction with approximate angle of 30^o. Contour lines of swirling strength show that the strip at the inclined shear layer, located just at the boundary of high and low velocity regions, is rich of small eddies. These eddies typically initiates at gravel crests and move downstream with positive normal velocity, so transferring to upper part of the flow field. Vortices are stronger near the

bed and attenuate during their flapping transport and stretching moving downstream. However, in many instants it has been observed that these packets are able to reach the water surface. These features are consistent with previous findings of Roy et al. (2004) and Detert et al. (2010).

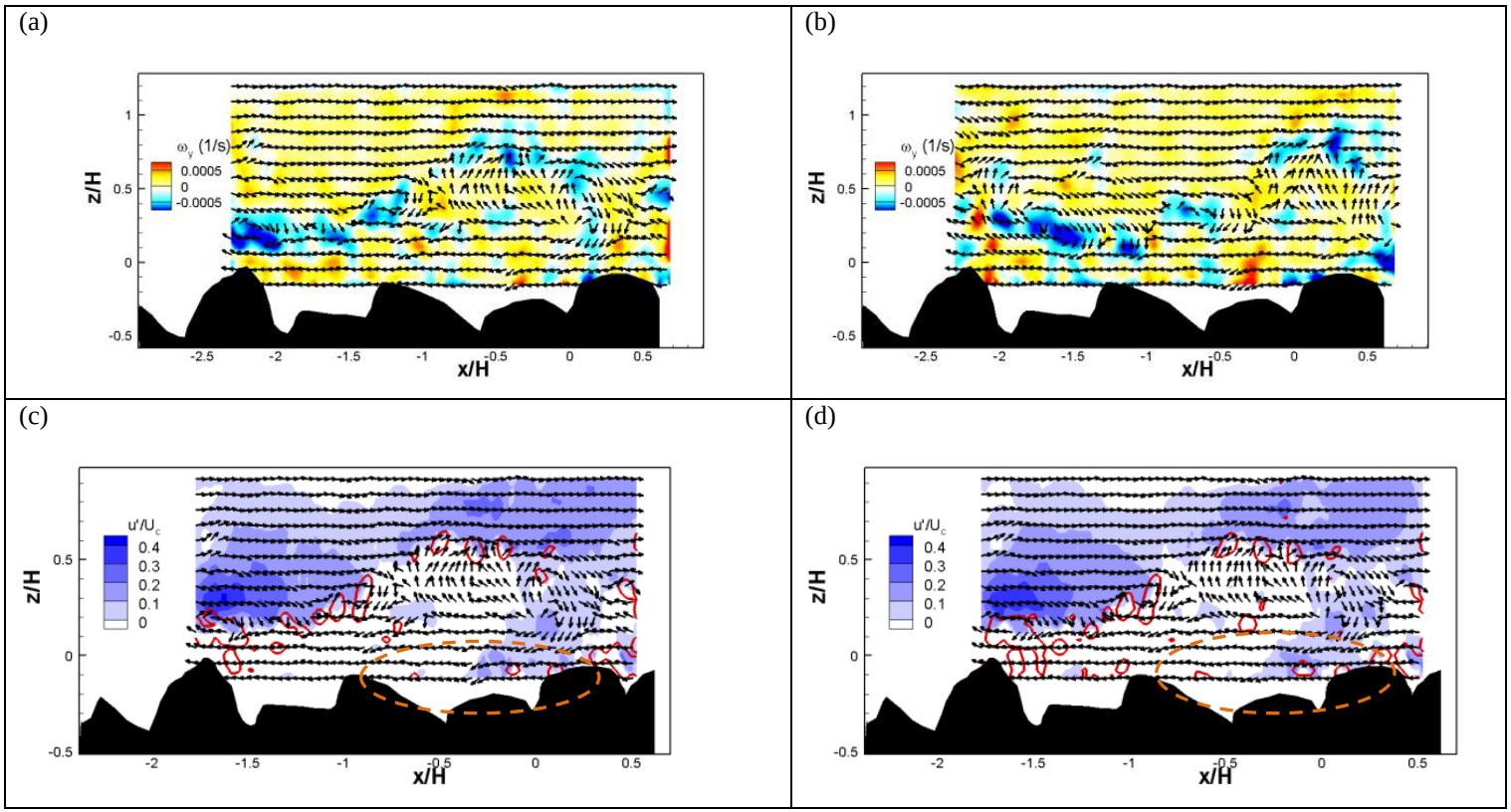

Figure 5-12: Sequence of two snapshots of instantaneous velocity fields with Δt=80 ms in Run (I) vertical plane 3. In (a) and (b) colour map shows vorticity and vector based on Galilean decomposition u_c=[0.85 U, 0], while in .c and .d colour map shows streamwise velocity fluctuation and red lines swirling strength. Photos (a) and (c) are at t=2.202s, photos (b) and (d) are at t=2.282s.

Obviously not only these kinds of vortices could be present, other kinds of coherent structures over rough bed have been detected in previous works, such as hairpin vortexes (Volino et al., 2007) or horseshoe-type vortexes around large protruding pebbles (Bomminayuni and Stoesser, 2011). Therefore, the description here presented is far to be exhaustive of the complex flow field in the near bed region, and has only the aim to highlight what seems to be the kind of coherent structure which mostly seems to mark the near bed turbulence dynamics.

In Figure 5-13, similar to Figure 5-12, two sequence of instantaneous vorticity, Galilean vector field decomposition (u_c=[0.53U, 0]), swirling strength, and streamwise Reynolds velocity fluctuation are shown for the horizontal layer acquisition in Run (I). In Figure 5-13, vortices are generated and then transported downstream. Meanwhile they convey downstream, they get out of the measurement layer. Also, typical picture of streaky structure of elongated high and low velocities can be identified. Similar streaky structure has been observed in previous studies above rough bed (Defina, 1996; Nino and Garcia, 1996; Detert et al., 2010) and are consistent with the '*chessboard*' pattern with regions of lower and higher velocities described by Detert et al. (2010).

In Figure 5-13, horizontal black dashed lines are corresponded to maximum of low and high time averaged streamwise velocity strips shown in Figure 5-1a, b, c. Comparison of instantaneous streaky structure with dashes lines shows that velocity fluctuations are stronger along these lines (Figure 5-13c, d) and also the sign of vorticity changes in this region (Figure 5-13a, b). In agreement with what are seen in Figure 5-13, Mejia-Alvarez and Christensen (2013) and Barros and Christensen (2014) observed that sign of longitudinally elongated vortexes are changed (swirling strength equal to zero ($\lambda = 0$)) in the center of time averaged velocity strips. This consistency express that, as highlighted by Barros and Christensen (2014), the vortical motion of the flow can provide a mechanism for generation and maintenance of the time averaged velocity strips.

While streaky structure in rough beds was seen in Figure 5-13, it is worth to be noted that in some regions there are also persistency of vertical axis vortex presence. As an example, some regions are highlighted with yellow circle dashed lines, which are the regions of strong protrusion of isolated gravel crest. In these

regions, vortices generate and then convey downstream through streaky structure. This shows that unlike smooth walls, locations of vortexes generation do not distribute randomly through bottom of the channel and they are mostly occured around gravel crests.

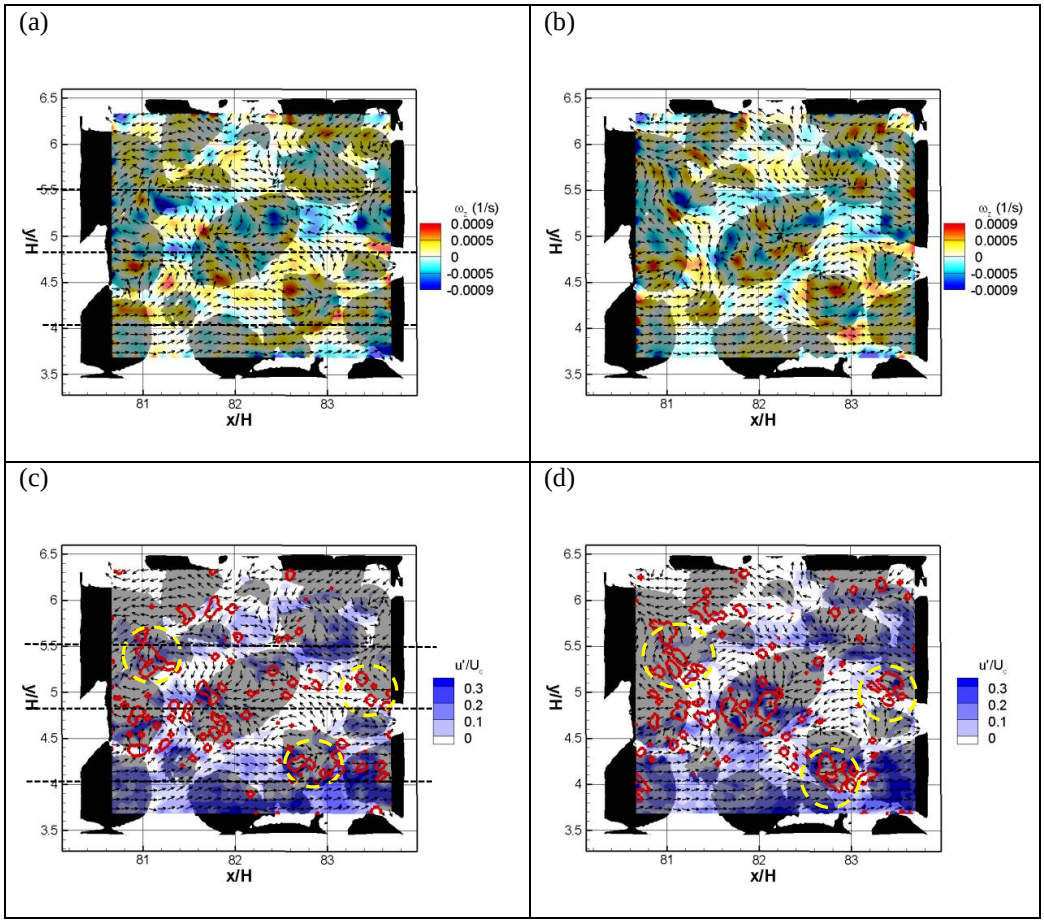

Figure 5-13: Sequence of two snapshots of instantaneous velocity fields with D*t*=80ms in Run (I) and in gravel crest. In (a) and (b) plots colour map shows vorticity and vector based on Galilean decomposition u_c=[0.53 U, 0]. In (c) and (d) plots colour map shows streamwise velocity fluctuation and red lines swirling strength. Photos (a) and (c) are at *t*=2.202s, photos (b) and (d) are at *t*=2.282s.

6 Sediment Transport Process and Turbulent Flow

Abstract:

This chapter is complementary analysis of the data. In this chapter, turbulent flow is considered in the context of sediment transport. At first vertical component of the velocity is analysed through modified Wei and Willmarth (1991)'s method presented in "Theoretical Background" chapter. Also, results of applying quadrant analysis to our experimental data are reported in this section. It was found that momentum flux is generally upward along water depth. Below gravel crests, asymmetry of mean vertical velocity is negative. In this region, momentum flux due to the turbulence is also downward. However, our results show that below gravel crests form induced vertical stress contributes noticeable upward momentum flux. The behaviour of vertical velocity is in agreement with occurrence of bursting process through water depth. Analysis of this chapter shows that movement of vertical flow and momentum transport are also in agreement with bed topography.

6.1 ANALYSIS OF WEI AND WILLMARTH (1991)'S METHOD

In the first step, mean values of vertical velocity in the vertical planes are considered. Figure 6-1a depicts contour maps of the vertical velocity normalized with respect to u_* in the vertical plane (1) for run (I). In previous studies, it has been observed that vertical velocity is positive in upstream side and negative in downstream side of roughness elements. As an example, Dancey et al. (2000) found positive and negative vertical velocity, respectively, in the zones upstream and downstream of uniformly-distributed balls. In the case of random gravel bed, Mclean and Nikora (2006) observed that the form induced component of vertical velocity ($\widetilde{w}$) is positive and negative in upstream and downstream sides. This behavior is in agreement with spatial organization of vertical velocity in horizontal layer described in previous chapter. In Figure 6-1a and in the near bed region ($z/\sigma_l < 2.5$), the vertical velocity is heterogeneous with patches of high positive and negative values. In analogy to what observed in previous studies and also present study measurements in horizontal layer, the spatial variation of vertical velocity is in agreement with the bed topography. Indeed, in Figure 6-1a at the upstream face of the gravel crests, flow is diverted upwards, while at the downstream face, downward flow occurs.

In Figure 6-1b, profiles of double averaged vertical velocity normalized with cross-section averaged streamwise velocity ($\langle\overline{W}\rangle/U_{ave}$ where U_{ave} is cross-section averaged streamwise velocity) is shown. Values of cross-section averaged streamwise velocity are reported in Table 3-1. In order to satisfy the continuity equation, double averaged vertical velocity should be zero. Profiles in Figure 6-1b show that along water depth normalized double averaged vertical velocities are smaller than 0.005 (Black bold line in Figure 6-1b). In near bed region ($\frac{z}{H} < 0$) and only in Run (II) and (III) $\langle\overline{W}\rangle/U_{ave}$ is higher than 0.005, albeit the values are not significantly high $|\langle\overline{W}\rangle/U_{ave}| < 0.02$. These small non-zero values, especially in near bed region, can be associated with the PIV measurements uncertainty. Therefore, as the continuity assumption is almost satisfied for the present study experimental data, turbulent fluctuations of vertical velocity can be examined through Wei and Willmarth (1991)'s method.

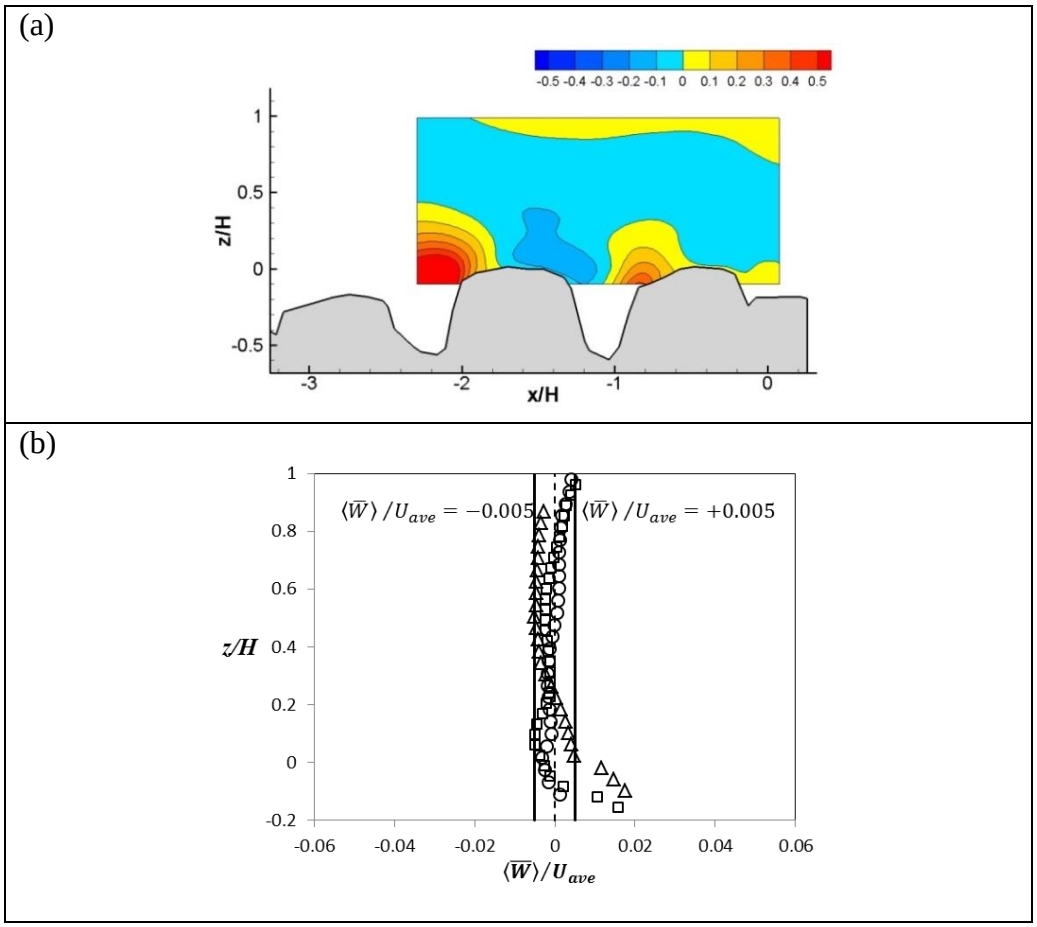

Figure 6-1: (a) Contour map of non-dimensional vertical velocity ($\overline{w}/u_*$) in vertical plane 1 for Run (I) (b) Profiles of double averaged vertical velocity normalized with area averaged streamwise velocity.

In Figure 6-2 the difference in the magnitude of upward vertical velocity ($|\overline{w_+}|$) and downward vertical velocity ($|\overline{w_-}|$) normalized with respect to u_* in the vertical plane 1 (Figure 6-2a) and the horizontal layer 1mm above gravel crests (Figure 6-2b) for run (I) are shown. The value of $|\overline{w_+}|$ and $|\overline{w_-}|$ expresses respectively the intensity of upward and downward flows. Based on Figure 6-2a, along most of the water depth $|\overline{w_+}|$ is higher than $|\overline{w_-}|$. So, high magnitude vertical velocity with short duration are common in most parts of the water column. However, in the near bed region $|\overline{w_+}|$ is lower than $|\overline{w_-}|$. There is also a consistency between variation of $|\overline{w_+}| - |\overline{w_-}|$ and bed topography, which is more clear in Figure 6-2b. Location of the regions that $|\overline{w_+}|$ is lower than $|\overline{w_-}|$ is mostly at the

downstream side of the gravels, while in the upstream side of the gravel crests usually $|\overline{w_+}|$ is higher than $|\overline{w_-}|$. This shows that high intensity with short duration upward flow is dominant in upstream side of gravel crests, while in downstream of gravel crests high intensity with short duration downward flow is common. However, flow around some gravels, due to orientation, spacing and shape of gravels, do not follow this rule. Like present results, Dancey et al. (2000) also found high negative values of $(|\overline{w_+}| - |\overline{w_-}|)/u_*$ on the downstream side of roughness elements, although their results do not show high positive values of $(|\overline{w_+}| - |\overline{w_-}|)/u_*$ in upstream side of roughness elements.

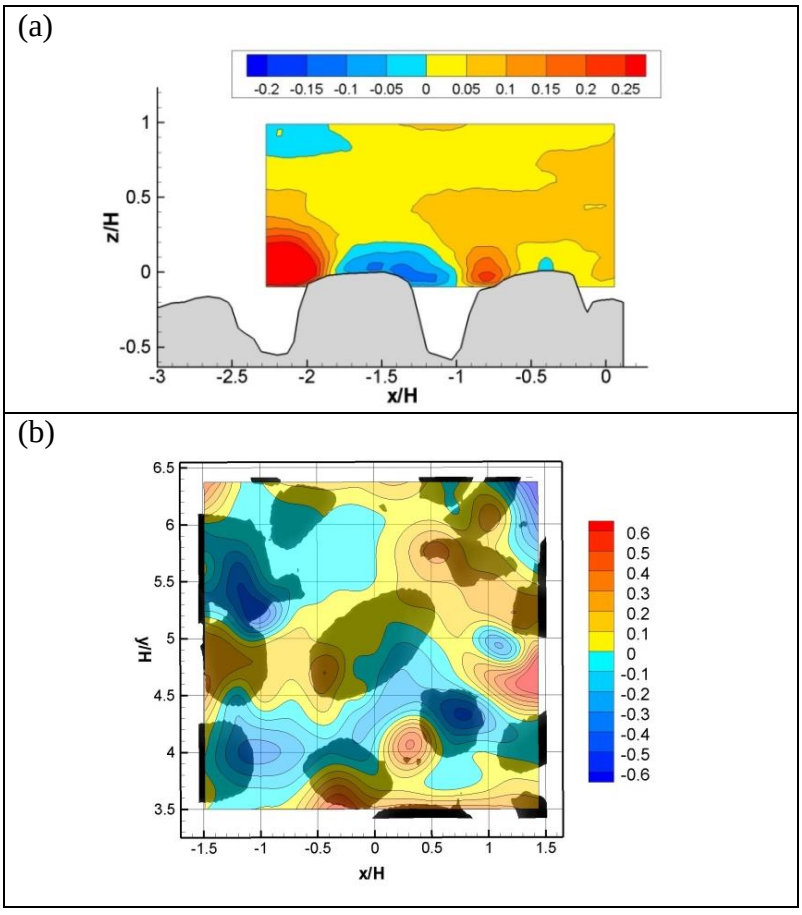

Figure 6-2: Contour map of $(|\overline{w_+}| - |\overline{w_-}|)/u_*$ (a) in vertical plane 1 (b) in horizontal layer 1mm above the crest for Run (I), flow from left to right.

For smooth bed, profiles of $(|\overline{w_+}| - |\overline{w_-}|)/u_*$ mostly have positive values, except in in $10 < z_+ < 30$ (where $z_+ = zu_*/\nu$) values of $(|\overline{w_+}| - |\overline{w_-}|)/u_*$ become negative (Wei and Willmarth, 1991). In rough bed, Dancey et al. (2000) found positive values of $(|\overline{w_+}| - |\overline{w_-}|)/u_*$ in the zone above roughness elements. Contour maps of $(|\overline{w_+}| - |\overline{w_-}|)/u_*$ above roughness elements in Dancey et al. (2000)'s study also shows noticeable spatial variation. As discussed in the theoretical background, to better consider near bed spatial variation, analysis of Wei and Willmarth (1991) should be supported by double averaging method. The double averaged profiles of $(|\overline{w_+}| - |\overline{w_-}|)/u_*$ for all three runs are reported in Figure 6-3a. The profiles for all three runs are positive in the region away from bed ($z/H > 0.1$). However, near the bed region ($z/H < 0.1$) profiles of run (II) and run (III) become negative, while run (I) is still positive. In all three runs the maximum positive asymmetry is located in the middle of the water column ($z/H = 0.5$). This means that, high intensity with short duration upward flow generally find in the region away from bed, while below gravel crests high intensity with short duration downward flow is common. Different behavior of run (I) in comparison to run (II) and run (III) can be attributed to slight variation in vertical planes location of run (I) as to run (II) and run (III). In fact, in run (I) upstream side of gravels are mostly captured in PIV collected photos. Therefore, the double averaged of $(|\overline{w_+}| - |\overline{w_-}|)/u_*$ is still positive.

In addition to the profiles of $\langle|\overline{w_+}| - |\overline{w_-}|\rangle/u_*$ (Figure 6-3a), the profiles of $|\langle\overline{w}\rangle_+|$ and $|\langle\overline{w}\rangle_-|$ difference are also shown in Figure 6-3b. This difference can be a representative for asymmetrical spatial variation of vertical velocity. In the region far from the bed ($0.2 < z/H < 0.6$) the absolute value of $|\langle\overline{w_+}\rangle| - |\langle\overline{w_-}\rangle|/u_*$ is smaller than 0.02. In the near bed region ($z/H < 0.1$), a rising trend of $|\langle\overline{w_+}\rangle| - |\langle\overline{w_-}\rangle|/u_*$ is notified which leads to positive values below gravel crests. The positive values of $|\langle\overline{w_+}\rangle| - |\langle\overline{w_-}\rangle|/u_*$ below gravel crests are higher in comparison to the values observed in the middle of water column. This means that below gravel crests, where form induced stress should consider, asymmetrical spatial variation of time averaged vertical velocity is also significant. Moreover, the positive value of $|\langle\overline{w_+}\rangle| - |\langle\overline{w_-}\rangle|/u_*$ in this region shows that large area has negative amplitude. These large negative areas offset by small area with high

positive vertical velocity which can push particles away from a gravel bed.

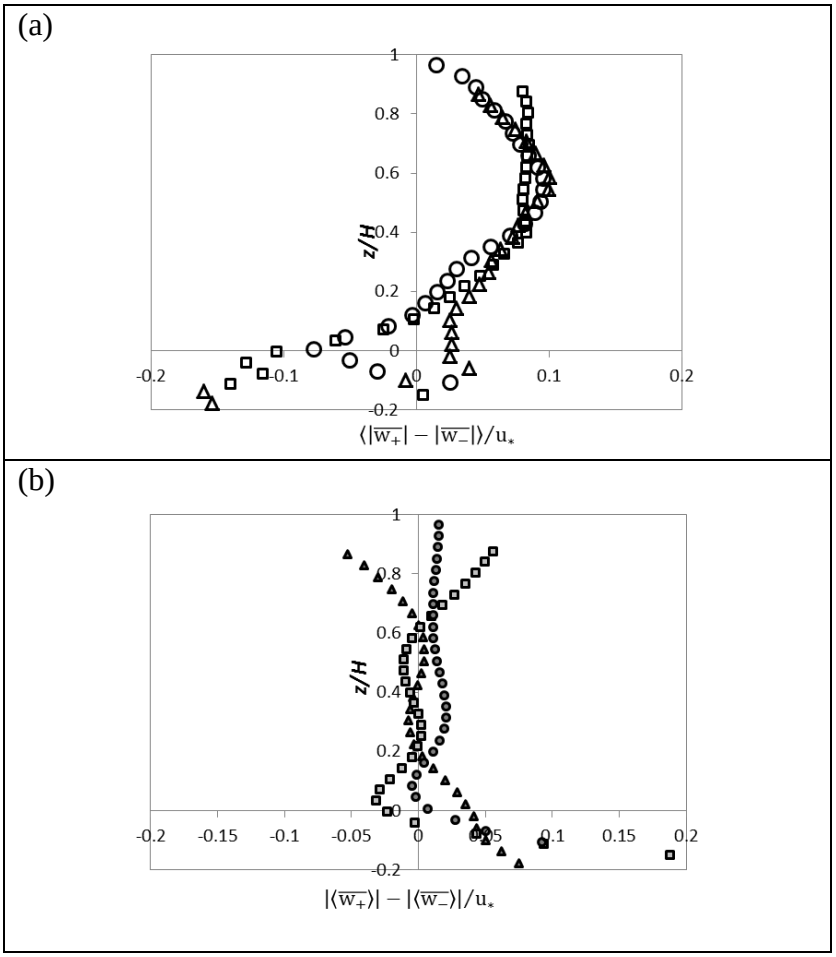

Figure 6-3: Profiles of (a) $\langle|\overline{w_+}| - |\overline{w_-}|\rangle/u_*$(open symbols) (b) $|\langle\overline{w_+}\rangle| - |\langle\overline{w_-}\rangle|/u_*$ (filled symbols) for three Runs; Δ Run (I); □ Run (II) ○ Run (III).

Figure 6-4 displays the spatial pattern of mean net vertical momentum flux due to velocity fluctuations. The values are normalized with respect to $u_*{}^2$. Similar to the observed distribution of mean vertical velocity, Figure 6-4a shows that $\overline{w'^2}^{NF}$ (Eq. (2-9)) in the vertical plane is mostly positive above the gravel crests. However, below the gravel crests there are some regions where negative values of $\overline{w'^2}^{NF}$ are found. Referring to both contour maps (Figure 6-4a and b) it is observed that in general negative values of $\overline{w'^2}^{NF}$ are found downstream of the gravels. Also, local

positive maximum of $\overline{w'^2}^{NF}$ are mostly found in upstream side of the gravels. Different to what have been seen in present study, Dancey et al. (2000) found that vertical net turbulent momentum flux is positive over the whole of their horizontal measurement layer above roughness elements. However, vertical mean flow and vertical momentum flux without mean vertical velocity subtraction in Dancey et al. (2000) measurements has negative values in the downstream side and local maximum positive values in upstream side of the roughness elements. They finally concluded that downward momentum flux is caused by mean flow motion, while upward momentum flux is attributed to turbulent velocity fluctuations.

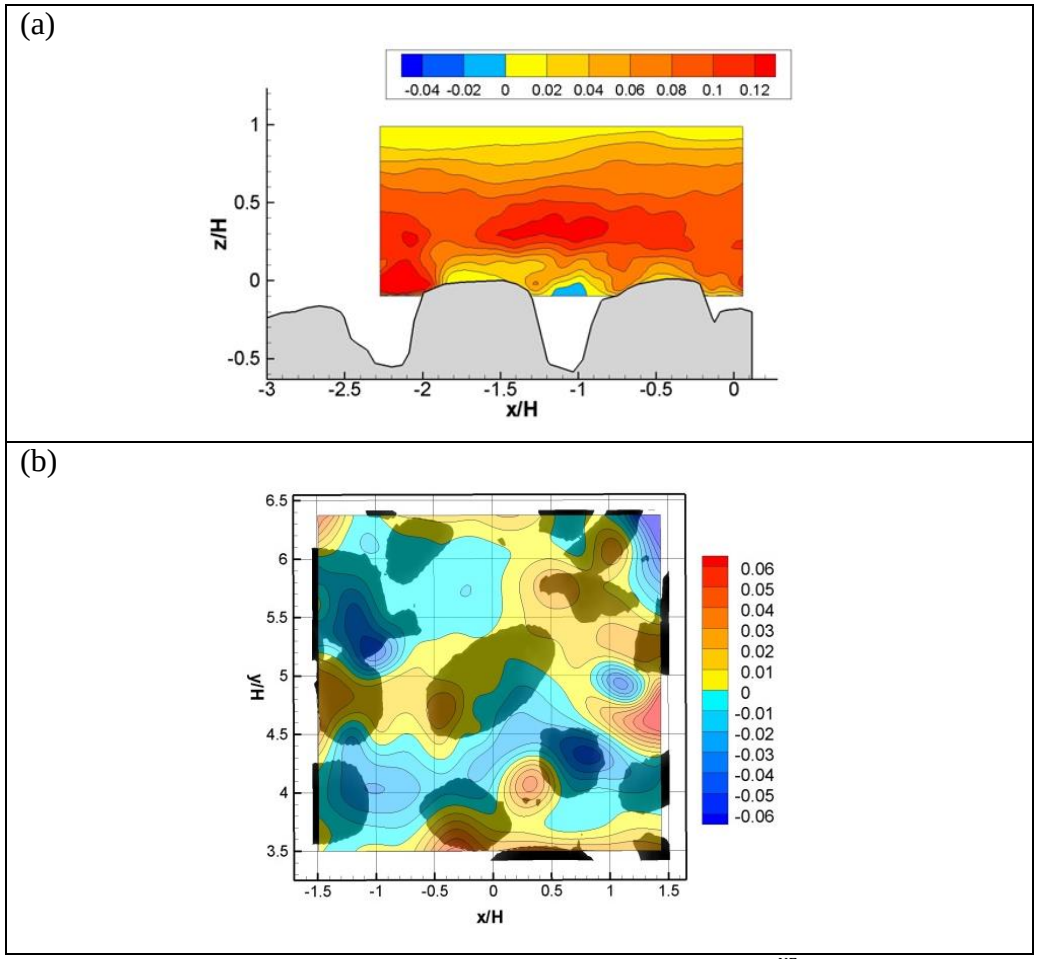

Figure 6-4: Contour map of non-dimensional vertical net momentum flux ($\frac{\overline{w'^2}^{NF}}{u_*^2}$) (a) in vertical plane 1 (b) in horizontal layer 1mm above the crest in Run (I), flow from left to right.

To further explore vertical momentum flux, the double averaging method was applied to the turbulent momentum flux. In Figure 6-5, profiles of double averaged upward and downward turbulent and form induced momentum fluxes are shown. The values are dimensionalized with second power of shear velocity. Both upward and downward turbulent momentum fluxes increase from water surface toward the bed. Near bed region ($z/H < 0.4$ in Figure 6-5a and $z/H < 0.3$ in Figure 6-5b) both upward and downward turbulent momentum fluxes become approximately constant. The exact location of maximum values of positive and negative turbulent momentum fluxes are not clear, however it seems that it is located in gravel crests. Finally, below gravel crests both upward and downward momentum fluxes attenuate abruptly. Note that reduction of upward turbulent momentum flux is much faster than downward turbulent momentum flux.

The form induced upward and downward momentum fluxes are not noticeable far from gravel bed. Near gravel bed ($z/H < 0.1$), both $\langle \widetilde{w}^2 \rangle_+ / u_*^2$ and $\langle \widetilde{w}^2 \rangle_- / u_*^2$ become significant. Near gravel crests ($-0.1 < z/H < 0.1$), dimensionless upward and downward momentum fluxes due to the spatial fluctuation are smaller than 0.3, while dimensionless upward and downward turbulent momentum fluxes are larger than 0.8. This expresses that although both upward and downward form induced momentum fluxes are not high, they are not negligible in comparison to upward and downward turbulent momentum fluxes.

The profiles of double averaged vertical net turbulent momentum flux ($\langle \overline{w'^2}^{NF} \rangle / u_*^2$) are shown in Figure 6-6a. The profiles of all three runs are observed to have maximum positive values in the middle of the water column ($z/H = 0.5$). The values decline from $z/H = 0.5$ to water the surface where $\langle \overline{w'^2}^{NF} \rangle / u_*^2$ is approximately equal to zero. From $z/H = 0.5$ towards the gravel bed $\langle \overline{w'^2}^{NF} \rangle / u_*^2$ reduce and for the zone below the gravel crests ($z/H < 0.0$) values become negative. Similar to this study, for the condition that bed forms are present, Bennett et al. (1998) found the maximum of vertical net turbulent momentum flux in $z/H = 0.5$. In agreement to Dancey et al. (2000), we found a region ($0.0 \leq z/H < 0.1$) where mean turbulent momentum flux is upward (Figure 6-6a), while magnitude of downward motions exceeds from upward motions (Figure 6-3a). Note that Dancey et al. (2000) measurements are only limited to a small horizontal layer

just above roughness elements. Below the gravel crests ($z/H < 0.0$), we observed that both vertical mean flow and momentum flux attributed to flow fluctuations were toward the bed (Figure 6-6a).

In Figure 6-6b, the net vertical momentum flux due to spatial heterogeneity of vertical velocity component ($\langle\widetilde{w}^2\rangle^{NF}/u_*^2$) is also shown. The values are negligible above the gravel crests. However in the near bed region ($z/H < 0.1$), they have an incremental trend to reach positive values. Comparison of Figure 6-6a and b shows that $\langle\widetilde{w}^2\rangle^{NF}/u_*^2$ and net turbulent vertical momentum flux are nearly at the same order of magnitude. It is interesting since as highlighted, in Figure 6-5 upward and downward form induced momentum fluxes are significant in comparison to upward and downward turbulent momentum fluxes, while their differences reaches approximately to the same order of magnitude. Near gravel bed, net turbulent and form induced momentum fluxes present opposite behaviors. Specifically, while near gravel bed $\langle\widetilde{w}^2\rangle^{NF}/u_*^2$ is upward directed, the $\langle\overline{w'^2}^{NF}\rangle/u_*^2$ is negative (tendency to transport mass in downward with turbulent momentum flux and upward with form induced momentum flux).

To better compare contribution of $\langle\widetilde{w}^2\rangle^{NF}/u_*^2$ and $\langle\overline{w'^2}^{NF}\rangle/u_*^2$ to vertical momentum flux, the total vertical net momentum flux (TNWF from Eq. (2-18)) is shown in Figure 6-6c. Profiles of all three runs in the region away from the bed ($z/H > 0.1$) are identical to the double averaged vertical net momentum flux profiles (Figure 6-6a) due to time fluctuations. However, in the near bed region ($z/H < 0.1$) the simultaneous effects of net momentum flux due to both time and space fluctuations is noticeable. It seems that in a level below gravel crests ($z/H < -0.1$) the values of form induced momentum fluxes are smaller than the values of vertical turbulent momentum flux and so total vertical net momentum flux become negative. However, from our data it is difficult to judge about the exact location of negative total vertical net momentum flux below gravel crests.

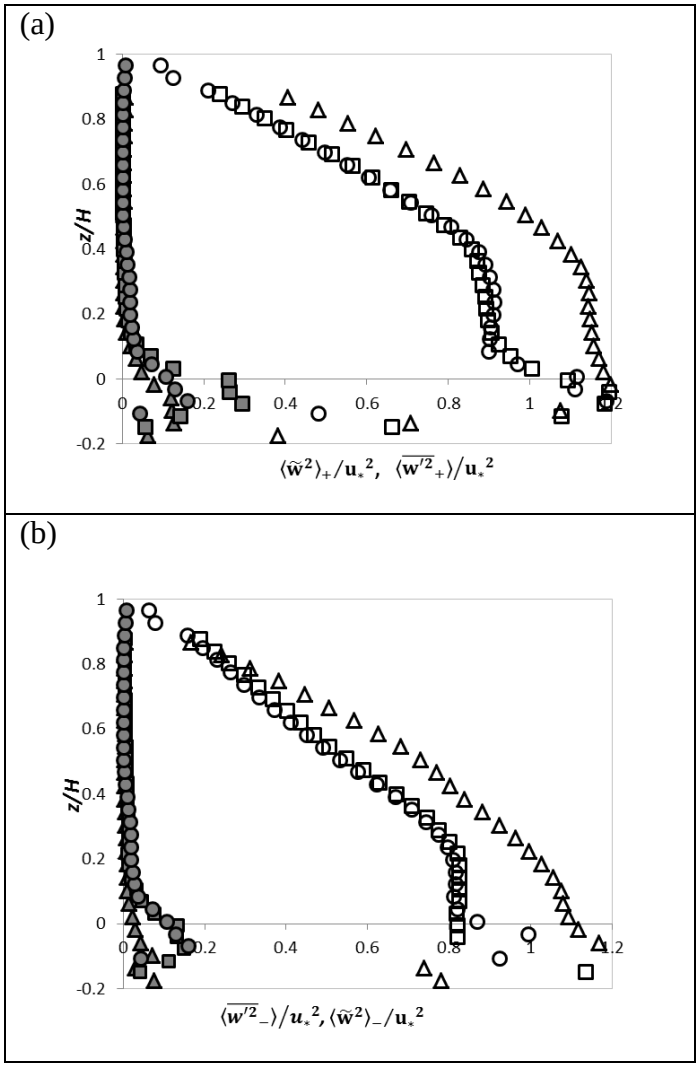

Figure 6-5: Profiles of double averaged (a) upward momentum flux profiles (b) downward momentum flux profiles (open symbols due to the turbulence; filled symbols due to the spatial fluctuations).

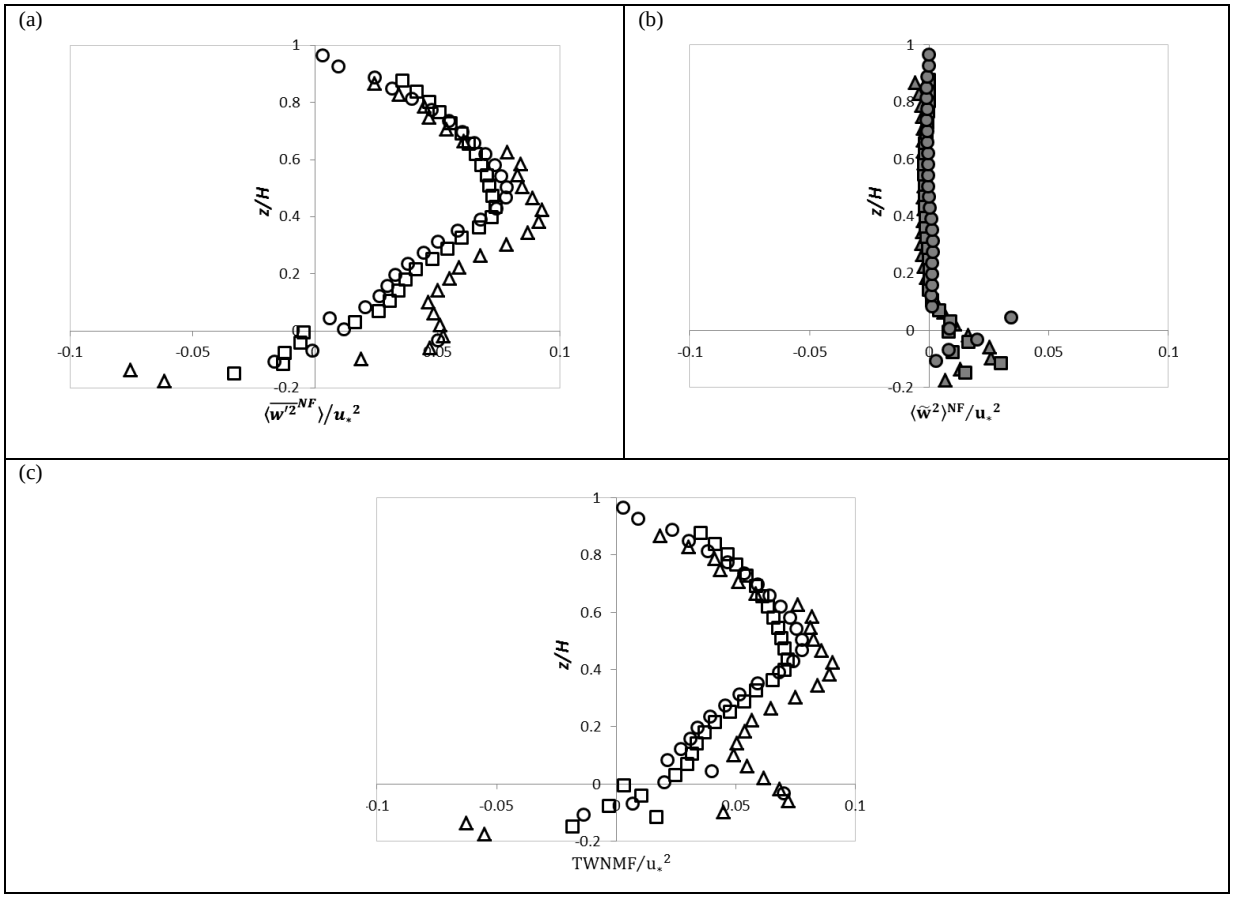

Figure 6-6: Profiles of (a) double averaged vertical net momentum flux profiles ($\frac{\langle \overline{w'^2}^{NF} \rangle}{u_*^2}$) (open symbols) (b) vertical net momentum flux due to spatial heterogeneity ($\langle \tilde{w}^2 \rangle^{NF} / u_*^2$) (filled symbols) (c) total net vertical momentum flux (TWNMF/u_*^2) (open symbols) for three Runs; Δ Run (I); □ Run (II) ○ Run (III).

6.2 QUADRANT ANALYSIS RESULTS

To compare the behaviour of vertical velocity with respect to the bursting process, quadrant analysis was undertaken. In Figure 6-7, the results of this quadrant analysis in run (I) and in plane (1) are shown. In this Figure, contributions of each quadrant to Reynolds shear stress are normalized with respect to u_*^2. Also, as discussed in Bursting Process Detecting Method (page 42), it has been assumed that the hole size (χ) equal to 1.0 is suitable for detection of bursting process. Many studies showed that in open channel quadrant 4 and quadrant 2 are the main contributors to Reynolds shear stress (Kline et al., 1967; Nezu and Nakagawa, 1993). This issue arises because quadrant 2 and 4 are attributed to sweep and ejection events, while quadrant 1 and 3 do not correlated to any specific coherent structure (Nezu and Nakagawa, 1993). Ejection is mostly happened in the region far from the bed, while sweep is more common in the near bed (Grass, 1971; Nezu and Nakagawa, 1993). Similar results is also reported for rough bed open channel flows (Grass, 1971; Raupach et al., 1991; Nezu and Nakagawa, 1993; Papanicolaou et al., 2001; Hardy et al., 2007; Dey and Das, 2012). Grass (1971) and Raupach et al. (1991) found that the effect of quadrant 2 is noticeable in region far from the bed, while the effect of quadrant 4 is confined in the near bed region. In present study, almost everywhere absolute values of contributions from quadrant 2 (Figure 6-7b) and quadrant 4 (Figure 6-7d) are higher than contributions from quadrant 1 (Figure 6-7a) and quadrant 3 (Figure 6-7c). In the near bed region ($z/\sigma_l < 3$), all contour maps are heterogeneous. Hardy et al. (2009) also found spatial variation of different quadrants at $z/H < 0.15$. The larger area that was affected by bed topography ($z/H < 0.35$) in the present study compared to that by Hardy et al. (2009) can be explained by different configuration of bed topography (discussed in chapter 4, Gravel Bed Characteristics, page 65) and larger value of roughness length scale in this research. In Figure 6-7b it is clear that second quadrant is more common above gravel crests, while below gravel crests fourth quadrant is more common. From vertical planes measurements it was possible to determine spatial organization of quadrant events near bed region. To further investigate the spatial variation of four quadrants with respect to bed topography, quadrant analysis was repeated for the horizontal layers.

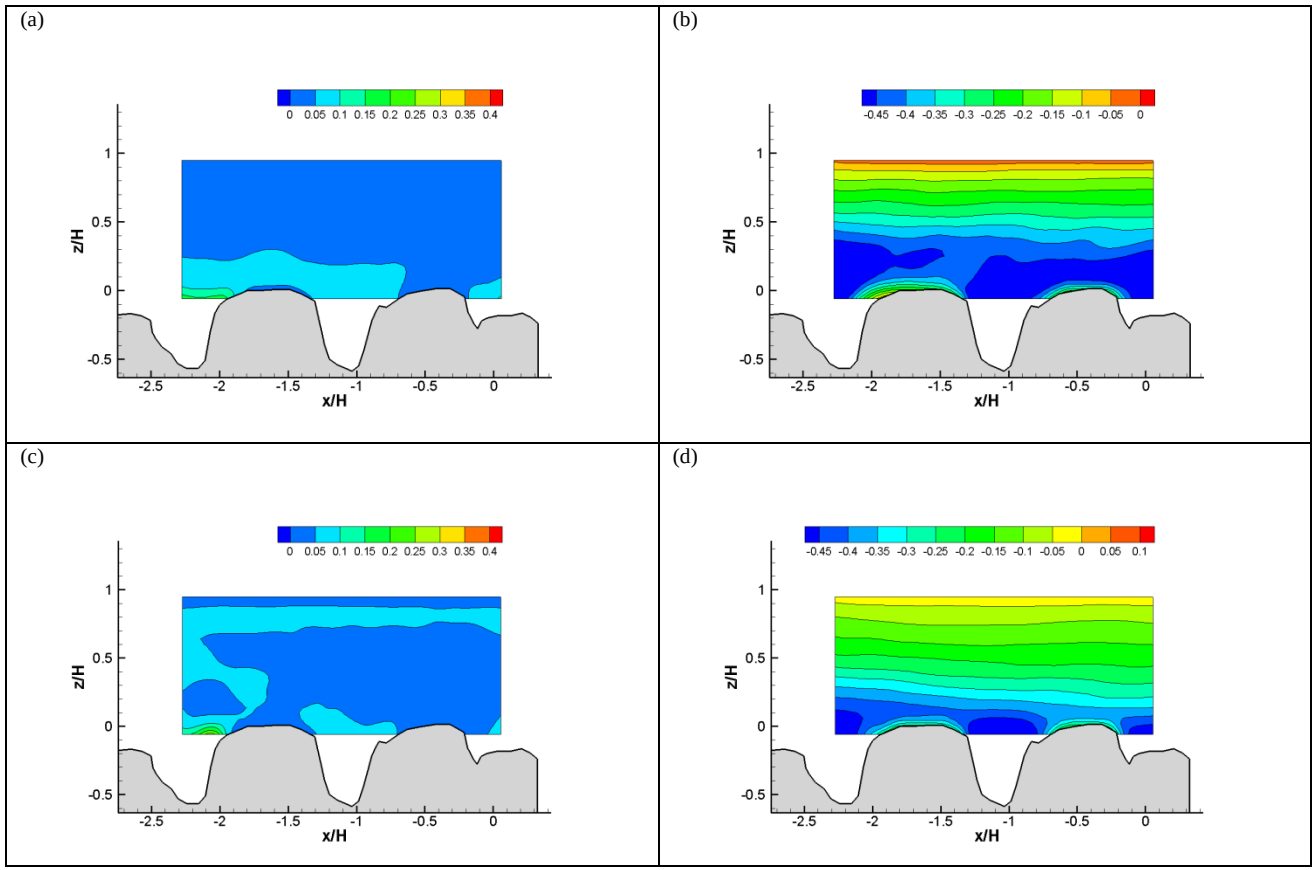

Figure 6-7: Contour map of non-dimensional Reynolds shear stress ($\overline{u'w'}/u_*^2$) for different events with $\chi = 1.0$ in vertical plane for Run (I), Plane 1; (a) quadrant 1, (b) ejection events, (c) quadrant 3, (d) quadrant 4.

The results of quadrant analysis in horizontal layers show an agreement between occurrence of sweep and ejection events and bed topography. As example results of quadrant analysis in horizontal layer and for Run (I) are shown in Figure 6-8. In all contour maps in Figure 6-8 (a: quadrant 1, b: quadrant 2, c: quadrant 3 and d: quadrant 4) like previous figures gravel crests are also shown in the background. These contour maps show that $\overline{u'w'}/{u_*}^2$ vary spatially with respect to bed topography for all quadrants. More precisely, quadrant 2 (ejection events) mostly occurs in the upstream side of gravel crests, while quadrant 4 (sweep) is common in downstream side of gravel crests. Described interaction of bed topography and quadrant results is also reported by Hardy et al. (2009). They found alternating patterns of quadrant 2 and 4 in upstream and downstream sides of gravel crests.

This finding is in agreement with spatial variation of near bed flow field described in Time Averaged Turbulence Statistics (page 76). Upward diverted flow before gravel crests by sweep and downward diverted flow after gravel crests by ejection can be consistent with occurrence of separation and reattachment respectively upstream and downstream of gravel crests. In addition to the spatial variation of different quadrants in relation to bed topography, contour maps of all quadrants show longitudinally elongated strips of high and low values. High and low strips in contour maps of quadrant 1 (Figure 6-8a) and 2 (Figure 6-8b) have approximately the same locations. Like quadrant 1 and 2, locations of high and low strips of quadrant 3 (Figure 6-8c) and 4 (Figure 6-8d) are similar. For different runs, while there is slight variation in the location of these strips, they are clearly visible. These strips can be important for sediment transport in open channel as they can cause sand ribbon formation (Nezu and Nakagawa, 1993).

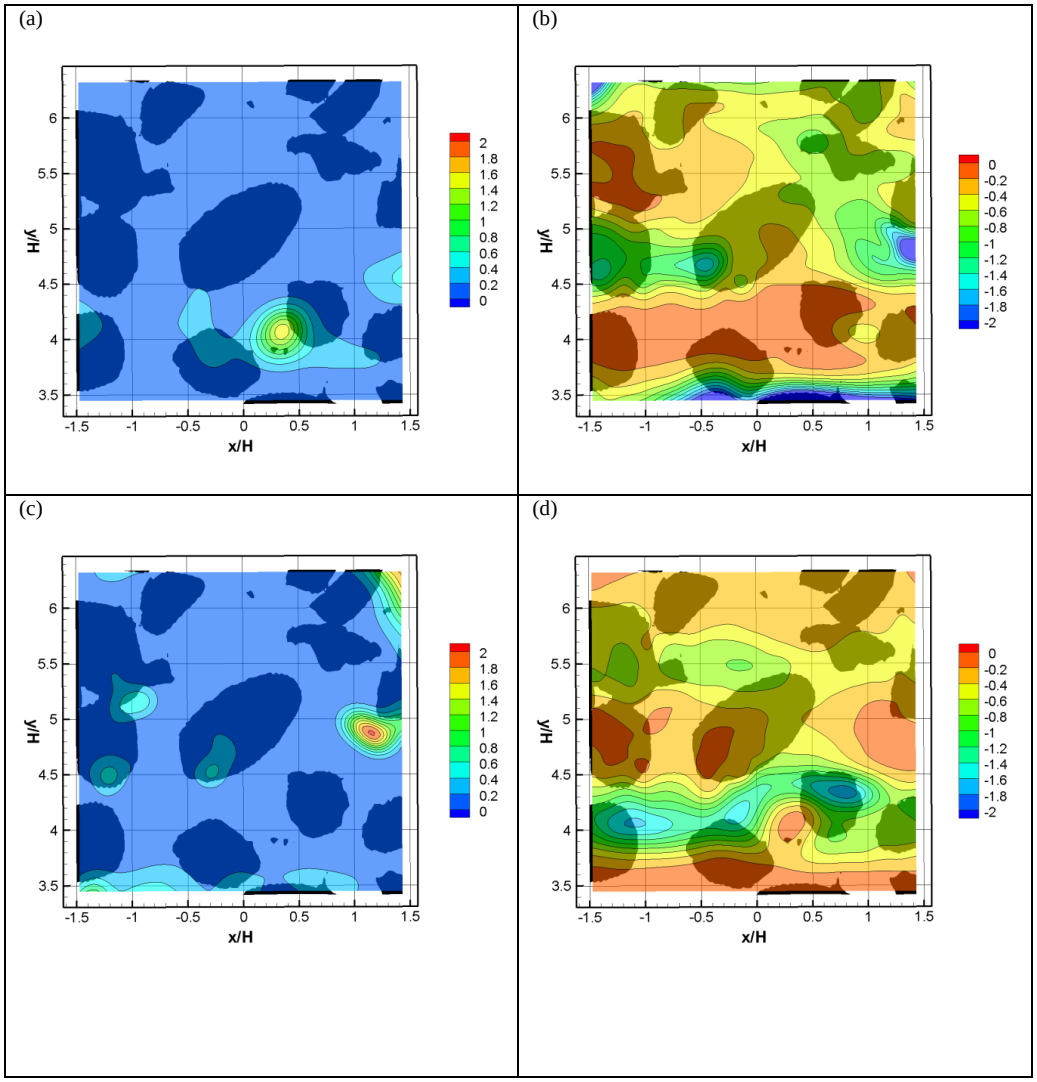

Figure 6-8: Contour map of non-dimensional Reynolds shear stress ($\overline{u'w'}/u_*^2$) for different events with $\chi = 1.0$ in horizontal layer for Run (II); (a) quadrant 1, (b) ejection events, (c) quadrant 3, (d) quadrant 4.

In rough bed flows, to deeper study contribution of different quadrants especially in the near bed region double averaging is commonly used (Mignot et al., 2009b; Sarkar and Dey, 2010; Dey and Das, 2012). Results of applying the double averaging method to present study quadrant analysis are shown in Figure 6-9. The double averaged profiles are made non-dimensional with second power of shear

velocity. Also, in order to better observe variation of quadrant analysis with the hole size (χ), results of quadrant analysis without eliminating mild fluctuations ($\chi = 0.0$) is also reported in Figure 6-9. Previous studies showed that fractional contribution of all quadrants reduces with increase of hole size (Nezu and Nakagawa, 1993; Mignot et al., 2009b). In Figure 6-9, the red lines refer to quadrant analysis with $\chi = 0.0$ and black lines refer to quadrant analysis with $\chi = 1.0$. The results show that like previous studies, the double averaged profiles of different quadrants reduce by increase of the hole size. However, the general shape of the profiles along the water depth in different hole sizes approximately remains similar, except for some slight variations are noticeable for quadrant 1 and 3, especially in the near bed region. These slight variations can be attributed to the measurement uncertainty. In fact, from results of quadrants analysis (Figure 6-9) it can be better observed that quadrants 1 and 3 (Figure 6-9a and c) have smaller contributions to Reynolds shear stress than quadrants 2 and 4 (Figure 6-9a and c). So, as quadrant 1 and 3 are less likely to occur than quadrants 2 and 4, the uncertainty of quadrants 1 and 3 would be more significant.

Double averaged shear stress values in quadrant 1 (Figure 6-9a) increase towards the bed and then decline below the gravel crests. In all three runs maximum is located below gravel crests. This behavior does not change with (Figure 6-9a, black spots) or without (Figure 6-9b, red spots) considering the hole size. Results of previous studies show that double averaged profile of quadrant 1 varies similar to double averaged quadrant 1 in present study with maximum value located below gravel crests (Mignot et al., 2009b; Sarkar and Dey, 2010; Dey and Das, 2012).

Ejection events (Figure 6-9b) values also increase from the water surface towards the bed. Values reach a maximum in region between $0.1 < z/H < 0.5$ in different runs and then they reduce towards the bed. Like quadrant 1, the general trend of double averaged profiles in quadrant 2 approximately remain constant with and without considering hole size. Although the shape of double averaged Reynolds shear stress profiles of present study are similar to what are reported in the other researches (Mignot et al., 2009b; Sarkar and Dey, 2010; Dey and Das, 2012), there is no agreement on the location of the maximum. In Mignot et al. (2009b) study, maximum of $\langle \overline{u'w'} \rangle / u_*^2$ for ejection events is near gravel crests. In contrast, data of

Sarkar and Dey (2010) and Dey and Das (2012) shows this maximum far from the bed ($z/H \approx 0.7$). In summary, these observations express that ejection is more common above gravel crests, while there is not an agreement on the location of the maximum.

Results of quadrant 3 with $\chi = 1.0$ (black spots in Figure 6-9c) depict an increase from the lowest points toward middle of the channel ($z/H \approx 0.5$) and then a reduction toward the water surface. However, results of run (I) are slightly different below gravel crests and near water surface. These differences can also be resulted by measurement uncertainty. The results of quadrant 3 without eliminating small fluctuations (red spots in Figure 6-9c) is slightly different from the results of quadrant analysis with $\chi = 1.0$. These profiles are similar to the profiles of quadrant 1 with a maximum below gravel crests. In other studies profiles of quadrant 3 also have maximum below gravel crests and it is very similar to the profiles of quadrant 1 (Mignot et al., 2009b; Sarkar and Dey, 2010; Dey and Das, 2012). However, contour maps of quadrant analysis in Hardy et al. (2009) shows higher values of quadrant 3 far from gravel crests.

Finally, contribution of quadrant 4 to Reynolds shear stress (Figure 6-9d) starts from near zero at water surface and increases linearly toward the bed. The profiles of quadrant 4 contribution to Reynolds shear stress also do not show a significant change with or without eliminating small fluctuations. Similar profiles are also reported for quadrant 4 contribution in previous studies (Mignot et al., 2009b; Sarkar and Dey, 2010; Dey and Das, 2012).

As has been discussed, Mignot et al. (2009b) and Dey and Das (2012) found that $\langle \overline{u'w'} \rangle / u_*^2$ of ejection events is higher than sweep events in region above gravel crests. Also, they showed that below gravel crests ($z/H < -0.1$), contribution of sweep events is higher than ejection events. The same results are also found in present study. There is also a region slightly below gravel crests ($0.0 < z/H < -0.1$) that Mignot et al. (2009b) found the highest contributions from sweep events, while Dey and Das (2012) reported highest contributions from ejection events. Results of present study (Figure 6-9) show that like what is reported by Mignot et al. (2009b) in this region, contributions of sweep events is higher than contributions of ejection events.

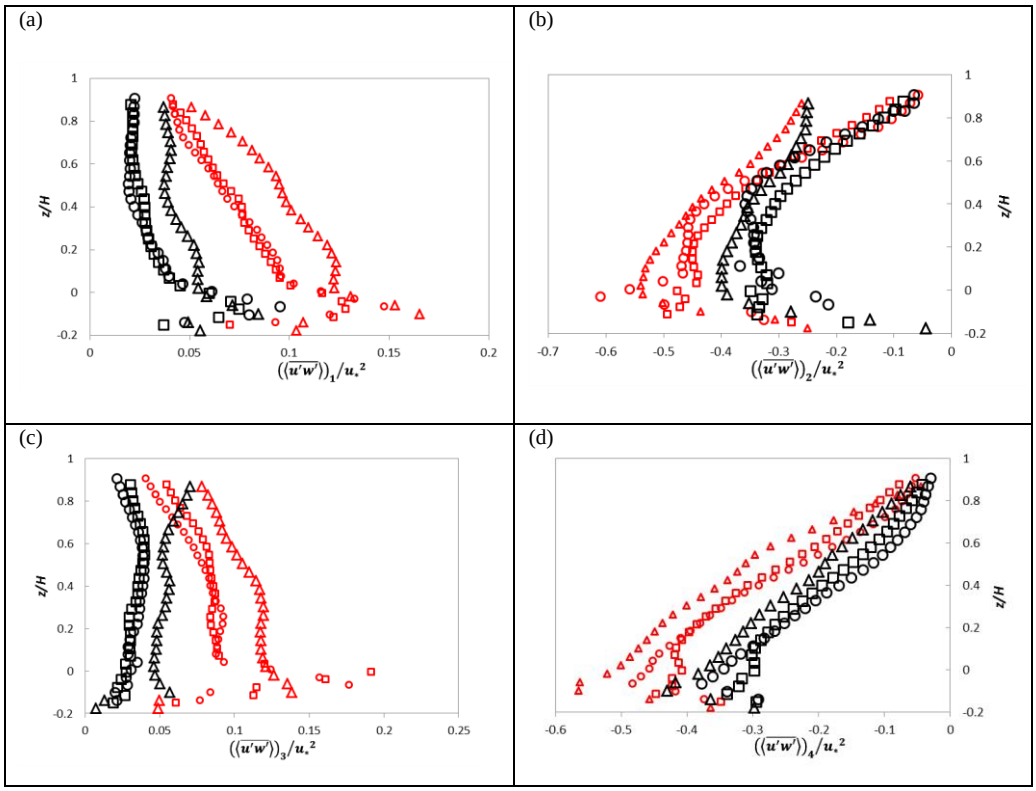

Figure 6-9: Double averaged profiles of non-dimensional Reynolds shear stress ($\langle\overline{u'w'}\rangle/u_*^2$) for (a) quadrant 1 (b) ejection events (c) quadrant 3 (d) quadrant 4 for three Runs (Δ Run (I); □ Run (II); ○ Run (III)) with $\chi = 0.0$ (red spots) and $\chi = 1.0$ (black spots).

In order to also study contributions of sweep and ejection on vertical momentum flux ($\overline{w'^2}$), fractional contributions of different quadrants to vertical momentum flux are calculated and are shown in Figure 6-10. The results show that in general vertical variation of fractional contributions of different quadrants to vertical momentum flux are similar to fractional contributions of quadrants to Reynolds shear stress. The main contributors are quadrant 2 and 4. From Figure 6-10b it is clear that along water depth and above gravel crests the contributions of quadrant 2 is higher than other three quadrants (Figure 6-10a, c, d). However, below gravel crests contributions of quadrant 4 (Figure 6-10d) to vertical momentum flux is the highest. Quadrant 2 (Figure 6-10b) reaches to maximum values in $0.2 < z/H < 0.5$, while quadrant 4 increases toward the bed and has the highest values below gravel crests. This behavior is different from results reported

for smooth bed conditions. In smooth bed, Wei and Willmarth (1991) showed that in any location along z-direction, the contribution of quadrant 2 is higher than other three quadrants. However, in the case of gravel bed, protrusion of roughness elements cause formation of a layer between roughness elements where contribution of quadrant 4 is higher than other quadrants that is caused by dominance of sweep events.

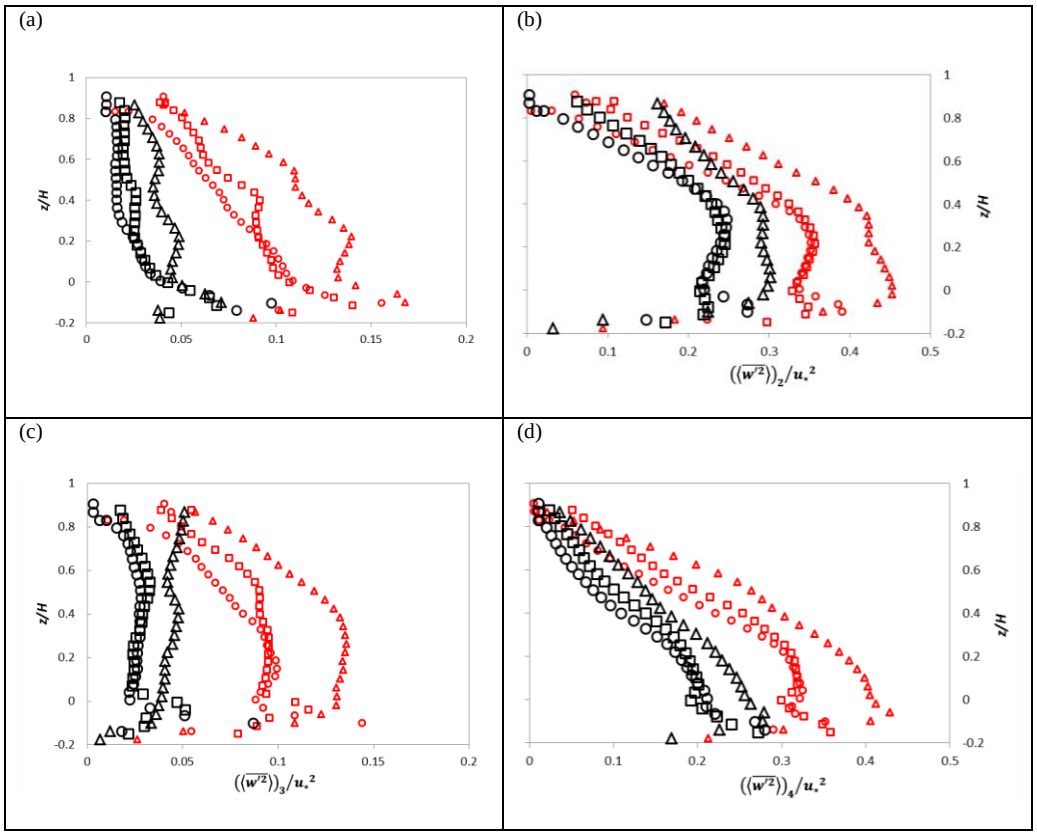

Figure 6-10: Double averaged profiles of non-dimensional vertical momentum flux ($\langle\overline{w'^2}\rangle/u_*^2$) for (a) quadrant 1 (b) ejection events (c) quadrant 3 (d) quadrant 4 for three Runs (Δ Run (I); □ Run (II); ○ Run (III)) with $\chi = 0.0$ (red spots) and $\chi = 1.0$ (black spots).

The variation of double averaged profiles of quadrant 1 and 3 contributions to vertical momentum flux (Figure 6-10a, c) are also similar to quadrant 1 and 3 contributions to Reynolds shear stress (Figure 6-9a, c). Contribution of quadrant 1 increases along water depth and has maximum around gravel crests. The general

shape of the contributions of quadrant 1 profiles are similar with and without applying the hole size. Profile of double averaged contribution of quadrant 3 with $\chi = 0.0$ also increases from water surface toward the bed. From these profiles, it can be assumed that the maximum contributions of quadrant 1 and 3 take place at the gravel crests region. Contribution of quadrant 3 with $\chi = 1.0$ increases from water surface to $z/H \approx 0.5$ and reduces toward the bed.

To summarize the information reportedin this chapter, schematically variation of sweep and ejection events together with the results of vertical velocity analysis along water depth are shown in Figure 6-11. Also, the results of Wei and Willmarth (1991) analysis is summarized in Table 6-1. Based on Figure 6-11 and Table 6-1, there is an agreement between occurrence of sweep and ejection events and the results of vertical velocity analysis. Below gravel crests, net vertical turbulent momentum flux is negative where there is prevalence of sweep events. There is also significant positive form induced net momentum flux below gravel crests. Near gravel crests ($0.0 < z/H < 0.1$), in general there is only weak net vertical turbulent momentum flux, which is consistent with the existence of the balance between sweep and ejection events. Note that both sweep and ejection events are common near gravel crests, while they do not exceed each other. Far from both water surface and gravel bed ($0.1 < z/H$) net turbulent momentum flux is upward due to dominance of ejection events. In this region, form induced net momentum flux is negligible. Finally, near water surface there is not any noticeable net vertical turbulent momentum flux. Negligible net momentum flux is resulted by the lack of sweep and ejection events at water surface. This is different from negligible net momentum flux near gravel crests ($0.0 < z/H < 0.1$) where there is a balance between occurrence of sweep and ejection events.

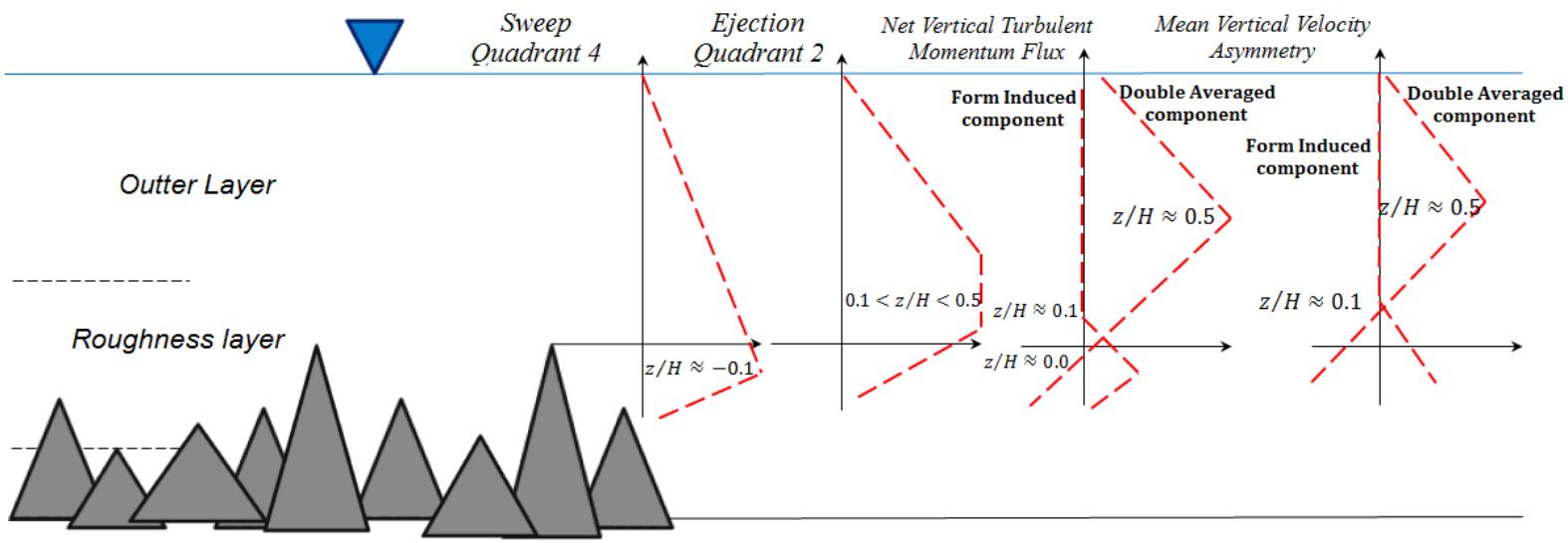

Figure 6-11: Schematic comparison of quadrant analysis and analysis of vertical velocity.

At the end, it should be stress out that despite explanations presented in this chapter about net turbulent momentum flux due to both time and spatial fluctuations, below gravel crests bed geometry is also important. As discussed in theoretical background, the last term in Eq.(2-3) ($\int_z^{z_c} \frac{1}{\Phi}\frac{\partial \Phi}{\partial z}(\rho\langle\overline{w'^2}\rangle + \rho\langle\widetilde{w}^2\rangle + \langle\bar{p}\rangle)$) which is caused by the variation of roughness geometry function in the vertical direction cause a complicated relation of different terms of the momentum equation in the vertical direction. In other words, geometry of gravel bed does not give only form induced vertical momentum flux. The main difficulty is to recall this term below gravel crests with bed geometry parameters.

Table 6-1: Summary of contributions of vertical velocity fluctuations to upward and downward motions.

Region	***Upward Contributions***	***Downward Contributions***
Far From Bed ($z/H > 0.1$)	- Net vertical turbulent momentum flux. - Asymmetry of mean vertical velocity in time.	No Contributions
Above Gravel Crests ($0.0 < z/H < 0.1$)	- Net vertical turbulent momentum flux. - Asymmetry of form induced vertical velocity. - Net vertical form induced momentum flux.	- Asymmetry of time averaged vertical velocity.
Below Gravel Crests ($z/H < -0.1$)	- Asymmetry of form induced vertical velocity. - Net vertical form induced momentum flux.	- Net vertical turbulent momentum flux. - Asymmetry of time averaged vertical velocity.

7 Discussion

Abstract:

In this chapter, results reported in the previous three chapters are discussed deeper. At first, turbulent flow structure in near bed region is discussed respect to formation of secondary currents and bed topography effects. Then, results of turbulent flow structure are compared with a limited number of qualitative experimental measurements in the presence of fine particles. Finally, a method was suggested in order to consider near bed spatial variation of turbulent flow characteristics in suspension threshold (Rouse criterion).

7.1 FLOW STRUCTURE NEAR GRAVEL BED REGION

In present study, measurements of three components velocity field in near bed horizontal layer have been combined with two dimensional velocity measurements in streamwise vertical planes. This combination provides the opportunity to analyze in detail the characteristics of the flow field at intermediate submergence conditions, with particular attention to the near bed region. Moreover, characteristics of the present measurements (such as ratio of vector spacing to bed materials size, measurement frequency, aspect ratio and relative submergence variations) which are different from those reported in the literature (e.g. by Manes et al., 2007; Cooper and Tait, 2008; Hardy et al., 2009), allow us to depict the properties of the flow field at a higher degree of detail with respect to the past.

In the near bed region two features of the velocity field are evident: formation of streamwise striped structure which alternates in transversal direction and, at the same time, formation of a patchy structure of the flow field induced by bed topography. Measurements in near bed horizontal layer show that longitudinal velocities are organized in high and low velocity strips. High velocity strips show downward motion (negative *w* velocity) and vice-versa upward motion is noticed for low velocity strips. Moreover, sign of spanwise velocities changes at about the middle of the high and low velocity strips. Conformal to time averaged velocity, 2^{nd} order velocity moments are organized in striped structures. Besides, 2D velocity measurements performed in different vertical planes are consistent with the presence of striped structure all along the flow depth. All these features of the flow field lead us to infer that striped structure is given by presence of secondary currents.

Mechanism for secondary currents formation can be explained by vorticity equation in *x* direction (Einstein and Li, 1958; Nezu and Nakagawa, 1993) which shows that secondary currents are formed where turbulence is anisotropic (spanwise turbulent intensity (σ_v) different to normalwise turbulent intensity (σ_w)) and flow is spatially heterogeneous (Einstein and Li, 1958; Nikora et al., 1998b). Actual observations are consistent with this mechanism. Following Einstein and Li (1958), enhancement of secondary currents are related to different roughnesses between side and bed walls (Rodríguez and García, 2008; Albayrak and Lemmin, 2011). In contrast, Belcher and Fox (2009) expressed that presence of secondary currents in

region further from side walls is not necessarily side wall effect but it can be attributed to vortex stretching induced by bed roughness.

Nezu and Nakagawa (1993) stated that secondary currents are strong in near side wall regions ($y/H \leq 2.5$). However, our measurements show that in a gravel bed open channel, secondary currents can still be present even in region far from side walls ($y/H > 2.5$) and can extend toward the center of the channel. Similar results have been already reported in the literature (Nikora et al., 1998b; Rodríguez and García, 2008; Albayrak and Lemmin, 2011). In particular Rodríguez and García (2008) reported presence of secondary currents in the central part of the flume, while their aspect ratio was close to that of present experiments (B/H equal to 6.3 and 8.5). On the other hand, Albayrak and Lemmin (2011)'s measurements in very wide open channel ($B = 2.45m$) with very high aspect ratio (B/H up to 20) show that, while secondary currents are clear even for $y/H > 2.5$, no well-defined secondary current cell is found in the central zone. Both the authors agree that origin of secondary currents rely on the difference between bed and side wall roughnesses. There is also experimental evidence that increase in these roughnesses difference seems to enhance secondary currents (Rodríguez and García, 2008). However, present results in Flow Type (II) show that, contrary to what expected, striped structure is more evident at lower relative submergence, for which aspect ratio is higher and difference between side and bed roughness is smaller (see page 60, Table 3-1). Measurements of Cooper and Tait (2010) and Cooper et al. (2013) show that by relative submergence reduction, both FITI and spatial variance of DATI increase in the near bed region, so indicating that the heterogeneity of the flow field produced by gravel protrusions increases. Therefore it can be argued that far from the side wall, *"local"* heterogeneity at the bed can assume a significant role, in addition to difference of bed-side wall roughnesses, in secondary current enhancement.

Another important point concerning presence of secondary currents is related to the definition of required distance from inlet for the flow to be fully developed. Generally, in laboratory open channel measurements, achievement of fully-development flow conditions can be verified applying available formulas (e.g. Kirkgöz and Ardiçlioğlu, 1997; Nikora et al., 1998b), which are mainly based on the

comparison of streamwise velocity profiles measured in the center of cross sections, at different longitudinal x positions. In presence of secondary currents, similar to main flow, the secondary current cells should require a minimum length to properly develop and become independent from entrance conditions. There is a lack of study on minimum required length for fully development of secondary current cells and this topic is beyond the scope of this work. However if the aforementioned velocity profiles measurement in different transversal locations at a certain longitudinal position with UDV and averaging in cross-section could be considered a statistically significant sampling among different secondary current cells, then the achievement of a fully developed transversally averaged velocity profile could be a reasonable criterion to indirectly check also the fully development of secondary current cells.

The small ratio of vector spacing to size of bed material in present experiments provided us the possibility to detect the disturbances of near bed flow field induced by bed topography, which overlaps and interferes with the strip structure induced by secondary currents. The horizontal layer flow velocities (Figure 5-1 and Figure 5-3) show that protrusions of gravel crests tend to locally induce flow diversions in lateral directions. The features of lateral diversion are quite irregular and seem also dependent on local orientation and shape of the pebbles that originate it. Moreover, at the downstream side region of gravel crests streamwise velocity tends to decelerate and normalwise component tends to be downward directed, while at the upstream side region upward motion tends to prevail. This behavior is contradictory to the finding of Cooper and Tait (2008) who did not find any coherency between near bed flow and bed topography. The main reason that Cooper and Tait (2008) did not see this behavior could be related to larger value of l_{IA}/D_{50} in their measurement ($l_{IA}/D_{50} \approx 0.2$) in comparison to present study measurement ($l_{IA}/D_{50} = 0.05$). Unlike Cooper and Tait (2008), Buffin-Bélanger et al. (2006) reported that bed micro topography cause spatial structure in near bed flow characteristics. They found that maximum and minimum magnitude of total velocity occurred at top of protuberant gravel crests and at the downstream side of large obstacles, respectively. Also, Mclean and Nikora (2006) found that in gravel bed, normal and streamwise form induced velocity components ($\tilde{u}, \tilde{w}$) have behavior consistent with bed elevations. Similar to us, they also found

that $\widetilde{w}$ usually have maximum values (positive) at upstream side and minimum values (negative) at downstream side.

To quantitatively analyze the effects of bed topography on the structure of the near bed flow field previously qualitatively described, 2D cross-correlations between different time averaged velocity components measured in the horizontal layer and bed elevations are calculated, based on the following equation:

$$R(\mathrm{n}\Delta x, m\Delta y) = \left(\frac{1}{(N-n)\times(M-m)} \sum_{i=-N+n}^{N-n} \sum_{j=-M+m}^{M-m} (u_k(x_i, y_i) - \bar{u}_k) \times \left(z(x_i + \mathrm{n}\Delta x, y_j + m\Delta y) - \bar{z}\right)\right) / \left(\sqrt{\sigma_l{}^2(x_N, y_M)\sigma_{u_k}{}^2(x_N, y_M)}\right) \quad (7\text{-}1)$$

Where $R(n\Delta x, m\Delta y)$ is cross-correlation, $n\Delta x, m\Delta y$ are streamwise and spanwise spatial lags in cross-correlation, $\Delta x, \Delta y$ are sampling intervals which can be positive or negative, k subscript represents different components of velocity, $\sigma_l{}^2$ is variance of bed elevation, $\sigma_{u_k}{}^2$ is variance of k-th component of time averaged velocity and N, M are total number of measuring points in x and y directions.

Results of 2D cross-correlation are shown in Figure 7-1. Cross-correlograms of streamwise velocity and bed elevations ($R_{\bar{u}z}$; Figure 7-1a, b, c) have lower absolute maximum values (in all three runs: $|R_{\bar{u}z}|_{MAX} \approx 0.3$) compared with spanwise velocity to bed elevations cross-correlograms ($|R_{\bar{v}z}|_{MAX} \approx 0.5$; Figure 7-1d, e, f) and with normalwise velocity to bed elevations cross-correlograms ($|\mathrm{R}_{\bar{w}z}|_{\mathrm{MAX}} \approx 0.4$; Figure 7-1g, h, i). Therefore, among three different components of velocity, spanwise and normalwise velocity components are more affected by bed topography and deserve to be better analyzed. Cross-correlograms of spanwise velocity component show a patchy structure (Figure 7-1d, e, f) for small negative $m\Delta x$ sampling intervals, a positive peak located at $m\Delta y/D_{50} \approx +0.25$ and a negative local peak located at $m\Delta y/D_{50} \approx -1$ are noticed. At the same time, for small positive $m\Delta x$ sampling intervals, a mirrored situation take place, with a positive peak located at $m\Delta y/D_{50} \approx -1$, while the negative is at $m\Delta y/D_{50} \approx +0.25$. Peaks are clear and evident for all the runs, despite their position slightly change with relative submergence. These features are compatible with a diverging flow immediately upstream a crest and its subsequent convergence immediately downstream, as, indeed, it is recognizable.

As far as normalwise velocity component cross-correlograms is concerned (Figure 7-1g, h, i), a positive peak is evident for all the runs at small negative $m\Delta x$ sampling intervals, at $m\Delta y/D_{50} \approx -0.25$, which is consistent with upward motion immediately upstream gravel crests. For small positive sampling intervals a negative peak is noticeable again at $m\Delta y/D_{50} \approx 0.25$, but the position tends to progressively shift from $m\Delta x \approx +0.5$ to $m\Delta x \approx +1$ for increasing relative submergence. This behavior of the cross-correlogram is consistent with downflow motion at downstream side of gravel crests. It has to be pointed out that by increasing relative submergence, a progressive decrease of the absolute value of both the maximum and minimum correlation peak values take place. This fact, together with the corresponding progressive downstream shift of minimum peak, may be interpreted as further evidence that skimming flow tends to develop for increasing Reynolds number, that is in present case for increasing relative submergence.

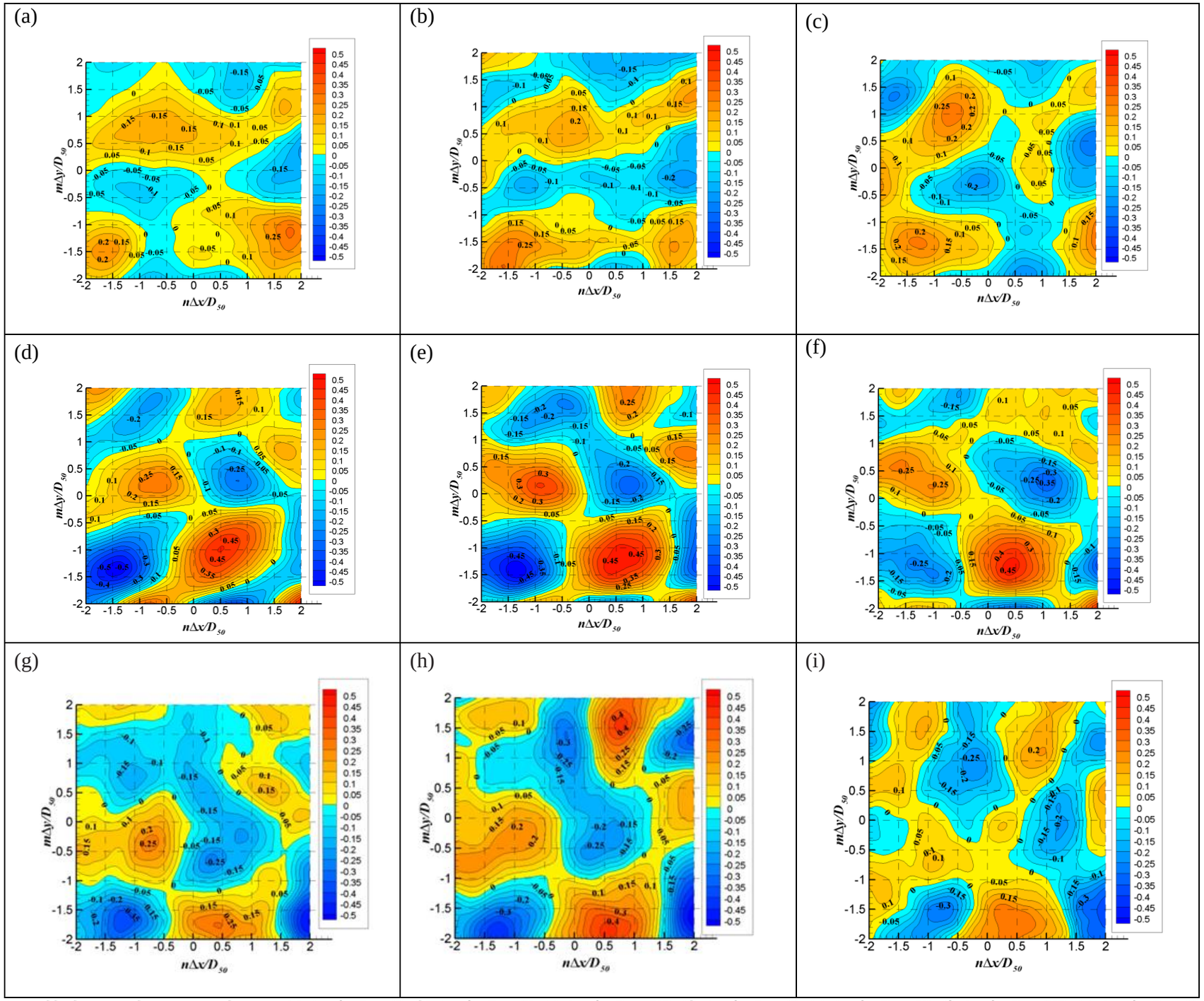

Figure 7-1: Near bed velocity and bed topography cross-correlogram: (a) $R_{\bar{u}z}$ for Run (I); (b) $R_{\bar{u}z}$ for Run (II; (c) $R_{\bar{u}z}$ for Run (III); (d) $R_{\bar{v}z}$ for Run (I); (e) $R_{\bar{v}z}$ for Run (II); (f) $R_{\bar{v}z}$ for Run (III); (g) $R_{\bar{w}z}$ for Run (I); (h) $R_{\bar{w}z}$ for Run (II); (i) $R_{\bar{w}z}$ for Run (III).

7.2 DOUBLE AVERAGED TURBULENT CHARACTERISTICS

Results of applying double averaged method show that by increase of relative submergence streamwise DATI (Figure 5-7a) do not show any significant dependence on the relative submergence and normalwise DATI (Figure 5-7b) reduces all along the flow depth with relative submergence. Normalwise FITI profiles (Figure 5-7b) do not varies significantly with increase of relative submergence. Streamwise FITI profiles (Figure 5-7a) tend to increase only in the roughness layer with relative submergence. Although in previous studies observed profiles of normalwise FITI are also invariable with relative submergence (Manes et al., 2007; Cooper et al., 2013), dependence on relative submergence of streamwise component of FITI in present study is different from what has been reported. Cooper et al. (2013) found that streamwise FITI are higher in shallower flow conditions, while they remain approximately constant in Manes et al. (2007). These differences only in part can be explained by the different characteristics of the bed topography, such as the width of the gravel layer or the size and shape of roughness elements in different studies. Moreover, it has to bear in mind that the FITI are much more sensitive than spatial averaged turbulence quantities to both the minimum required size of spatial averaging and to the density of measurements (Cooper and Tait, 2010). Therefore no definitive conclusion can be drawn from the data and more detailed measurements are necessary to better determine dependence of form-induced stresses on relative submergence.

Applying log-law to velocity profiles shows that both additive constant and hydrodynamics roughness length vary with relative submergence (see page 90, Double Averaged Velocity Profile). However, in order to consider log-law fully applicable we believe that these values should remain constant with relative submergence changes. Variations of zero plane displacement level d are noticed in present results, but no clear trend can be depicted (Figure 5-8, Figure 5-9, Figure 5-11). Differences in obtained additive constants and hydrodynamic roughness lengths can be explained by variation of estimated d from Eq.(5-2). Two reasons for this variation are conceivable: firstly uncertainty in estimation of d, κ by Eq.(5-2) and Eq.(5-3) and secondly weakness of logarithmic velocity profile

behavior. Estimation of d, κ is based on the derivative of velocity, which is highly sensitive to small measurement errors. So, estimation of d, κ and log-law bounds can have large confidence interval. But, if the uncertainty of measurement is accepted, results show that none approximations given by Eq.(5-1) in Figure 5-11 are suitable for this type of flow and other kind of velocity profiles should be considered. An alternative approach could be mixing layer proposed by Katul et al. (2002). This approximation is supported by formation of wake zones at the downstream side of gravel crests, with inflection point in velocity profile, as indeed have been observed also in present data near some gravel crest.

7.3 TURBULENT FLOW AND SEDIMENT TRANSPORT

The information obtained from analysis of vertical velocity and quadrant analysis highlights the importance of spatial variability of flow characteristics in near bed region. Results of Wei and Willmarth (1991)'s method and quadrant analysis show that spatial organization of near bed flow is affected by bed topography. Figure 6-7 and Figure 6-8 showed that sweep event is more common at downstream side of gravel crests, while at upstream side of gravels ejection events mostly tend to take place. Figure 6-8 also shows that near bed flow organizes in a longitudinally striped structure alternating in transversal direction, so that where time averaged upward flow is common, downward flow is rare and vice versa. These strips are resulted by the presence of secondary current notified in the measurement. In the case of rough bed, intrusion of obstacles (in the case of present study, gravel crests) can trigger secondary currents in wide open channel (aspect ratio higher than 5) (Nezu and Nakagawa, 1993; Schlichting et al., 2000). Presence of these longitudinally strips can cause lateral transport of sediments which leads to formation of longitudinally bed-forms (Karcz, 1966; Nezu and Nakagawa, 1993). On the other side, it should be remembered that due to occurrence of upward and downward flow respectively in upstream and downstream side of gravels, sediments should be mostly deposited in downstream side and entrained from upstream side of gravel crests.

In order to compare the results of turbulent flow characteristics with real case of sediment transport, limited numbers of measurements in the presence of fine particles have been performed. In these measurements, we illustrate transport of fine materials above a rough bed. Rough bed materials were mixture of gravels ($D_{50} = 24.9mm$) and sandy materials ($D_{50} = 1.25mm$). Hydraulic conditions were adjusted so that rough bed materials remain immobile during measurements. The materials which was used as fine mobile partilces were a plastic material named bakelite (phenol-formaldehyde resin) with density (ρ_s) equal to 1553*kg/lit*. Two series of data have been collected during these measurements (named Series 1 and Series 2). Experimental conditions of these measurements are reported in Table 7-1. As reported in this table, aspect ratio of both measurements are in the same range of turbulent flow measurements. In Table 7-1, Rouse number (R_o) is also reported. Rouse numner is a non-demsional criterion which is used to determine the mode of the sediment transport. Originally, it is the ratio of mean settling velocity of fine particles (ω_s) and maximum of root mean square of vertical velocity $\left(\sqrt{\overline{w'^2}}\right)_{max}$ (Bagnold, 1966) :

$$R_o = \omega_s / \left(\sqrt{\overline{w'^2}}\right)_{max} \tag{7-2}$$

However, as root mean square of vertical velocity is approximately equal to shear velocity at gravel crests and scales with u_* (Bennett et al., 1998; Leeder et al., 2005), for simplicity shear velocity can be used instead of $\left(\sqrt{\overline{w'^2}}\right)_{max}$. Settling velocity in Rouse number is a function of shape, size and roughness of fine particles. For high Reynolds number, empirical formulas are available for estimation of settling velocity based on particle diameters. One of the most common form of these empirical formulas is as below (Cheng, 1997; Julien, 2010):

$$\omega_s = \frac{\nu}{D}\left[\sqrt{\frac{1}{4}\left(\frac{A}{B}\right)^{2/m} + \left(\frac{4}{3}\frac{{d_*}^3}{B}\right)^{1/m}} - \frac{1}{2}\left(\frac{A}{B}\right)^{1/m}\right]^m \tag{7-3}$$

Where D is diameter moveable material, A, B, m are the coefficients vary according to different authors. In present study, the coefficients suggested by Cheng (1997) are used ($A = 32.0, B = 1.0, m = 1.5$). Also, d_* is dimensionless particle diameter defined as:

$$d_* = \frac{(\rho_s - \rho)g}{\rho \nu^2} D \qquad (7\text{-}4)$$

Where ρ and ρ_s are respectively water and fine sediment density and g is acceleration of gravity equal to 9.8 m/s^2. When maximum of root mean square of vertical velocity (or shear velocity) is higher than settling velocity (i.e. Rouse number smaller than 1), it can be assumed that suspended sediments transport is initiated (Bagnold, 1966; Van Rijn, 1984; Leeder et al., 2005). In both measurements, Rouse number is smaller than 1 (Table 7-1). This means that at least some parts of fine particles are transported in suspension.

Table 7-1: Characteristics of measurements in the presence of fine sediment.

	Q (*lit/min*)	H (*mm*)	S (-)	B (*mm*)	B/H (-)	D (μm)	U_* (*m/s*)	ω_s (*m/s*)	R_o (-)
Series 1	420	50	0.002	400	8	500	0.031	0.027	0.85
Series 2	320	40	0.002	400	10	425-500	0.028	0.025	0.89

Results obtained from these visualizations are shown in Figure 7-2 and Figure 7-3. Top view of fine particles transport for both series 1 and series 2 are shown in Figure 7-2. In both measurements, formation of sand ribbons is clear. Lateral distance between two consecutive sand bars (δ) is approximately two times of water depth. This ratio is in agreement with lateral spacing of lower longitudinal velocity zones of secondary currents observed by Kinoshita (1967) and Albayrak and Lemmin (2011), but higher than values observed in present study turbulent flow measurements. The difference between lateral spacing in turbulent flow field measurements and visualization measurements in present study can be related to bed topography. As highlighted by Mejia-Alvarez and Christensen (2013) and Barros and Christensen (2014) and also discussed in present study (page 76, Time Averaged Turbulence Statistics), bed topography can affect location of secondary

currents cells. In present study, the bed topography of the channel which is used for the visualization measurements (mixture of immobile sand and gravel) is different from the bed topography of the channel used in turbulent flow measurements (only gravel). Presence of sand in the matrix of gravels reduces protrusions of roughness elements and it also changes bed characteristics such as mean bed elevations, roughness length scales, profile of streamwise averaged bed elevations. As it has been highlighted by Barros and Christensen (2014) bed elevations is related to the locations of secondary currents cells. Therefore, the difference in bed topography in turbulent flow field measurements and visualization measurements causes different lateral spacing of lower longitudinal velocity zones of secondary currents and sand bars.

Similar straight sand ribbons are commonly notified in natural rivers (Karcz, 1966). In rough bed open channel and in the presence of mobile fine materials, cellular secondary currents and sand ribbons interact mutually. Presence of sand ribbons can stabilize secondary currents, while occurrence of upward and downward movement in secondary current cells can cause formation of sand ribbons (Nezu and Nakagawa, 1984; Nezu and Nakagawa, 1993). However, observation of secondary currents in gravel bed and without presence of mobile materials could be an indication for this assumption that secondary currents cause formation of longitudinally bed forms.

In addition to the presence of sand ribbons, it is found that erosion and deposition of fine materials are in agreement with bed topography. This fact can be seen in Figure 7-3. As it is clear, fine particles are generally deposited in downstream side of gravel crests. However, in upstream side of gravel crests, most of fine particles are eroded (see dashes curves in Figure 7-3a, b). This observation is also consistent with occurrence of sweep and ejection respective in upstream and downstream sides of gravels.

(a)

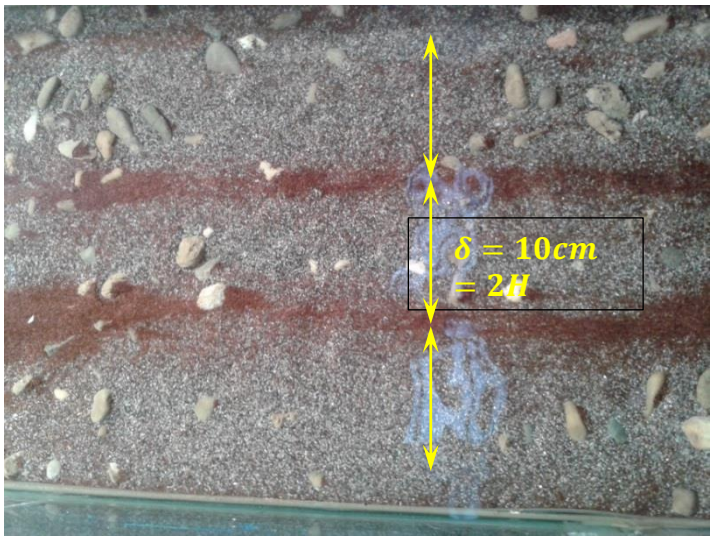

(b)

Figure 7-2: Formation of sand ribbons in rough bed (a) series 1 (b) series 2.

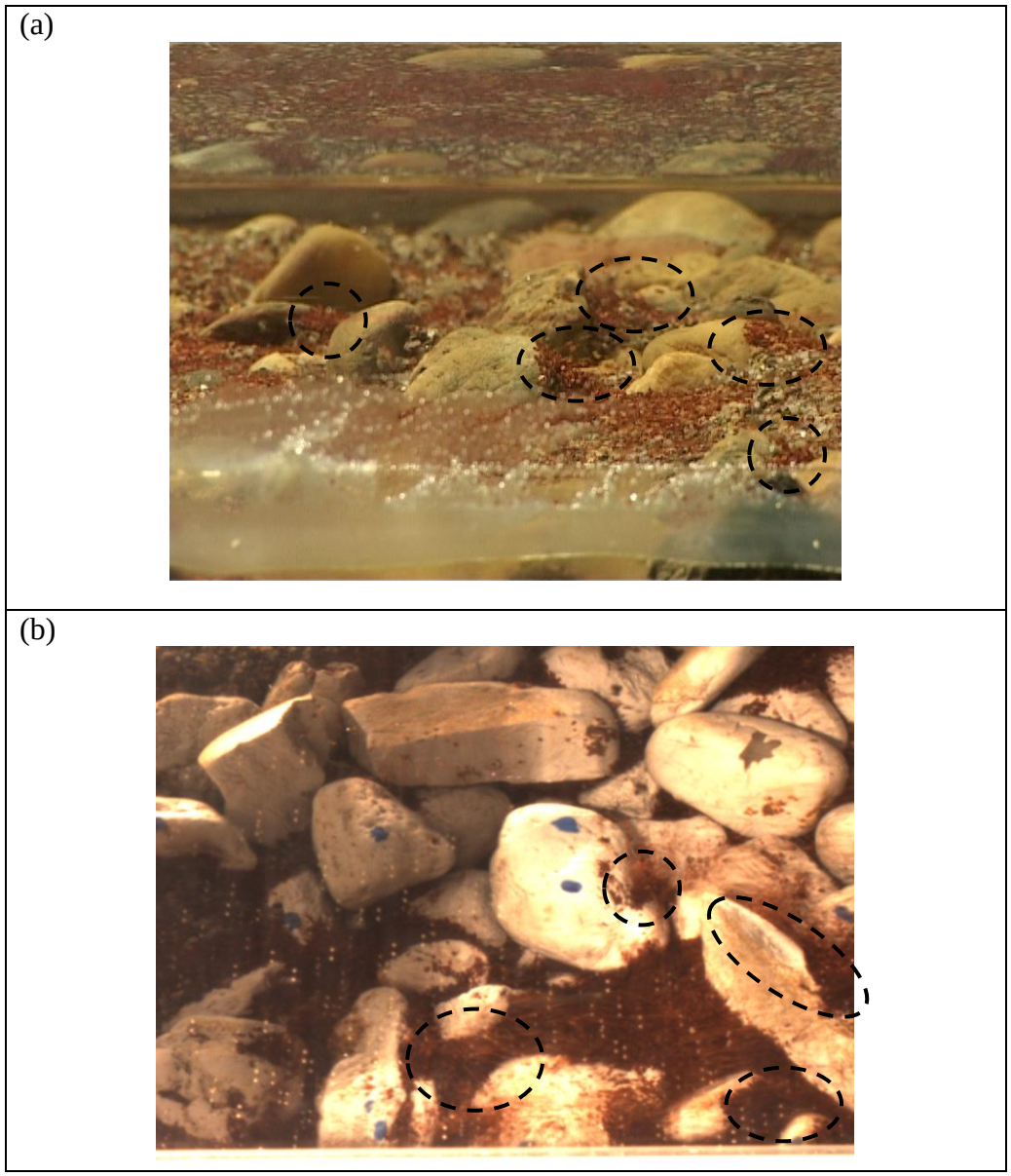

Figure 7-3: Pattern of fine sediment erosion and deposition in comparison to bed topography (a) side view (b) plan view.

Results of the flow field measurements and flow visualizations show that some areas such as upstream side of gravel crests and velocity strips with low streamwise velocity and positive vertical velocity actively participate in sediment transport. In fact, the spatial variation of flow quantities, such as Reynolds shear

stress and vertical turbulent momentum, causes formation of preferential zones for entrainment or deposition of fine particles. However, simultaneous effects of bed topography and secondary currents causes complex spatial distribution of turbulent flow characteristics in near bed region and consequently it causes complex spatial distribution of the preferential zones for entrainment or deposition of fine particles. Therefore, given this spatial heterogeneity, not all the bed contributes in the same way in sediment transport process.

In order to consider spatial variation of flow characteristics in sediment transport criteria, in present study a method has been developed. Here, we only focus on suspension threshold (i.e. Rouse criterion (see Eq. (7-2))). However, it is possible to extend the proposed method to other sediment transport thresholds. The method consists in applying point threshold criterion for entrainment into suspension, based on the local values of turbulence parameters. As expressed in Eq. (7-2), originally, Rouse number is the ratio of settling velocity in the power of two and maximum value of vertical momentum flux. The threshold is applied at the bed region. More precisely, the threshold (Rouse criterion) is applied to point values of the root mean square of vertical velocity component ($\sqrt{\overline{w'^2}}$) at the gravel crests, where ejection events tends to prevail. There are three reasons for this choice: Firstly, analysis of double averaging in present study (page 87, Double Averaged Turbulence Statistics) and also in previous studies (Manes et al., 2007; Mignot et al., 2009a; Dey and Das, 2012) shows that the maximum value of $\langle\overline{w'^2}\ \rangle$ is located near gravel crests. Secondly, as shown in previous chapter (page 101, Sediment Transport Process and Turbulent Flow), below gravel crests is dominated by downward motions associated with sweep events. Therefore, higher value of $\overline{w'^2}$ below gravel crests in comparing to the value in gravel crests is resulted by downward motions which do not support suspended movement of particles. Lastly, there is a discussion by Leeder et al. (2005) on the importance of $d\overline{w'^2}/dz$ on the suspended transport of particles. They explained that turbulent acceleration (increase of $d\overline{w'^2}/dz$) prevent loss of suspended transport capacity. While in gravel bed flows, prediction of $d\overline{w'^2}/dz$ variation is difficult, analysis of $d\langle\overline{w'^2}\rangle/dz$ shows that it increases from bed to around gravel crest and above gravel crests, it decreases. So, level of gravel crests is also approximate endpoint of accelerative trend of $d\langle\overline{w'^2}\rangle/dz$.

It has been proposed that sediments are transported in suspension if Rouse number is smaller than a critical value. The critical value is defined as:

$$R_{o\,cr} = \frac{\omega_s}{\left(\sqrt{\overline{w'^2}}\right)_{max}} \tag{7-5}$$

where $R_{o\,cr}$ is critical value of Rouse number and ω_s is calculated by Eq. (7-3). Sediment transport is in suspended mode when Rouse number is smaller than $R_{o\,cr}$. As mentioned a few paragraphs above, for initiation of suspended transport critical Rouse number ($R_{o\,cr}$) is 1.0 (Van Rijn, 1984; Leeder et al., 2005).

In present study, local values of Rouse number calculated based on $\overline{w'^2}$ in the horizontal layer 1mm above gravel crests are compared with critical value and the ratio $\Omega = R_o/R_{o\,cr}$ is introduced. In order to produce a contour map which shows the regions participate in suspended sediment transport, a new function is identified as follow:

$$\Psi(\mathrm{x,y}) = \begin{cases} 1 & if \quad \Omega < 1 \\ 0 & if \quad \Omega > 1 \end{cases} \tag{7-6}$$

This function is a detecting function which is equal to 1 when suspension criterion Eq. (7-5) is satisfied and when suspension criterion is not satisfied, Ψ will be zero. For better illustrating of this fact, by assuming an arbitrary diameter and density for fine materials ($D = 1.5mm, \rho_s = 2650\,kg/m^3$), contour map of suspension transport threshold (Ψ) were calculated and shown in Figure 7-4. In this figure, the area with blue color is the area which participated in the suspended transport (Ω>1). As someone can see, based on these contour maps with a constant threshold, some parts of measurement region participate in suspension and some parts do not participate in all three runs. While there are slight differences in location of preferential zones of different runs due to the slight change in the location of secondary currents cells, in general there is consistency in location of preferential zones in different runs.

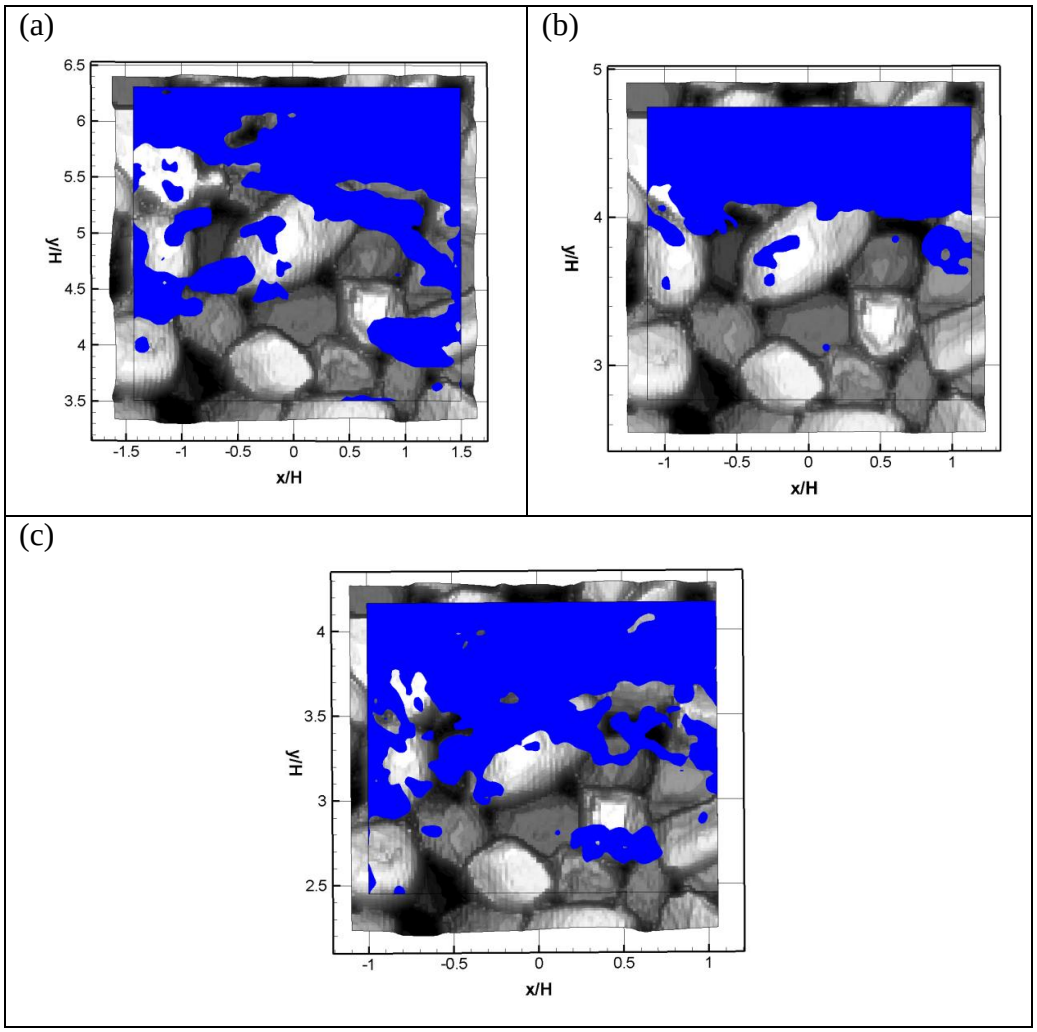

Figure 7-4: Contribution region to suspended sediment transport for D = 0.25mm (a) Run (I) (b) Run (II) (c) Run (III).

Following this approach, it is proposed to consider the ratio of the area participated in suspension to total measurement area, i.e.:

$$\langle \Psi \rangle = \frac{1}{A_o} \iint_{A_o} \Psi \, \mathrm{d}A_o \tag{7-7}$$

where ⟨Ψ⟩ is the ratio of area participated in suspension to total measurement area and A_o is total measurement area.

For three runs of present study, this ratio for different hypothetical particle diameters are calculated and shown in Figure 7-5. As one can see, trend of these curves are approximately similar. In small sediment diameter, ⟨Ψ⟩ is high showing that most of the region participate to entrainment with suspension and as the diameter of mobile materials increases, the percentage of the contribution area participates into suspended transport reduces. Therefore, a graph like Figure 7-5 which shows percentage of the area in gravel bed participates in the suspension proposed instead of original constant Rouse criteria.

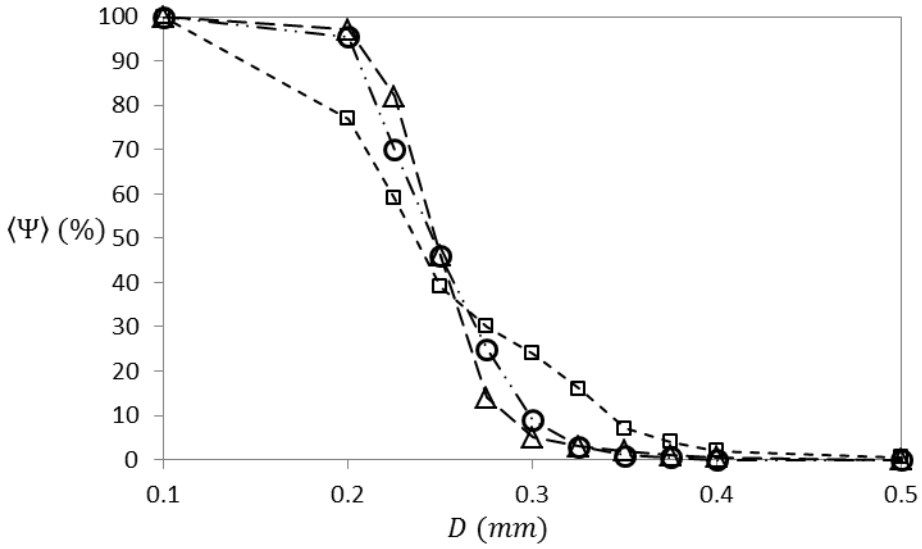

Figure 7-5: Diagram of area participated in suspended sediment transport to total area for different sediment diameters for three different Runs; Δ Run (I); □ Run (II) ○ Run (III).

8 Conclusions

Abstract:

In this chapter, the main findings in the present research and the importance of these results are reported. Also, some recommendations for future studies are explained.

8.1 SUMMARY

This thesis aims to study transport of fine sediment in the matrix of gravel bed. Laboratory open channel flume is used to experimentally study the structure of gravel bed turbulent flow as for possible application for sediment transport in the intermediate submergence conditions (flow type (II)). The main core of the present study is based on detailed analysis of these laboratory measurements. To this end, Stereoscopic Particle Image Velocimetry at near bed horizontal layer and Digital Particle Image Velocimetry in vertical planes for three different hydraulic conditions are employed together with laser scanning of the bed elevations. Spatial organization of velocity field was analyzed in a horizontal layer 1mm above gravel crests and in three vertical planes at different transversal locations. Double averaging method was applied to experimental data, in order to examine effects of relative submergence on turbulence characteristics and performance of logarithmic law. Also, analysis of quadrants and vertical velocity is applied to study turbulent flow in the context of sediment transport.

In summary, the analysis of the data leads to the following findings:

1- The near bed flow field is affected by both gravel bed protrusions and presence of secondary currents. Patchiness of velocity contour maps in the horizontal layer can be ascribed to gravel bed protrusions, while secondary currents induce striped structure in time averaged velocity field.

2- Gravel bed protrusions divert flow from main direction to the lateral directions. The results of mean velocities cross-correlations to bed elevations show that the effect of bed topography is stronger for spanwise and normalwise velocity components. Indeed, cross-correlograms of normalwise velocity to bed elevations show a tendency of upward flow at upstream side of gravels and down flow at downstream side of gravels. Spanwise velocity component to bed elevations correlograms are in agreement with formation of flow separation and reattachment in gravel crests surrounding area.

3- Lateral spacing of the captured strips of low streamwise velocity in the horizontal layer PIV data are approximately 1.2 times of water depth. The same value is also notified for lateral spacing of positive and negative strips of normalwise and spanwise velocities. This value is smaller than the value observed in

previous studies which are in around two times the water depth. Smaller lateral spacing in the present study can be explained with new observations which longitudinally elongated velocity strips are affected by bed topography, specifically for higher roughness. More precisely, it was observed that low and high streamwise velocity (positive and negative vertical velocity) strips are located where streamwise averaged bed elevations is respectively lower and higher than the mean bed elevations.

4- The results of applying logarithmic law in Flow Type (II) show that all parameters even additive constant change by relative submergence. As a result, if the uncertainty in calculation of velocity gradient would be accepted, strong variations of log-law bounds and parameters (C, d, z_o) challenge present parameterization method of logarithmic law in Flow Type (II). Therefore, other alternative approaches such as mixing layer should be considered for this type of flow.

5- Streamwise double averaged turbulent intensity (DATI) profiles in near bed region slightly reduce by increase of relative submergence. Normalwise double averaged turbulent intensity profiles show a more marked decrease all along the flow depth for increasing relative submergence. Moreover, normalwise form induced turbulent intensity (FITI) profiles are almost independent of relative submergence, as reported in the literature. Streamwise form induced turbulent intensity profiles show contradictory results to what reported by the others (see page 87, Double Averaged Turbulence Statistics and page 131, Double Averaged Turbulent Characteristics). These differences can be attributed to differences in gravel bed characteristics of various studies and also to uncertainty related to high sensitivity of form induced turbulent intensity to measurement properties such as the minimum required size of spatial averaging and the density of the measurements points.

6- Analysis of vertical velocity shows that above gravel crests and far from the bed, asymmetry of mean flow is positive and vertical turbulent momentum flux is upward, while below gravel crests asymmetry of mean flow is negative vertical turbulent momentum flux is downward. In $0.0<z/H<0.1$, we noticed that asymmetry of mean flow is negative, while turbulent momentum flux is upward. It

is also found that vertical momentum flux resulted by form induced component is not significant, except below gravel crests which is upward in to the water column. Net vertical momentum flux due to spatial fluctuations is significant also in comparision to turbulent vertical momentum flux.

7- The results of quadrants analysis is conformal to the results of vertical velocity analysis. Profiles of double averaged ejection events reach to maximum between $0.1 < z/H < 0.5$ depending on the measurement conditions. This shows that high upward momentum flux above gravel crests and in the lower half of the flow depth is caused by prevalence of ejection events. Moreover, profiles of double averaged sweep events increases linearly toward the bed, where they reach to the maximum values. So, downward momentum flux below gravel crests can also be attributed to prevalence of sweep events which are particularly vigorous at and below gravel crests.

8- It is found that spatial variation of vertical momentum flux is compatible with bed topography. Turbulent momentum flux is in downward direction in the downstream side of gravel crests, while upward turbulent momentum flux is generally happened in the upstream side of gravel crests. This spatial variation is in agreement with prevalence of sweep and ejection events respectively in downstream and upstream sides of gravel crests.

9- Qualitative observation in the real case of fine sediments presence in the matrix of rough bed is in agreement with the results of turbulent flow characteristics. Formation of sand ribbons due to secondary currents is clearly notified. Deposition is mostly occurred in downstream side of gravel crests where sweep is common. In the upstream side of gravels, where ejection is common, fine particles are generally eroded.

10- The results of present study shows that in general some regions (e.g. upstream side of gravel crests and velocity strips with low streamwise velocity and positive vertical velocity) more actively can participate in transport, while other regions (e.g. downstream side of gravel crests and velocity strips with high streamwise velocity and negative vertical velocity) do not participate. In order to consider this spatial variation in transport threshold criteria such as Rouse criterion, it is suggested to compare local values of related turbulent flow characteristics with

related thresholds. In this case, the ratio of total area which participates in sediment transport to the total measurement area can better represent fine sediment transport process in an immobile heterogeneous bed.

8.2 RECOMMENDATIONS FOR FUTURE STUDIES

Gravel Bed Turbulent Flow in Presence of Mobile Fine Particles: Within this thesis we highlighted relationship between near bed turbulent flow structure, bed topography and fine particle sediment transport. However, all of the PIV measurements are done in the conditions of clear water (i.e. without presence of mobile fine materials). In this case, relative level of fine particles elevation is important and has two opposite effects. On one side, sand level can change bed topography and on the other side sand level specifies the level of available mobile fine materials (Grams and Wilcock, 2007). From the measurements of the present study, the effects of bed topography have been highlighted. However, from these measurements it is not possible to address the importance of fine materials presence. Experimental measurement of the flow field in the presence of fine mobile materials can provide some information on the importance of fine particles availability.

Secondary Flow in Gravel Bed: In the present study, it has been observed that secondary currents are formed in channel with aspect ratio higher than 5 and also in region far from side walls ($y/H > 2.5$). During present study measurements, only three different hydraulic conditions are covered. Also, PIV measurements were carried out just in the central zone of the channel. Therefore, we were not able to recognize to what extend secondary currents in all cross-section are present (i.e. no information did not obtained about flow field near side walls). Also, we could not clearly explain the reason that secondary currents are still formed in the central part of the channel with aspect ratio higher than 5. Stereoscopic PIV measurements in cross-section, perpendicular to streamwise direction could help to better see and analyze secondary currents in gravel beds.

Flow Structure in Low Submergence Condition: Turbulent flow structure with relative submergence higher than 5 and smaller than 40 is studied in the present study and also in a number of previous studies. However, low submergence condition with relative submergence smaller than 5 is not considered properly. In the

case of low submergence, different from high and intermediate submergence conditions, effects of bed roughness are extended to water surface (Nikora et al., 2007b) and so it can be expected that no logarithmic region is formed. The different structure of the flow in addition to prevalence of this condition in the nature leads researchers to study low submergence flows (Flow Type (I)). Moreover, possible importance of relative submergence in secondary currents formation is another motivation for study of turbulent flow with low relative submergence.

Numerical Simulation of Gravel Bed Flows: In the present study, flow field measurements are coupled with measurements of bed elevations. As bed characteristics are fully described in the present study, constructing a model in order to numerically solve the flow field is also possible. With the use of a strong numerical model such as large eddy simulation (LES) velocity field can solve in high resolution in both time and space for realistic Reynolds numbers. This is useful in obtaining information on those parts of the flows that are hardly observable in the laboratory measurements (e.g. bottom of roughness layer). Also, it can be helpful for developing a conceptual transfer model for fine particles in a matrix of gravel bed.

Reference

Aberle, J. (2007), Measurements of armour layer roughness geometry function and porosity, *Acta Geophysica,* 55**,** 23-32.

Aberle, J., Koll, K. & Dittrich, A. (2008), Form induced stresses over rough gravel-beds, *Acta Geophysica,* 56**,** 584-600.

Aberle, J. & Nikora, V. (2006), Statistical properties of armored gravel bed surfaces, *Water Resources Research,* 42**,** W11414.

Acornley, R. M. (1999), Water temperatures within spawning beds in two chalk streams and implications for salmonid egg development, *Hydrological Processes,* 13**,** 439-446.

Adrian, R. J., Christensen, K. T. & Liu, Z. C. (2000a), Analysis and interpretation of instantaneous turbulent velocity fields, *Experiments in Fluids,* 29**,** 275-290.

Adrian, R. J., Meinhart, C. D. & Tomkins, C. D. (2000b), Vortex organization in the outer region of the turbulent boundary layer, *Journal of Fluid Mechanics,* 422**,** 1-54.

Albayrak, I. & Lemmin, U. (2011), Secondary currents and corresponding surface velocity patterns in a turbulent open-channel flow over a rough bed, *Journal of Hydraulic Engineering,* 137**,** 1318-1334.

Armitage, P. D. & Blackburn, J. H. (2001), The macroinvertebrate fauna of the Holy Stream, a small tributary of the River Frome, Dorset, *Proceedings of the Dorset Natural History and Archeological Society* 123**,** 95-100.

Armitage, P. D. & Cannan, C. E. (2000), Annual changes in summer patterns of mesohabitat distribution and associated macroinvertebrate assemblages, *Hydrological Processes,* 14**,** 3161-3179.

Bagnold, R. A., (1966), An approach to the sediment transport problem from general physics, *Geological survey proffessional paper 442-I.*

Bandyopadhyay, P. R. & Watson, R. D. (1988), Structure of rough-wall turbulent boundary layers, *Physics of Fluids (1958-1988),* 31**,** 1877-1883.

Barros, J. M. & Christensen, K. T. (2014), Observations of turbulent secondary flows in a rough-wall boundary layer, *Journal of Fluid Mechanics,* 748**,** null-null.

Bayazit, M. (1976), Free surface flow in a channel of large relative roughness, *Journal of Hydraulic Research,* 14**,** 115-126.

Belcher, B. J. & Fox, J. F. (2009), Laboratory measurements of 3-D flow patterns and turbulence in straight open channel with rough bed, *Journal of Hydraulic Research,* 47**,** 685-688.

Benedict, L. H. & Gould, R. D. (1996), Towards better uncertainty estimates for turbulence statistics, *Experiments in Fluids,* 22**,** 129-136.

Bennett, S. J., Bridge, J. S. & Best, J. L. (1998), Fluid and sediment dynamics of upper stage plane beds, *Journal of Geophysical Research: Oceans,* 103**,** 1239-1274.

Blaschke, A. P., Steiner, K.-H., Schmalfuss, R., Gutknecht, D. & Sengschmitt, D. (2003), Clogging Processes in Hyporheic Interstices of an Impounded River, the Danube at Vienna, Austria, *International Review of Hydrobiology,* 88**,** 397-413.

Bo, T., Fenoglio, S., Malacarne, G., Pessino, M. & Sgariboldi, F. (2007), Effects of clogging on stream macroinvertebrates: An experimental approach, *Limnologica - Ecology and Management of Inland Waters,* 37**,** 186-192.

Bogard, D. G. & Tiederman, W. G. (1986), Burst detection with single-point velocity measurements, *Journal of Fluid Mechanics,* 162**,** 389-413.

Bomminayuni, S. & Stoesser, T. (2011), Turbulence Statistics in an Open-Channel Flow over a Rough Bed, *Journal of Hydraulic Engineering,* 137**,** 1347-1358.

Boulton, A. J. (2007), Hyporheic rehabilitation in rivers: restoring vertical connectivity, *Freshwater Biology,* 52**,** 632-650.

Boulton, A. J., Findlay, S., Marmonier, P., Stanley, E. H. & Valett, H. M. (1998), THE FUNCTIONAL SIGNIFICANCE OF THE HYPORHEIC ZONE IN STREAMS AND RIVERS, *Annual Review of Ecology and Systematics,* 29**,** 59-81.

Braza, M., Perrin, R. & Hoarau, Y. (2006), Turbulence properties in the cylinder wake at high Reynolds numbers, *Journal of Fluids and Structures,* 22**,** 757-771.

Brunke, M., (1998), *The Influence of Hydrological Exchange Patterns on Environmental Gradients and Community Ecology in Hyporheic Interstices of a Prealpine River*.

Brunke, M. & Gonser, T. O. M. (1997), The ecological significance of exchange processes between rivers and groundwater, *Freshwater Biology,* 37**,** 1-33.

Buffin-Bélanger, T., Rice, S., Reid, I. & Lancaster, J. (2006), Spatial heterogeneity of near-bed hydraulics above a patch of river gravel, *Water Resources Research,* 42**,** W04413.

Buffin-Bélanger, T. & Roy, A. G. (1998), Effects of a pebble cluster on the turbulent structure of a depth-limited flow in a gravel-bed river, *Geomorphology,* 25**,** 249-267.

Burkholder, B. K., Grant, G. E., Haggerty, R., Khangaonkar, T. & Wampler, P. J. (2008), Influence of hyporheic flow and geomorphology on temperature of a large, gravel-bed river, Clackamas River, Oregon, USA, *Hydrological Processes,* 22**,** 941-953.

Chen, C., Packman, A. I. & Gaillard, J.-F. (2008), Pore-scale analysis of permeability reduction resulting from colloid deposition, *Geophysical Research Letters,* 35**,** L07404.

Cheng, N. (1997), Simplified Settling Velocity Formula for Sediment Particle, *Journal of Hydraulic Engineering,* 123**,** 149-152.

Clarke, S. J. & Wharton, G. (2001), Sediment nutrient characteristics and aquatic macrophytes in lowland English rivers, *Science of The Total Environment,* 266**,** 103-112.

Cooper, J. & Tait, S. (2008), The spatial organisation of time-averaged streamwise velocity and its correlation with the surface topography of water-worked gravel beds, *Acta Geophysica,* 56**,** 614-641.

Cooper, J. R., Aberle, J., Koll, K. & Tait, S. J. (2013), Influence of relative submergence on spatial variance and form-induced stress of gravel-bed flows, *Water Resources Research,* 49**,** 5765-5777.

Cooper, J. R. & Tait, S. J. (2010), Spatially representative velocity measurement over water-worked gravel beds, *Water Resources Research,* 46**,** W11559.

Dancey, C. L., Balakrishnan, M., Diplas, P. & Papanicolaou, A. N. (2000), The spatial inhomogeneity of turbulence above a fully rough, packed bed in open channel flow, *Experiments in Fluids,* 29**,** 402-410.

Davis, A., Marshak, A., Wiscombe, W. & Cahalan, R. (1994), Multifractal characterizations of nonstationarity and intermittency in geophysical fields: Observed, retrieved, or simulated, *Journal of Geophysical Research: Atmospheres,* 99**,** 8055-8072.

Defina, A., (1996), Transverse spacing of low-speed streaks in a channel flow over a rough bed, *In:* P. J. Ashworth, S. L. B., J. L. Best,S. J. Mc Lelland (ed.) *Coherent Flow Structures in Open Channels*: John Wiley & Sons.

Descloux, S., Datry, T., Philippe, M. & Marmonier, P. (2010), Comparison of Different Techniques to Assess Surface and Subsurface Streambed Colmation with Fine Sediments, *International Review of Hydrobiology,* 95**,** 520-540.

Detert, M., (2008), *Hydrodynamic processes at the water-sediment interface of stream beds,* PhD, university of Karlsruhe.

Detert, M., Nikora, V. & Jirka, G. H. (2010), Synoptic velocity and pressure fields at the water–sediment interface of streambeds, *Journal of Fluid Mechanics,* 660**,** 55-86.

Dey, S. & Das, R. (2012), Gravel-bed hydrodynamics: double-averaging approach, *Journal of Hydraulic Engineering,* 138**,** 707-725.

Diplas, P. & Parker, G., (1992), Deposition and removal of fines in gravel-bed streams, *In:* Billi, P. a. H., R. D. And Thorne C. R. And Tacconi P. (ed.) *Dynamics of gravel-bed rivers,* Chichester: Wiley publisher.

Dong, L. F., Smith, C. J., Papaspyrou, S., Stott, A., Osborn, A. M. & Nedwell, D. B. (2009), Changes in Benthic Denitrification, Nitrate Ammonification, and Anammox Process Rates and Nitrate and Nitrite Reductase Gene Abundances along an Estuarine Nutrient Gradient (the Colne Estuary, United Kingdom), *Applied and Environmental Microbiology,* 75**,** 3171-3179.

Dong, S., Karniadakis, G. E., Ekmekci, A. & Rockwell, D. (2006), A combined direct numerical simulation–particle image velocimetry study of the turbulent near wake, *Journal of Fluid Mechanics,* 569**,** 185-207.

Doussan, C., Poitevin, G., Ledoux, E. & Detay, M. (1997), River bank filtration: modelling of the changes in water chemistry with emphasis on nitrogen species, *Journal of Contaminant Hydrology,* 25**,** 129-156.

Drake, T. G., Shreve, R. L., Dietrich, W. E., Whiting, P. J. & Leopold, L. B. (1988), Bedload transport of fine gravel observed by motion-picture photography, *Journal of Fluid Mechanics,* 192**,** 193-217.

Eglin, I., Roeck, U., Robach, F. & Tremolieres, M. (1997), Macrophyte biological methods used in the study of the exchange between the Rhine river and the groundwater, *Water Research,* 31**,** 503-514.

Einstein, H. & Li, H. (1958), Secondary currents in straight channels, *Transaction of American Geophysical Union,* 39**,** 1085-1088.

Finnigan, J. (2000), Turbulence in Plant Canopies, *Annual Review of Fluid Mechanics,* 32**,** 519-571.

Florio, D. D., Felice, F. D. & Romano, G. P. (2002), Windowing, re-shaping and re-orientation interrogation windows in particle image velocimetry for the investigation of shear flows, *Measurement Science and Technology,* 13**,** 953.

Gaudio, R., Miglio, A. & Dey, S. (2010), Non-universality of von Kármán's κ in fluvial streams, *Journal of Hydraulic Research,* 48**,** 658-663.

George, W. K. (2007), Is there a universal log law for turbulent wall-bounded flows?, *Philosophical Transactions of the Royal Society A: Mathematical, Physical and Engineering Sciences,* 365**,** 789-806.

Goring, D. G., Nikora, V. & Mcewan, I., (1999), Analysis of the texture of gravel beds using 2-D structure functions, *River, Coastal, and Estuarine Morphodynamics: Proceedings of the IAHR Symposium,*, Genova, Italy.

Grabowski, R. C., Droppo, I. G. & Wharton, G. (2011), Erodibility of cohesive sediment: The importance of sediment properties, *Earth-Science Reviews,* 105**,** 101-120.

Grams, P. E. & Wilcock, P. R. (2007), Equilibrium entrainment of fine sediment over a coarse immobile bed, *Water Resources Research,* 43**,** W10420.

Grass, A. J. (1971), Structural features of turbulent flow over smooth and rough boundaries, *Journal of Fluid Mechanics,* 50**,** 233-255.

Guala, M., Tomkins, C. D., Christensen, K. T. & Adrian, R. J. (2012), Vortex organization in a turbulent boundary layer overlying sparse roughness elements, *Journal of Hydraulic Research,* 50**,** 465-481.

Hardy, R. J., Best, J. L., Lane, S. N. & Carbonneau, P. E. (2009), Coherent flow structures in a depth-limited flow over a gravel surface: The role of near-bed turbulence and

influence of Reynolds number, *Journal of Geophysical Research: Earth Surface,* 114**,** F01003.
Hardy, R. J., Best, J. L., Lane, S. N. & Carbonneau, P. E. (2010), Coherent flow structures in a depth-limited flow over a gravel surface: The influence of surface roughness, *Journal of Geophysical Research: Earth Surface,* 115**,** F03006.
Hardy, R. J., Lane, S. N., Ferguson, R. I. & Parsons, D. R. (2007), Emergence of coherent flow structures over a gravel surface : a numerical experiment, *Water resources research.,* 43**,** W03422.
Heppell, C. M., Wharton, G., Cotton, J. a. C., Bass, J. a. B. & Roberts, S. E. (2009), Sediment storage in the shallow hyporheic of lowland vegetated river reaches, *Hydrological Processes,* 23**,** 2239-2251.
Hiscock, K. M. & Grischek, T. (2002), Attenuation of groundwater pollution by bank filtration, *Journal of Hydrology,* 266**,** 139-144.
Hoover, T. M. & Ackerman, J. D. (2004), Near-bed hydrodynamic measurements above boulders in shallow torrential streams: Implications for stream biota, *Journal of Environmental Engineering and Science,* 3**,** 365-378.
Hunt, J. C. R., Wray, A. A. & Moin, P. (1988), Eddies, Stream, and Convergence Zones in Turbulent Flows, *Center For Turbulence Research,* Report CTR-S88.
Ibisch, R., Seydell, I. And Borchardt, D. (2009), Influence of periphyton biomass dynamics on biological colmation proccesses in the hyporheic zone of a gravel bed river (River Lahn, Germany), *Advanced Liminology* 61**,** 87-104.
Jeong, J. & Hussain, F. (1995), On the identification of a vortex, *Journal of Fluid Mechanics,* 285**,** 69-94.
Jimenez, J. (2004), Turbulent flows over rough walls, *Annual Review of Fluid Mechanics,* 36**,** 173-196.
Jones, J. I., Murphy, J. F., Collins, A. L., Sear, D. A., Naden, P. S. & Armitage, P. D. (2012), THE IMPACT OF FINE SEDIMENT ON MACRO-INVERTEBRATES, *River Research and Applications,* 28**,** 1055-1071.
Julien, P. Y., (2010), *Erosion and Sedimentation,* Cambridge University Press.
Karcz, I. (1966), Secondary currents and the configuration of a natural stream bed, *Journal of Geophysical Research,* 71**,** 3109-3112.
Katul, G., Wiberg, P., Albertson, J. & Hornberger, G. (2002), A mixing layer theory for flow resistance in shallow streams, *Water Resources Research,* 38**,** 1250.
Kinoshita, R. (1967), An Analysis of the Movement of Flood Waters by Aerial Photography Concerning Characteristics of Turbulence and Surface Flow, *Journal of the Japan society of photogrammetry,* 6**,** 1-17.
Kirkgöz, M. & Ardiçlioğlu, M. (1997), Velocity Profiles of Developing and Developed Open Channel Flow, *Journal of Hydraulic Engineering,* 123**,** 1099-1105.
Kline, S. J., Reynolds, W. C., Schraub, F. A. & Runstadler, P. W. (1967), The structure of turbulent boundary layers, *Journal of Fluid Mechanics,* 30**,** 741-773.
Koll, K., (2006), Parameterisation of the vertical velocity profile in the wall region over rough surfaces, *In:* Rui M.L. Ferreira, E. C. T. L. A., Joao G.A.B. Leal, Antonio H. Cardoso (ed.) *River Flow,* Lisbon, Portugal.
Kondolf, G. M. & Mathews, W. V. G., (1991), Management of Coarse Sediment in Regulated Rivers of California, Berkeley, USA: Technical report, University Califonia.
Krause, S., Hannah, D. M. & Fleckenstein, J. H. (2009), Hyporheic hydrology: interactions at the groundwater-surface water interface, *Hydrological Processes,* 23**,** 2103-2107.
Krause, S., Hannah, D. M., Fleckenstein, J. H., Heppell, C. M., Kaeser, D., Pickup, R., Pinay, G., Robertson, A. L. & Wood, P. J. (2011), Inter-disciplinary perspectives on processes in the hyporheic zone, *Ecohydrology,* 4**,** 481-499.

Kuhnle, R., Wren, D., Langendoen, E. & Rigby, J. (2013), Sand Transport over an Immobile Gravel Substrate, *Journal of Hydraulic Engineering,* 139**,** 167-176.

Lamarre, H. & Roy, A. G. (2005), Reach scale variability of turbulent flow characteristics in a gravel-bed river, *Geomorphology,* 68**,** 95-113.

Lambs, L. (2004), Interactions between groundwater and surface water at river banks and the confluence of rivers, *Journal of Hydrology,* 288**,** 312-326.

Lavoie, P., Avallone, G., Gregorio, F., Romano, G. P. & Antonia, R. A. (2007), Spatial resolution of PIV for the measurement of turbulence, *Experiments in Fluids,* 43**,** 39-51.

Leeder, M. R. (1983), On the dynamics of sediment suspension by residual Reynolds stresses—confirmation of Bagnold's theory, *Sedimentology,* 30**,** 485-491.

Leeder, M. R., Gray, T. E. & Alexander, J. a. N. (2005), Sediment suspension dynamics and a new criterion for the maintenance of turbulent suspensions, *Sedimentology,* 52**,** 683-691.

Lefebvre, S., Marmonier, P. & Pinay, G. (2004), Stream regulation and nitrogen dynamics in sediment interstices: comparison of natural and straightened sectors of a third-order stream, *River Research and Applications,* 20**,** 499-512.

Li, W. a. Z., L. S (1997), edimentary facies and tectonic setting of the cretaceous in the suhongtu-yingen basin, *Scientia Geologica Sinica,* 32**,** 387-396.

Lu, S. S. & Willmarth, W. W. (1973), Measurements of the structure of the Reynolds stress in a turbulent boundary layer, *Journal of Fluid Mechanics,* 60**,** 481-511.

Macisaac, H. J. & Rocha, R. (1995), Effects of suspended clay on zebra mussel (dreissena polymorpha) faeces and pseudofaeces production, *Archiv für Hydrobiologie,* 135.

Manes, C., Pokrajac, D. & Mcewan, I. (2007), Double-Averaged Open-Channel Flows with Small Relative Submergence, *Journal of Hydraulic Engineering,* 133**,** 896-904.

Maridet, L. & Philippe, M. (1995), Influence of substrate characteristics on the vertical distribution of stream macroinvertebrates in the hyporheic zone, *International Review of Hydrobiology,* 91**,** 101-105.

Marusic, I., Mckeon, B. J., Monkewitz, P. A., Nagib, H. M., Smits, A. J. & Sreenivasan, K. R. (2010), Wall-bounded turbulent flows at high Reynolds numbers: Recent advances and key issues, *Physics of Fluids (1994-present),* 22**,** -.

Mccloskey, T. F. & Finnemore, E. J. (1996), Estimating Hydraulic Conductivities in an Alluvial Basin from Sediment Facies Models, *Ground Water,* 34**,** 1024-1032.

Mclean, S. R. & Nikora, V. I. (2006), Characteristics of turbulent unidirectional flow over rough beds: Double-averaging perspective with particular focus on sand dunes and gravel beds, *Water Resources Research,* 42**,** W10409.

Mejia-Alvarez, R. & Christensen, K. T. (2013), Wall-parallel stereo particle-image velocimetry measurements in the roughness sublayer of turbulent flow overlying highly irregular roughness, *Physics of Fluids (1994-present),* 25**,** -.

Mignot, E., Barthelemy , E. & Hurther, D. (2009a), Double-averaging analysis and local flow characterization of near-bed turbulence in gravel-bed channel flows, *Journal of Fluid Mechanics,* 618**,** 279-303.

Mignot, E., Hurther, D. & Barthelemy, E. (2009b), On the structure of shear stress and turbulent kinetic energy flux across the roughness layer of a gravel-bed channel flow, *Journal of Fluid Mechanics,* 638**,** 423-452.

Mueller, M., Pander, J., Wild, R., Lueders, T. & Geist, J. (2013), The effects of stream substratum texture on interstitial conditions and bacterial biofilms: Methodological strategies, *Limnologica - Ecology and Management of Inland Waters,* 43**,** 106-113.

Narasimha, R., Kumar, S. R., Prabhu, A. & Kailas, S. V. (2007), Turbulent flux events in a nearly neutral atmospheric boundary layer, *Philosophical Transactions of the Royal Society A: Mathematical, Physical and Engineering Sciences,* 365**,** 841-858.

Nelson, J. M., Shreve, R. L., Mclean, S. R. & Drake, T. G. (1995), Role of Near-Bed Turbulence Structure in Bed Load Transport and Bed Form Mechanics, *Water Resources Research,* 31**,** 2071-2086.

Nezu, I. & Nakagawa, H. (1984), Cellular Secondary Currents in Straight Conduit, *Journal of Hydraulic Engineering,* 110**,** 173-193.

Nezu, I. & Nakagawa, H., (1993), *Turbulence in Open-Channel Flows,* A.A. Balkema.

Nezu, I. & Sanjou, M. (2011), PIV and PTV measurements in hydro-sciences with focus on turbulent open-channel flows, *Journal of Hydro-environment Research,* 5**,** 215-230.

Nikora, V., (2007), Hydrodynamics of gravel-bed rivers: scale issues, *In:* Habersack, H., Piégay, H. & Rinaldi, M. (eds.) *Gravel bed rivers IV: from process understanding to river restoration*: Elsevier.

Nikora, V., Goring, D., Mcewan, I. & Griffiths, G. (2001), Spatially Averaged Open-Channel Flow over Rough Bed, *Journal of Hydraulic Engineering,* 127**,** 123-133.

Nikora, V., Koll, K., Mclean, S., Dittrich, A. & Aberle, J., Zero-plane displacement for rough-bed open-channel flows, *In:* Bousmar, D. & Zech, Y., eds. international conference on fluvial hydraulics, River Flow 2002, 2002.

Nikora, V., Mcewan, I., Mclean, S., Coleman, S., Pokrajac, D. & Walters, R. (2007a), Double-Averaging Concept for Rough-Bed Open-Channel and Overland Flows: Theoretical Background, *Journal of Hydraulic Engineering,* 133**,** 873-883.

Nikora, V., Mclean, S., Coleman, S., Pokrajac, D., Mcewan, I., Campbell, L., Aberle, J., Clunie, D. & Koll, K. (2007b), Double-Averaging Concept for Rough-Bed Open-Channel and Overland Flows: Applications, *Journal of Hydraulic Engineering,* 133**,** 884-895.

Nikora, V. & Rowiński, P. (2008), Rough-bed flows in geophysical, environmental, and engineering systems: Double-Averaging Approach and its applications, *Acta Geophysica,* 56**,** 529-533.

Nikora, V. & Walsh, J. (2004), Water-worked gravel surfaces: High-order structure functions at the particle scale, *Water Resources Research,* 40**,** W12601.

Nikora, V. I., Goring, D. G. & Biggs, B. J. F. (1998a), On gravel-bed roughness characterization, *Water Resources Research,* 34**,** 517-527.

Nikora, V. I., Goring, D. G. & Biggs, B. J. F., (1998b), *Silverstream eco-hydraulics flume : hydraulic design and tests,* Wellington, New-Zealand, Scientific and Industrial Research Publishing.

Nino, Y. & Garcia, M. H. (1996), Experiments on particle—turbulence interactions in the near–wall region of an open channel flow: implications for sediment transport, *Journal of Fluid Mechanics,* 326**,** 285-319.

Nogaro, G., Datry, T., Mermillod-Blondin, F., Descloux, S. & Montuelle, B. (2010), Influence of streambed sediment clogging on microbial processes in the hyporheic zone, *Freshwater Biology,* 55**,** 1288-1302.

Nogaro, G., Mermillod-Blondin, F., François- Carcaillet, F., Gaudet, J.-P., Lafont, M. & Gibert, J. (2006), Invertebrate bioturbation can reduce the clogging of sediment: an experimental study using infiltration sediment columns, *Freshwater Biology,* 51**,** 1458-1473.

Packman, A. I. & Mackay, J. S. (2003), Interplay of stream-subsurface exchange, clay particle deposition, and streambed evolution, *Water Resources Research,* 39**,** 1097.

Papanicolaou, A., Diplas, P., Dancey, C. & Balakrishnan, M. (2001), Surface Roughness Effects in Near-Bed Turbulence: Implications to Sediment Entrainment, *Journal of Engineering Mechanics,* 127**,** 211-218.

Pellachini, C., (2011), *Modelling fine sediment transport over an immobile gravel bed,* PhD, University of Trento.

Pokrajac, D., Campbell, L., Nikora, V., Manes, C. & Mcewan, I. (2007), Quadrant analysis of persistent spatial velocity perturbations over square-bar roughness, *Experiments in Fluids,* 42**,** 413-423.

Pokrajac, D., Finnigan, J. J., Manes, C., Mcewan, I. & Nikora, V., (2006), On the definition of the shear velocity in rough bed open channel flows, *River Flow 2006, Two Volume Set*: Taylor & Francis.

Pope, S. B., (2000), *Turbulent Flows*, Cambridge University Press.

Prasad, A. K. (2000), Stereoscopic particle image velocimetry, *Experiments in Fluids,* 29**,** 103-116.

Prasad, A. K., Adrian, R. J., Landreth, C. C. & Offutt, P. W. (1992), Effect of resolution on the speed and accuracy of particle image velocimetry interrogation, *Experiments in Fluids,* 13**,** 105-116.

Pretty, J. L., Hildrew, A. G. & Trimmer, M. (2006), Nutrient dynamics in relation to surface–subsurface hydrological exchange in a groundwater fed chalk stream, *Journal of Hydrology,* 330**,** 84-100.

Raffel, M., Willert, C. E., Wereley, S. T. & Kompenhans, J., (2007), *Particle Image Velocimetry: A Practical Guide*, Springer.

Raupach, M. R., Antonia, R. A. & Rajagopalan, S. (1991), Rough-Wall Turbulent Boundary Layers, *Applied Mechanics Reviews,* 44**,** 1-25.

Raupach, M. R. & Shaw, R. H. (1982), Averaging procedures for flow within vegetation canopies, *Boundary-Layer Meteorology,* 22**,** 79-90.

Rehg, K. J., Packman, A. I. & Ren, J. (2005), Effects of suspended sediment characteristics and bed sediment transport on streambed clogging, *Hydrological Processes,* 19**,** 413-427.

Righetti, M. & Romano, G. P. (2004), Particle–fluid interactions in a plane near-wall turbulent flow, *Journal of Fluid Mechanics,* 505**,** 93-121.

Robert, A. (1991), Fractal properties of simulated bed profiles in coarse-grained channels, *Mathematical Geology,* 23**,** 367-382.

Rodríguez, J. F. & García, M. H. (2008), Laboratory measurements of 3-D flow patterns and turbulence in straight open channel with rough bed, *Journal of Hydraulic Research,* 46**,** 454-465.

Roy, A., Eacute, G., Buffin-Bélanger, T., Lamarre, H., Egrave, Eacute, Ne & Kirkbride, A. D. (2004), Size, shape and dynamics of large-scale turbulent flow structures in a gravel-bed river, *Journal of Fluid Mechanics,* 500**,** 1-27.

Sambrook Smith, G. H. & Nicholas, A. P. (2005), Effect on flow structure of sand deposition on a gravel bed: Results from a two-dimensional flume experiment, *Water Resources Research,* 41**,** W10405.

Sanders, I. A., Heppell, C. M., Cotton, J. A., Wharton, G., Hildrew, A. G., Flowers, E. J. & Trimmer, M. (2007), Emission of methane from chalk streams has potential implications for agricultural practices, *Freshwater Biology,* 52**,** 1176-1186.

Sarkar, S. & Dey, S. (2010), Double-averaging turbulence characteristics in flows over a gravel bed, *Journal of Hydraulic Research,* 48**,** 801-809.

Scarano, F. (2002), Iterative image deformation methods in PIV, *Measurement Science and Technology,* 13**,** R1.

Schälchli, U. (1992), The clogging of coarse gravel river beds by fine sediment, *Hydrobiologia,* 235-236**,** 189-197.

Scheurer, K., Alewell, C., Bänninger, D. & Burkhardt-Holm, P. (2009), Climate and land-use changes affecting river sediment and brown trout in alpine countries—a review, *Environmental Science and Pollution Research,* 16**,** 232-242.

Schlichting, H., Gersten, K. & Gersten, K., (2000), *Boundary-Layer Theory*, MacGraw-Hill.

Selley, R. C., (2000), *Applied Sedimentology*, Elsevier Science.

Shvidchenko, A. B. & Pender, G. (2001), Macroturbulent structure of open-channel flow over gravel beds, *Water Resources Research,* 37**,** 709-719.

Singh, K., Sandham, N. & Williams, J. (2007), Numerical Simulation of Flow over a Rough Bed, *Journal of Hydraulic Engineering,* 133**,** 386-398.

Smits, A. J., Mckeon, B. J. & Marusic, I. (2011), High–Reynolds Number Wall Turbulence, *Annual Review of Fluid Mechanics,* 43**,** 353-375.

Snarski, S. R. & Lueptow, R. M. (1995), Wall pressure and coherent structures in a turbulent boundary layer on a cylinder in axial flow, *Journal of Fluid Mechanics,* 286**,** 137-171.

Soloff, S. M., Adrian, R. J. & Liu, Z.-C. (1997), Distortion compensation for generalized stereoscopic particle image velocimetry, *Measurement Science and Technology,* 8**,** 1441.

Statzner, B. & Sagnes, P. (2008), Crayfish and fish as bioturbators of streambed sediments: Assessing joint effects of species with different mechanistic abilities, *Geomorphology,* 93**,** 267-287.

Sterk, G., Jacobs, A. F. G. & Van Boxel, J. H. (1998), The effect of turbulent flow structures on saltation sand transport in the atmospheric boundary layer, *Earth Surface Processes and Landforms,* 23**,** 877-887.

Sternecker, K., Wild, R. & Geist, J. (2013), Effects of substratum restoration on salmonid habitat quality in a subalpine stream, *Environmental Biology of Fishes,* 96**,** 1341-1351.

Stromberg, J. C. & Tiller, R. (1996), Effects of groundwater decline on riparian vegetation of semiarid regions: the San Pedro, Arizona, *Ecological Applications*
6**,** 113-131.

Sutherland, A. J. (1967), Proposed mechanism for sediment entrainment by turbulent flows, *Journal of Geophysical Research,* 72**,** 6183-6194.

Tamburrino, A. & Gulliver, J. S. (2007), Free-surface visualization of streamwise vortices in a channel flow, *Water Resources Research,* 43**,** W11410.

Thomas, A. S. W. & Bull, M. K. (1983), On the role of wall-pressure fluctuations in deterministic motions in the turbulent boundary layer, *Journal of Fluid Mechanics,* 128**,** 283-322.

Tigrek, S. & Aras, T., (2011), *Reservoir Sediment Management*, Taylor & Francis.

Trimmer, M., Maanoja, S. & G., H. A. (2010), Potential carbon fixation via methane oxidation in well-oxygenated riverbed gravels, *Limnology and Oceanography,* 55**,** 560-568.

Van Rijn, L. (1984), Sediment Transport, Part II: Suspended Load Transport, *Journal of Hydraulic Engineering,* 110**,** 1613-1641.

Velickovic, B. (2005), Colmation as one of the processes in interaction between the groundwater and surface water, *Facta Universitatis* 3**,** 165–172.

Volino, R. J., Schultz, M. P. & Flack, K. A. (2007), Turbulence structure in rough- and smooth-wall boundary layers, *Journal of Fluid Mechanics,* 592**,** 263-293.

Von Bertrab, M. G., Krein, A., Stendera, S., Thielen, F. & Hering, D. (2013), Is fine sediment deposition a main driver for the composition of benthic macroinvertebrate assemblages?, *Ecological Indicators,* 24**,** 589-598.

Wang, J., Dong, Z., Chen, C. & Xia, Z. (1993), The effects of bed roughness on the distribution of turbulent intensities in open-channel flow, *Journal of Hydraulic Research,* 31**,** 89-98.

Warren, L. L., Wotton, R. S., Wharton, G., Bass, J. a. B. & Cotton, J. A. (2009), The transport of fine particulate organic matter in vegetated chalk streams, *Ecohydrology,* 2**,** 480-491.

Webb, B. W., Hannah, D. M., Moore, R. D., Brown, L. E. & Nobilis, F. (2008), Recent advances in stream and river temperature research, *Hydrological Processes,* 22**,** 902-918.

Webb, R. H. & Leake, S. A. (2006), Ground-water surface-water interactions and long-term change in riverine riparian vegetation in the southwestern United States, *Journal of Hydrology,* 320**,** 302-323.

Wei, T. & Willmarth, W. W. (1989), Reynolds-number effects on the structure of a turbulent channel flow, *Journal of Fluid Mechanics,* 204**,** 57-95.

Wei, T. & Willmarth, W. W. (1991), Examination of v-velocity fluctuations in a turbulent channel flow in the context of sediment transport, *Journal of Fluid Mechanics,* 223**,** 241-252.

Weitbrecht, V., Seol, D.-G., Negretti, E., Detert, M., Kühn, G. & Jirka, G. H. (2011), PIV measurements in environmental flows: Recent experiences at the Institute for Hydromechanics in Karlsruhe, *Journal of Hydro-environment Research,* 5**,** 231-245.

Westerweel, J. & Scarano, F. (2005), Universal outlier detection for PIV data, *Experiments in Fluids,* 39**,** 1096-1100.

Wharton, G., Cotton, J. A., Wotton, R. S., Bass, J. a. B., Heppell, C. M., Trimmer, M., Sanders, I. A. & Warren, L. L. (2006), Macrophytes and suspension-feeding invertebrates modify flows and fine sediments in the Frome and Piddle catchments, Dorset (UK), *Journal of Hydrology,* 330**,** 171-184.

Whitaker, S., (1999), *The Method of Volume Averaging*, Springer.

Willmarth, W. W. & Lu, S. S. (1972), Structure of the Reynolds stress near the wall, *Journal of Fluid Mechanics,* 55**,** 65-92.

Wohl, E., (2013), *Mountain Rivers*, Washington, D. C, American Geophysical Union.

Wood, P. J. & Armitage, P. D. (1997), Biological Effects of Fine Sediment in the Lotic Environment, *Environmental Management,* 21**,** 203-217.

Wood, P. J. & Armitage, P. D. (1999), Sediment deposition in a small lowland stream—management implications, *Regulated Rivers: Research & Management,* 15**,** 199-210.

Wood, P. J., Vann, A. R. & Wanless, P. J. (2001), The response of Melampophylax mucoreus (Hagen) (Trichoptera: Limnephilidae) to rapid sedimentation, *Hydrobiologia,* 455**,** 183-188.

Wren, D. G., Langendoen, E. J. & Kuhnle, R. A. (2011), Effects of sand addition on turbulent flow over an immobile gravel bed, *Journal of Geophysical Research: Earth Surface,* 116**,** F01018.